UNCLASSIFIED

AD 282 055

Reproduced
by the

ARMED SERVICES TECHNICAL INFORMATION AGENCY
ARLINGTON HALL STATION
ARLINGTON 12, VIRGINIA

UNCLASSIFIED

NOTICE: When government or other drawings, specifications or other data are used for any purpose other than in connection with a definitely related government procurement operation, the U. S. Government thereby incurs no responsibility, nor any obligation whatsoever; and the fact that the Government may have formulated, furnished, or in any way supplied the said drawings, specifications, or other data is not to be regarded by implication or otherwise as in any manner licensing the holder or any other person or corporation, or conveying any rights or permission to manufacture, use or sell any patented invention that may in any way be related thereto.

282055

62-4-5

Report No. P-61-17
Quarterly
Copy No. 65

June 25, 1962

ROHM & HAAS COMPANY

REDSTONE ARSENAL RESEARCH DIVISION

HUNTSVILLE, ALABAMA

REPORT NO. P-61-17

QUARTERLY PROGRESS REPORT
ON ENGINEERING RESEARCH (U)

June 15, 1961 to September 15, 1961

ORDNANCE CORPS, DEPARTMENT OF THE ARMY

CATALOGED BY ASTIA
AD No.

282055

AUG 14 1962
TISIA

ROHM & HAAS COMPANY

REDSTONE ARSENAL RESEARCH DIVISION
HUNTSVILLE, ALABAMA

REPORT NO. P-61-17

QUARTERLY PROGRESS REPORT ON

ENGINEERING RESEARCH (U)

Approved:

W. H. Groetzinger, III
Head, Engineering Section

Allen R. Deschere
General Manager

Contributing Staff:

Gerald F. Gillis
Charles H. Parr

June 25, 1962
(written June 15, 1962)

Work reported herein was carried out under the following contract

DA-01-021-ORD-5135

FOREWORD

This is one in a series of Quarterly Progress Reports issued by the Redstone Arsenal Research Division of the Rohm & Haas Company. The complete list of reports, together with approximate issuance dates, is shown below.

Inorganic Chemistry	Process Research	Physical Chemistry	Engineering Research
Jan. 25	Feb. 25	March 25	Jan. 10
April 25	May 25	June 25	April 10
July 25	August 25	Sept. 25	July 10
Oct. 25	Nov. 25	Dec. 25	Oct. 10

Interior Ballistics	Chemical and Propellant Processing	Air Force High Energy Propellant Program	A.R.P.A. Projects
Feb. 10	March 10	March 25	Jan. 15
May 10	June 10	June 25	April 15
August 10	Sept. 10	Sept. 25	July 15
Nov. 10	Dec. 10	Dec. 25	Oct. 15

The distribution of all reports is made according to the JANAF Mailing List plus approved supplements.

ROHM & HAAS COMPANY

REDSTONE ARSENAL RESEARCH DIVISION
HUNTSVILLE, ALABAMA

ABSTRACT

A method of numerical solution was developed for obtaining the stresses, strains, and displacements in a solid propellant grain of finite length subject to loadings of pressure, cure and thermal shrinkage, and axial acceleration. Although the method is applicable to any solid of revolution, the development was restricted to a propellant grain in the form of hollow, right, circular cylinder bonded at the outer periphery to a rigid motor case. The ends of the grain were treated for both bonded and free conditions. The analysis was limited to materials which are homogeneous, isotropic, elastic, and undergo small deformations. Results were obtained in dimensionless form which can be expressed in terms of only three independent variables - Poisson's ratio and the length-to-diameter and the inner-to-outer diameter ratios of the grain. The effect of these variables on the stress, strain, and displacement distributions in the propellant grain was examined.

The Raleigh-Ritz method was employed in conjunction with the principle of minimum potential energy to obtain expressions for the displacements in a propellant grain in the form of a hollow, right, circular cylinder bonded at the outer periphery to a rigid motor case and subjected to cure shrinkage. The analysis was limited to materials which are homogeneous, isotropic, elastic and undergo small deformations. Numerical results obtained from the displacement equations compare favorably with measured values and those obtained by a numerical solution using relaxation techniques.

TABLE OF CONTENTS

DEFORMATIONS AND STRESSES IN CASE-BONDED SOLID PROPELLANT GRAINS OF FINITE LENGTH BY NUMERICAL METHODS

Charles H. Parr

Most existing stress-strain analyses of solid propellant grains have been based on conditions of plane strain, which is equivalent to assuming the grains to be of infinite length. These solutions are applicable to center sections of very long cylinders where the warping of cross sections in the axial direction is small. These plane strain solutions for pressure, thermal, and cure shrinkage loading have been developed adequately for circular cross-sections, small deformations, linearly elastic homogeneous materials, and constant material properties [1][1]. Significant advances have been made in plane strain analysis to include more complex cross sectional geometries [2], viscoelastic properties [3, 4], and large deformations [4].

The study of propellant grains of finite length has been neglected until recently. Shortly after the analysis described here was completed, two papers concerned with the analysis of hollow, right, circular cylinders using numerical methods were published [5, 6]. Solutions for stress distributions in cylinders of finite length subject to various boundary tractions in terms of continuous functions offer formidable difficulties even in classical elasticity theory [7, 8, 9]. If a continuous solution can be obtained, the numerical evaluation of the solution may be quite difficult, particularly in certain regions of the cylinder.

Following several abortive attempts at this Division to obtain closed form solutions for finite length grains in the form of hollow, right, circular cylinders with the required boundary conditions, it was decided to try two alternative approaches: (1) a numerical solution of the appropriate differential equations and (2) approximate solutions based on the principles of minimum energy. This section of this report is based on the numerical solution method.

---

[1]Numbers in brackets refer to references at the end of the report.

ANALYSIS

Problem Description

The most general end-effect problem in the mechanics of case-bonded solid propellant grains would consider a system of three concentric cylinders (motor case, liner, and propellant grain), the inner cylinder having a perforation of complicated geometry and all terminating in a complex non-symmetric, non-cylindrical fashion. The end conditions would vary both in contour and in the conditions of restraint on the propellant grain. Loading conditions would include internal pressurization, cure and thermal shrinkage, three-dimensional thermal gradients, and acceleration forces of arbitrary direction.

In addition, the propellant under some circumstances undergoes deformations of such magnitude that the theory of infinitesmial deformation is no longer valid to any acceptable degree of approximation; the propellant is viscoelastic, thus making the problem time and history dependent; the propellant is not isotropic in its response to stress; and the propellant is non-homogeneous.

The various mathematical theories of continuum mechanics are at such a stage of development that, with the exception of simultaneous large deformations and viscoelastic effects, a model closely describing the actual propellant grain can be formulated in differential equation form. However the complexity of the complete problem is such that it is doubtful that existing electronic digital computers could be utilized to obtain numerical results in reasonable times. More serious, however, is the lack of data on the viscoelastic response of propellants under multiaxial stress conditions. To date, there is not a single propellant whose viscoelastic behavior has been fully characterized, even for small deformations. This fact alone precludes the usefulness of the more sophisticated solution techniques available. Lack of data on propellants dictates a choice of obtaining a complex solution in terms of unmeasured physical parameters or obtaining a simpler solution which may not be compatible with reality.

Accordingly, to reduce this problem to one of a magnitude solvable by numerical methods on existing electronic digital computers in reasonable times and which will give reasonable qualitive information on end effects in a propellant grain, a model of the grain in the form of a hollow, right, circular cylinder of finite length with the outer periphery

bonded to a rigid motor case and with the ends either free or bonded to the case was considered. The cylinder material was considered to be homogeneous, isotropic, and elastic. Small deformation theory was used. The assumptions of case rigidity, isotropy, and small deformations are reasonable if (a) the interrelated factors of interface stress, case-propellant modulus ratio, and case thickness are such that the deflections of the motor case are small and (b) the maximum strains in the propellant are of the order of ten percent or less. These conditions are satisfied, in general, by motors which undergo thermal or cure shrinkage and acceleration loads but, in general, are not met by motors undergoing internal pressurization, in which case the validity of these assumption must be established in individual problems. This can be done by studying the plane strain solutions for both elastic and rigid motor cases. The assumption of homogeneity is adequate if stresses are only considered on the macroscopic level. The assumption of elasticity was made for simplicity although the extension of this method to include viscoelastic effects is under study.

Problem Formulation

The model used in this analysis is shown in Fig. 1. It consists of a hollow, right, circular cylinder of finite length which is bonded at the outer periphery to a rigid solid. The cylinder material was homogeneous, elastic, and isotropic. In the present study two types of end conditions were considered: (a) both ends free and (b) one end bonded to a rigid wall and the other end free. For cylinders with free ends under thermal or cure shrinkage loading or pressure loading an additional symmetry is introduced so that the numerical solution was carried out only for one-half of the length.

The cylinder was considered to be loaded by internal pressure on the inner radius and on each of the free ends; by a linear expansion, δ, which would have a negative value for shrinkage; and axial acceleration.

Stress functions introduced by Southwell [10], but which are described more clearly by Allen [11], were used for the numerical solution. These Southwell stress functions are particularly well adapted to the use of relaxation methods for the numerical solution of problems involving axial symmetry. Southwell shows that if two functions $\Phi(r, z)$ and $\Psi(r, z)$ satisfy the second order differential equations

$$\frac{\partial^2\Phi}{\partial r^2} - \frac{1}{r}\frac{\partial\Phi}{\partial r} + \frac{\partial^2\Phi}{\partial z^2} = 0 \tag{1}$$

and

$$\frac{\partial^2\Psi}{\partial r^2} - \frac{1}{r}\frac{\partial\Psi}{\partial r} + \frac{\partial^2\Psi}{\partial z^2} = \frac{\partial^2\Phi}{\partial z^2} \quad , \tag{2}$$

the compatability relations and equilibrium equation are satisfied for an elastic solid undergoing small deformations if the stresses are defined by

$$\sigma_r = \frac{1}{r}\left[\frac{\partial\Phi}{\partial r} + \frac{\partial\Psi}{\partial r}\right] - \frac{1}{r^2}\left[\Psi + [1-\nu]\,\Phi\right] \quad , \tag{3}$$

$$\sigma_\theta = \frac{\nu}{r}\frac{\partial\Phi}{\partial r} + \frac{1}{r^2}\left[\Psi + [1-\nu]\,\Phi\right] \quad , \tag{4}$$

$$\sigma_z = -\frac{1}{r}\frac{\partial\Psi}{\partial r} \quad , \text{ and} \tag{5}$$

$$\sigma_{rz} = \frac{1}{r}\frac{\partial\Psi}{dz} \quad , \tag{6}$$

where r, θ, z denote a cylindrical polar coordinate system, σ denotes stress, and ν denotes Poisson's ratio. Eqs. 1 through 6 were generalized to include the effects of body forces due to axial acceleration and propellant expansion due to temperature change and cure shrinkage. The addition of the expansion term has been discussed previously by Parr [12]. Acceleration terms are discussed by Southwell [13]. If the propellant cylinder is under an axial acceleration A and undergoes a linear expansion δ, the stresses and strains may still be defined in terms of stress functions which satisfy Eqs. 1 and 2. For convenience, Eqs. 1 through 6 and the allied strain and displacement equations were put into dimensionless form. Defining

$$\rho = \frac{r}{b} \quad , \qquad \sigma_\rho = \frac{\sigma_r}{E} \quad , \qquad \epsilon_\rho = \epsilon_r \quad ,$$

$$\eta = \frac{z}{b} \quad , \qquad \sigma_\Theta = \frac{\sigma_\theta}{E} \quad , \qquad \epsilon_\Theta = \epsilon_\theta \quad ,$$

$$Z = \frac{b\gamma A}{E} \quad , \qquad \sigma_\eta = \frac{\sigma_z}{E} \quad , \qquad \epsilon_\eta = \epsilon_z \quad ,$$

$$\phi = \frac{b^2\Phi}{E} \quad , \qquad \sigma_{\rho\eta} = \frac{\sigma_{rz}}{E} \quad , \qquad \epsilon_{\rho\eta} = \epsilon_{rz} \quad ,$$

$$\psi = \frac{b^2\Psi}{E} \quad , \qquad u_\rho = \frac{u_r}{b} \quad , \qquad u_\eta = \frac{u_z}{b} \quad ,$$

where u indicates displacement, ϵ indicates strain, b is the outer radius of the cylinder, γ is the density, and E is the elastic modulus of the cylinder, the partial differential equations for the stress function $\phi(\rho, \eta)$ and $\psi(\rho, \eta)$ may be written

$$\frac{\partial^2\phi}{\partial\rho^2} - \frac{1}{\rho}\frac{\partial\phi}{\partial\rho} + \frac{\partial^2\phi}{\partial\eta^2} = 0 \tag{7}$$

and

$$\frac{\partial^2\psi}{\partial\rho^2} - \frac{1}{\rho}\frac{\partial\psi}{\partial\rho} + \frac{\partial^2\psi}{\partial\eta^2} = \frac{\partial^2\phi}{\partial\eta^2} \quad . \tag{8}$$

The displacements, strains, and stresses are defined by

$$u_\rho = \frac{[1+\nu]}{\rho}\left[\psi + [1-\nu]\phi\right] + \rho\delta - \nu\rho\eta Z \quad , \tag{9}$$

$$u_\eta = -\frac{[1+\nu]}{\rho}\left[\int_o^\eta \frac{\partial\psi}{\partial\rho}\, d\eta + \nu\int_o^\eta \frac{\partial\phi}{\partial\rho}\, d\eta\right] + \eta\delta + \frac{\eta^2}{2}Z + f(\rho) \quad , \tag{10}$$

$$u_\theta = 0 \quad , \tag{11}$$

$$\epsilon_\rho = \frac{[1+\nu]}{\rho}\left\{\frac{\partial\psi}{\partial\rho} + [1-\nu]\frac{\partial\phi}{\partial\rho} - \frac{1}{\rho}\left[\psi + [1-\nu]\phi\right]\right\} + \delta - \nu\eta Z \quad , \tag{12}$$

$$\epsilon_\theta = \frac{[1+\nu]}{\rho^2}\left[\psi + [1-\nu]\phi\right] + \delta - \nu\eta Z \quad , \tag{13}$$

$$\epsilon_\eta = -\frac{[1+\nu]}{\rho}\left[\frac{\partial\psi}{\partial\rho} + \nu\frac{\partial\phi}{\partial\rho}\right] + \delta + \eta Z \quad , \tag{14}$$

$$\sigma_\rho = \frac{1}{\rho}\left[\frac{\partial\phi}{\partial\rho} + \frac{\partial\psi}{\partial\rho}\right] - \frac{1}{\rho^2}\left[\psi + [1-\nu]\phi\right] \quad , \tag{15}$$

$$\sigma_\theta = \frac{\nu}{\rho}\frac{\partial\phi}{\partial\rho} + \frac{1}{\rho^2}\left[\psi + [1-\nu]\phi\right] \quad , \tag{16}$$

$$\sigma_\eta = -\frac{1}{\rho}\frac{\partial\psi}{\partial\rho} + \eta Z \quad , \text{ and} \tag{17}$$

$$\sigma_{\rho\eta} = \frac{1}{\rho}\frac{\partial\psi}{\partial\eta} \quad . \tag{18}$$

The function $f(\rho)$ appearing in Eq. 10 will be discussed later. The dimensionless coordinate system is illustrated in Fig. 2. The origin of the η coordinate is taken at the motor midsection for symmetrical problems and at the left end of the cylinder for unsymmetrical problems.

Boundary Conditions

In addition to satisfying Eqs. 7 and 8, the stress functions ϕ and ψ have certain restrictions placed on them at the boundaries which are determined from the boundary conditions.

Boundary $\rho = \alpha$

On the inner boundary of the cylinder, $r = a$, the most general form of boundary conditions for the problem under consideration can be expressed as

$$\sigma_r = - p_2(z) \tag{19}$$

and

$$\sigma_{rz} = t_2(z) \quad , \tag{20}$$

where $p_2(z)$ is the normal pressure on the boundary and $t_2(z)$ is the shearing stress on the boundary. In dimensionless form, the inner boundary is $\rho = \alpha = \frac{a}{b}$ and the boundary conditions become

$$\sigma_\rho = - \frac{p_2(z)}{E} = - \Pi_2(\eta) \tag{21}$$

and

$$\sigma_{\rho\eta} = \frac{t_2(z)}{E} = T_2(\eta) \quad . \tag{22}$$

Boundary $\eta = H$

The free end of the cylinder was considered to be loaded by normal pressure $p_3(r)$ and shear stress $t_3(r)$. In dimensionless form this boundary becomes $\eta = H$ and the boundary conditions can be expressed as

$$\sigma_\eta = - \frac{p_3(r)}{E} = - \Pi_3(\rho) \tag{23}$$

and

$$\sigma_{\rho\eta} = \frac{t_3(r)}{E} = T_3(\rho) \quad . \tag{24}$$

Boundary $\rho = 1$

On the boundary $r = b$, or $\rho = 1$ in dimensionless form, the bonding to the rigid motor case requires zero radial and axial displacements. Hence in dimensionless form these boundary conditions become

$$u_\rho = 0 \tag{25}$$

and

$$u_\eta = 0 \ . \tag{26}$$

Boundary $\eta = 0$

1. Symmetrical Problems

For symmetrical problems the plane $\eta = 0$ was taken as the mid-section of the grain. From considerations of symmetry on the stresses and displacements it can be deduced that the symmetry boundary conditions are

$$\frac{\partial \phi}{\partial \eta} = 0 \tag{27}$$

and

$$\frac{\partial \psi}{\partial \eta} = 0 \ . \tag{28}$$

2. Unsymmetrical Problems

For unsymmetrical problems the plane $\eta = 0$ was taken at the left end of the cylinder.

(a) When this end is bonded to a rigid case the radial, and axial displacements are

$$u_\rho = 0 \tag{29}$$

and

$$u_\eta = 0 \ . \tag{30}$$

(b) When this end is free, the boundary conditions become analogous to Eqs. 23 and 24, i.e.,

$$\sigma_\eta = \Pi_1 (\rho) \tag{31}$$

and

$$\sigma_{\rho\eta} = T_1 (\rho) \ . \tag{32}$$

If the axial displacement is zero along the coordinate $\eta = 0$, the function $f(\rho)$ in Eq. 10 is zero. If the axial displacement is not zero along this coordinate, the function $f(\rho)$ must be separately evaluated. Since such cases are not considered in the results covered by this report, the evaluation of $f(\rho)$ will not be discussed further.

For the loadings considered in this report, the normal surface loads Π_i are considered constant and the shear loads T_i are all taken to be zero. The extension of the finite difference forms to variable loads is quite straightforward, however.

The reduction of Eqs. 7 through 32 to finite difference form and the method of solution is outlined in the Appendix.

RESULTS OF COMPUTATIONS

An inspection of the field equations of the stress function (Eqs. 7 and 8), the definition of dimensionless displacements, strains, and stresses (Eqs. 9 through 18), and the boundary conditions (Eqs. 21 through 32) reveals that the dimensionless displacements, strains, and stresses are linear functions of the load parameters δ, Z, Π_i, and T_i. Thus the parameters whose effects need investigation under each type of loading are Poisson's ratio, ν, and two geometric variables which were somewhat arbitrarily chosen to be the ratio of cylinder length-to-diameter, λ, and the outer-to-inner radius ratio, κ.

Some 90 problems with variations of these three parameters for various loads have been worked numerically. Tabulation of the variation of the four stresses and two displacements in critical areas as a function of these three parameters would require not only a discourse of considerable proportions but a massive amount of data reduction. Accordingly, the presentation of the results of these calculations is being prepared in two parts. This report will primarily be concerned with overall deformation effects and stresses at the midsection of such motors. This is in line with the interest of this Division in profile measurements as a nondestructive test and in the use of motors with propellant grains of the same geometry employed in this analysis for the determination of failure criteria.

The second part of the presentation of results consists of a more complete stress study and is being prepared by John Wise of Thiokol Chemical Corporation, Redstone Division, in the form of design charts suitable for use by rocket motor designers. This study will be published separately.

Shrinkage Loading

Fig. 3 shows the theoretical radial displacement of the inner radius for a grain with free ends 33 in. in length having an outer radius of 3 in. and an inner radius of 1 in. for four sets of Poisson's ratio and linear expansion factor. Superposed are measured displacements due to thermal and cure shrinkage from a 6C2-33 static test motor ($a = 1$, $b = 3$, $\ell = 33$), made with 112_{bw} nitrocellulose plastisol propellant. The measurements were made of the profile of the propellant in the static test motor had ceased to change with time, indicating that cure shrinkage was complete and viscoelastic effects were no longer affecting the profile. Neither of the properties ν or δ is known accurately for this propellant.

The computed displacements are directly proportional to δ, and therefore for a given ν it is possible to select a value of δ which fits the experimental data at the midsection of the motor.

Accordingly, displacement curves for $\nu = 0.49$ and $\nu = 0.50$ were fitted to the actual displacements at the midsection of the motor, giving values of δ of -0.0050 and -0.0043, respectively. (For this motor, the radial displacement at the center for $\nu = 0.5$ is 98.5% of the plane strain solution.) To demonstrate the effects of variations in Poisson's ratio and the linear expansion factor δ, curves are also shown for $\nu = 0.5$, $\delta = -0.0050$ and $\nu = 0.49$, $\delta = -0.0043$.

It can be seen that any value of Poisson's ratio from 0.50 to 0.49 (and perhaps lower) when combined with a suitable value of δ will give a reasonable fit to the experimental data. This suggests a method of determining Poisson's ratio if the unconstrained value of the shrinkage is known. The converse, however, would not apply since small errors in the value of Poisson's ratio would lead to large errors in the shrinkage. This demonstrates the dependence of the apparent shrinkage on the dilatancy or compressibility of the material.

Figs. 4 and 5 demonstrate the distortion produced in the longitudinal cross section of a long and a short grain under shrinkage loading. These grains had both ends free so that the deformations were symmetrical about the transverse centroidal plane. Fig. 6 demonstrates the distortion in a propellant grain with the left end fixed and Fig. 7 shows the corresponding dimensionless contour map of the stresses. It can be seen from Figs. 6 and 7 that there is little interaction of end effects so that the left side may be taken as being typical of rigidly bonded ends and the right side as being typical of free ends.

Figs. 8 through 10 demonstrate, respectively, the effect on the profile of Poisson's ratio, ν, length-to-diameter ratio, λ, and radius ratio, κ, on grains with free ends subjected to shrinkage loading.

The examples in Figs. 4 through 10 show results of the type that can be obtained with the solution method outlined here. A more detailed study was made to determine the values of λ, the length-to-diameter ratio which was needed to produce a condition of plane strain at the midsection of the propellant grain with free ends. Figs. 11 through 15 demonstrate the effect of the parameters λ, κ, and ν on the deviation of the radial displacement of the inside surface at the middle of various cylinders from the displacement of the inside surface in a cylinder of

infinite length. The dashed lines indicate areas where the data was insufficient to give reliable values. The ratio of the radial displacement at the inside radius to the inside radius, $\frac{u_a}{a}$, in a cylinder of infinite length is given [15] by

$$\frac{u_a}{a} = - \frac{[1+\nu][\kappa^2 - 1]\,\delta}{1 + [1 - 2\nu]\,\kappa^2} \quad . \tag{33}$$

From Figs. 11 through 15, it can be seen that the end effects are most extensive for $\nu = 0.5$ and decrease rapidly with decreasing ν. End effects become less extensive with decreasing radius ratio κ (decreasing web fraction). Since the end effects were most extensive for $\nu = 0.5$, the largest number of calculations were made for this value of Poisson's ratio.

By cross plotting Figs. 11 through 15, the ratio of radial displacements can be plotted as a function of reduced web $w^* = (b - a)/2b$, which is sometimes a more convenient parameter to use. A typical plot of this type is shown in Fig. 16 for $\nu = 0.5$ for various values of λ. The curve $\lambda = 0$ in Fig. 16 is plotted from the theoretical plane stress solution. Note that it does not reach 100% of the plane strain solution at $w^* = 0$. The assumptions of both plane strain and zero length are untenable and lead to the discontinuity shown here.

Figs. 17 through 22 show the circumferential and axial stresses at the midsection of the grain with free ends as a function of ν, λ, and κ. The dashed lines indicate areas where the data was insufficient to give reliable values of the stresses. The compressive values of axial stress for $\lambda < 1$ in Fig. 18, while surprising, are apparently correct. Several points were calculated in this area to establish this behavior.

One proposed method of testing propellants in a multiaxial stress field utilizes a rocket motor similar in all respects to the model discussed, with loading introduced by lowering of the temperature of the system. The differential thermal expansion of the case and propellant results in the type of shrinkage considered here. It is of interest to note since Poisson's ratio, ν, is a function of temperature, that as the temperature changes, not only will the displacement in a motor of given dimensions change but the shape of the displacement curve will also change, indicating that the stress field is also changing in form. Thus while Figs. 18 and 19 for $\nu = 0.5$ may be valid for a failure at room

temperature, the stresses at failure at a temperature of - 40°F need to be determined from another curve, say for $\nu = 0.40$.

Acceleration Loading

To date an extensive study of acceleration loads has not been made; however, such a study is in progress. Typical distortion plots are shown in Fig. 23 for a grain with both ends free and in Fig. 24 for a grain with one end free and one end fixed. The stress contours for the grain of Fig. 24 are shown in Fig. 25. Again, the end effects are well separated so that the right end is typical of a free end and the left end is typical of a fixed end.

One striking property of the cylinder with both ends free is that the stresses and defections are antisymmetric about the midsection. An interesting result of this fact is that the stresses and deflections at the midsection of any axially accelerated cylinder of finite length are exactly the same as the stresses and displacements everywhere in a similar cylinder of infinite length.

Pressure Loading

A few cases of pressure loading have been run. However, the usefulness of this solution is limited to relatively thick and stiff motor cases since the model assumes a rigid case. An additional limitation is imposed since the magnitude of strains under usual operation pressure will sometimes exceed the range of validity of the analysis. Details of the investigation for this loading will be presented at a later date.

DISCUSSION

Shrinkage Loading

It was determined that within the range of allowable strains in which the analysis is valid, say 10% or less, the end effects, expressed in dimensionless form are functions of only Poisson's ratio, ν, the ratio of outer-to-inner radius, κ, and the length-to-diameter ratio, λ. All three parameters affect the nature of the end effects significantly in their ranges of interest.

Only a few profiles of propellant grains are presented in this report; however, comparison of the many profiles which have been calculated showed that the apparent flatness of the deflection curve in the center section of the cylinder is not a reliable indication of the degree of approach to the plane strain condition. In actual measurements, the apparent flatness is further clouded by normal scatter of data.

Consideration of these factors, indicates that the use of case-bonded propellant cylinders for obtaining values of the thermal coefficient of expansion and of stress and strain at rupture is not at all straightforward and may lead to large errors if a plane strain analysis is used. For instance, suppose a motor with $K = 6$ and $\lambda = 4$ is used to predict the thermal coefficient of expansion. For $\nu = 0.50$ the deflection expected can be seen from Fig. 3 to be only 65% of the plane strain deflection. If the prediction is based on a plane strain solution, the apparent coefficient of thermal expansion would only be 65% of the true coefficient of thermal expansion. If, however, ν is known to be 0.49, the apparent coefficient of thermal expansion would be 84% of the true value. However, if ν is actually 0.49 for the propellant but it is assumed to be 0.50, the apparent coefficient of thermal expansion using Eq. 33 would be

$$84\% \times \frac{(\text{Plane strain displacement for } \nu = 0.49)}{(\text{Plane strain displacement for } \nu = 0.50)}$$

or 48.5% of the true value. Errors of a similar type could occur in the prediction of stresses and axial strains.

Viscoelastic Effects

The elastic solutions obtained here are applicable to viscoelastic materials at long times if the equilibrium moduli are used or for very short times if the glassy moduli are used. Since the tensile modulus occurs only in the dimensionless stress, pressure, and acceleration parameters, more general conclusions can be reached in certain cases. For instance with time independent Poisson's ratio, the viscoelastic strain and displacement solutions for shrinkage loading are the same as the elastic solutions. Further, although σ, δ, and E are functions of time, the dimensionless stresses $(\sigma/-\delta E)$ are constant, allowing the stresses to be evaluated if the time functionality of δ and E are known.

Additional viscoelastic solutions can be obtained by using the calculated numerical results for the elastic solution and utilizing numerical methods or other approximate methods for inversion of Laplace transforms. Such methods are under study and results will be reported at a later date.

Curved Ends

A computer program has been completed to investigate grains with curved ends which are bonded to the motor case. It is expected that the effects of the shape of the curved end on propellant stresses, strains,

and displacements will be studied using this program. This will be reported at a later date.

REFERENCES

1. Parr, C. H., "Stress-Strain Equations for Case Bonded Solid Propellant Grains", ARS Journal, Vol. 30, p. 778, (1960).
2. Wilson, Howard B., Jr., "Stresses Owing to Internal Pressure in Solid Propellant Grains" ARS Journal, Vol. 31, p. 309, (1961).
3. Lianis, George, "Stresses and Strains in Solid Propellants During Storage", ARS Paper No. 1592-61 presented at Solid Propellant Rocket Conference, February 1961.
4. Williams, M. L., Blatz, P.J., Schapery, R.A., "Fundamental Studies Relating to Systems Analysis of Solid Propellants", Final Report - GALCIT 101, Guggenheim Aeronautical Laboratory, California Institute of Technology, February 1961.
5. Conte, S. D., Miller, K.L., Sensenig, C.B., "The Numerical Solution of Axisymmetric Problems in Elasticity", Fifth Symposium on Ballistic Missile and Space Technology, Vol. IV, Academic Press, 1960, D.P. LeGalley, Editor.
6. Messner, A.M., "Propellant Grain Stress Analysis", Bulletin of the 17th Meeting of the JANAF-ARPA-NASA Solid Propellant Group, May, 1961, Vol. I (Confidential).
7. Pickett, Gerald, "Application of the Fourier Method to the Solution of Certain Boundary Problems in the Theory of Elasticity", J. Appl. Mech., Vol. 11, p. A-176, (1944).
8. Lewis, David W., "Circular Cylinders of Finite Length Subjected to Arbitrary Surface Tractions", Doctoral Dissertation, Northwestern University, August, (1958).
9. Prelog, E., "Elastostatik der Dicken Zylinderschalen", Acad. Serbe. Sci. Publ. Inst. Math., Vol. 5, p. 115, (1953).
10. Southwell, R. V., "Some Practically Important Stress-Systems in Solids of Revolution", Proceedings of the Royal Society, Series A, Vol. 180, pp. 367-396, (1942).
11. Allen, D. N. deG., "Relaxation Methods", McGraw-Hill, p. 134, (1954).
12. Rohm & Haas Company, Quarterly Progress Report on Engineering Research, No. P-59-5, April, 1957.

13. Southwell, R. V., "Relaxation Methods in Theoretical Physics", Vol. II, Oxford, p. 345, (1956).

14. Forsythe, G. E., "What Are Relaxation Methods", Chap. 17, Modern Mathematics for Engineers, edited by E. F. Beckenback, McGraw-Hill, (1956).

15. Rohm & Haas Company, Quarterly Progress Report on Weapons Research, No. P-57-5, April 1957.

APPENDIX

SOLUTION BY RELAXATION METHODS

Finite Difference Approximations

For the numerical solution of Eqs. 7 and 8, subject to appropriate boundary conditions, the cylinder cross section in the ρ, η plane was divided into a square mesh as illustrated in Fig. 2. Each intersection of the mesh was used as a nodal point for finite difference formulation. Using three-point central difference approximations from Taylor's series [11], the following approximations result.

$$\frac{\partial \phi}{\partial \rho} = \frac{\phi_{\rho + \Delta\rho} - \phi_{\rho - \Delta\rho}}{2\Delta\rho} \tag{A-1}$$

and

$$\frac{\partial^2 \phi}{\partial \rho^2} = \frac{\phi_{\rho + \Delta\rho} - 2\phi_{\rho} + \phi_{\rho - \Delta\rho}}{\overline{\Delta\rho}^2} \quad . \tag{A-2}$$

Similar expressions can be derived involving ψ and η. With the square mesh used, $\Delta\rho = \Delta\eta = h$.

Numeric subscripts corresponding to Fig. 26 were used to denote node location with respect to the central node. It should be understood that this notation applies to the neighborhood of the node of interest and is independent of the notation that locates a particular node in the body.

Applying relations of the types Eq. A-1 and A-2, Eqs. 7 and 8 can be expressed in finite difference form as

$$\frac{h}{2\rho}\left[\phi_4 - \phi_2\right] + \phi_1 + \phi_2 + \phi_3 + \phi_4 - 4\phi_0 = 0 \tag{A-3}$$

and

$$\frac{h}{2\rho}\left[\psi_4 - \psi_2\right] + \psi_1 + \psi_2 + \psi_3 + \psi_4 - 4\psi_0 - \phi_1 - \phi_3 + 2\phi_0 = 0 \quad . \tag{A-4}$$

The values of the stress functions at points in the interior of the body must satisfy the field equations in finite difference form, Eq. A-3 and A-4.

Finite Difference Form of the Boundary Conditions

In writing the central finite difference approximation for a normal gradient at a boundary, the resulting expression involves nodal points lying outside the boundary which are called fictitious nodes. By simultaneous application of the finite difference forms for the governing field equations and the boundary condition equations at the nodes on the boundary, these fictitious nodes can be eliminated. This is the standard procedure for hand relaxation as used by Southwell and others [11, 13].

Boundary $\rho = \alpha$

The boundary conditions to be considered are Eqs. 21 and 22 where Π_2 is a constant and $T_2 = 0$. Thus

$$\sigma_\rho = -\Pi_2 \tag{A-5}$$

and

$$\sigma_{\rho\eta} = 0 \quad . \tag{A-6}$$

Expressing these stresses in terms of the finite difference forms by the use of Eqs. 15 and 18 and relations of type expressed by Eq. A-1, the boundary conditions Eqs. A-5 and A-6 become

$$\phi_2 - \phi_4 + \psi_2 - \psi_4 - \frac{2[1-\nu]h}{\alpha}\,\phi_0 + 2\alpha h\Pi_2 = 0 \tag{A-7}$$

and

$$\psi_3 - \psi_1 = 0 \quad . \tag{A-8}$$

However since the relation

$$\frac{\partial \psi}{\partial \eta} = 0 \tag{A-9}$$

resulting from Eq. 18 and Eq. A-6 is valid at constant ρ, it may be integrated directly along the boundary to yield

$$\psi = \text{constant} \, .$$

Since there is one degree of arbitrariness in the stress functions (see Allen [11], p. 136), ψ on this boundary was taken as

$$\psi = 0 \quad . \tag{A-10}$$

Both Eqs. A-8 and A-9 are satisfied by the form, Eq. A-10. When combined with Eqs. A-3 and A-4 to eliminate the fictitious values ϕ_4 and ψ_4, and simplified by use of Eq. A-10, Eq. A-7 becomes

$$\phi_2 + \psi_2 - \left\{1 + [1-\nu]\,\frac{h}{\alpha}\left[1 + \frac{h}{2\alpha}\right]\right\}\phi_0 + h\alpha\Pi_2\left[1 + \frac{h}{2\alpha}\right] = 0 \quad . \tag{A-11}$$

Eq. A-10 and A-11 were used for the determination of stress functions on this boundary.

Similar manipulation of equations is necessary on all boundaries to achieve the most useful form of the boundary conditions.

Boundary $\eta = H$

Eq. 23 when combined with Eq. 17 can be written as

$$\frac{\partial \psi}{\partial \rho} = \rho[\Pi_3 + HZ] \quad . \tag{A-12}$$

which can be integrated along the boundary to give

$$\psi = \left[\frac{\rho^2 - \alpha^2}{2}\right][\Pi_3 + HZ] \quad . \tag{A-13}$$

Eq. 24 when combined with Eq. 18 and put into finite difference form yields

$$\psi_3 - \psi_1 = 0 \ , \tag{A-14}$$

which when combined with Eqs. A-3 and A-4 to eliminate the fictitious functions ϕ_1 and ψ_1 gives

$$\frac{h}{2\rho}\left[\phi_4 - \phi_2\right] + \phi_2 + \phi_4 - 2\phi_0 + 2\psi_3 - 2\psi_0 = 0 \ . \tag{A-15}$$

On the boundary $\eta = H$, the stress functions were determined with the use of Eqs. A-13 and A-15

Boundary $\rho = 1$

Eqs. 25 and 9 give one stress function directly in terms of the other,

$$\phi = -\frac{1}{1-\nu}\left[\psi + \frac{\delta}{1+\nu} - \frac{\nu\eta Z}{1+\nu}\right] \ . \tag{A-16}$$

The boundary condition given by Eq. 26,

$$u_\eta = 0 \ , \tag{A-17}$$

can be expressed as

$$\frac{\partial u_\eta}{\partial \eta} = \epsilon_\eta = 0 \ , \tag{A-18}$$

but with neglect of rigid body displacements. However proper application of Eq. 10 for calculation of u_η^* will alleviate this difficulty.

Hence the boundary condition Eq. 26 can be expressed equivalently as, with the use of Eq. 14 ,

$$\left[1+\nu\right]\left[\frac{\partial \psi}{\partial \rho} + \nu\,\frac{\partial \phi}{\partial \rho}\right] - \delta - \eta Z = 0 \ , \tag{A-19}$$

or, in finite difference form,

$$\psi_2 - \psi_4 + \nu\left[\phi_2 - \phi_4\right] - \frac{2h}{1+\nu}\left[\delta + \eta Z\right] = 0 \ . \tag{A-20}$$

When the fictitious functions ψ_2 and ϕ_2 are eliminated from Eq. A-20 by use of Eq. A-3 and A-4, there results

$$\psi_1 + \psi_3 + \psi_4 - \left[\frac{3-4\nu}{1-\nu}\right]\psi_0 + \nu\phi_4 + \frac{\delta}{1+\nu}\left\{\frac{\nu}{1-\nu} + \frac{h}{2}\left[2-h\right]\right\}$$

$$+ \frac{\eta Z}{1+\nu}\left\{\frac{h}{2}\left[2-h\right] - \frac{\nu^2}{1-\nu}\right\} = 0 \ . \tag{A-21}$$

Eqs. A-16 and A-21 were used for the determination of ϕ and ψ on this boundary.

Boundary $\eta = 0$

1. Symmetrical Problems

From Eqs. 27 and 28, the symmetry conditions can be reduced to

$$\phi_3 = \phi_1 \tag{A-22}$$

and

$$\psi_3 = \psi_1 \quad , \tag{A-23}$$

which give, by elimination of ϕ_3 and ψ_3 the fictitious values Eqs. A-3 and A-4, the equations which apply to the stress function on this boundary.

$$\frac{h}{2\rho}\,[\phi_4 - \phi_2] + 2\phi_1 + \phi_2 + \phi_4 - 4\phi_0 = 0 \tag{A-24}$$

and

$$\frac{h}{2\rho}\,[\psi_4 - \psi_2] + 2\psi_1 + \psi_2 + \psi_4 - 4\psi_0 - 2\phi_1 + 2\phi_0 = 0 \quad . \tag{A-25}$$

2. Unsymmetrical Problems

(a) When this end is bonded to a rigid case, Eqs. 29 and 30 apply. Eq. 29, with Eq. 9, gives a direct relation between the stress functions

$$\psi + [1-\nu]\phi + \frac{\rho^2}{1+\nu}\,[\delta - \nu\eta Z] = 0 \tag{A-26}$$

which simplifies for $\eta = 0$ to

$$\psi + [1-\nu]\phi + \frac{\rho^2 \delta}{1+\nu} = 0 \quad . \tag{A-27}$$

Eq. 30 is identically satisfied by the definition of u_η, Eq. 10, if $f(\rho) = 0$ and thus yields no additional boundary relations. However, if u_η = constant when η = constant, it is implied that

$$\frac{\partial u_\eta}{\partial \rho} = 0 \quad .$$

This relation is not useful applied to Eq. 30. However from the stress-strain relations

$$\epsilon_{\rho\eta} = 2[1+\nu]\,\sigma_{\rho\eta} = \frac{2[1+\nu]}{\rho}\,\frac{\partial \psi}{\partial \eta} \tag{A-28}$$

and by definition

$$\epsilon_{\rho\eta} = \frac{\partial u_\rho}{\partial \eta} + \frac{\partial u_\eta}{\partial \rho} \quad . \tag{A-29}$$

Combining the last three equations, there results

$$\frac{\partial u_\rho}{\partial \eta} = \frac{2[1+\nu]}{\rho} \frac{\partial \psi}{\partial \eta} \tag{A-30}$$

or, on expressing $\frac{\partial u_\rho}{\partial \eta}$ in terms of the stress functions,

$$2[1+\nu] \frac{\partial \psi}{\partial \eta} = [1+\nu]\left[\frac{\partial \psi}{\partial \eta} + [1-\nu] \frac{\partial \phi}{\partial \eta}\right] - \nu\rho^2 Z \quad , \tag{A-31}$$

which can be written in finite difference form as

$$\psi_1 - \psi_3 - [1-\nu][\phi_1 - \phi_3] + \frac{2\nu h\rho^2}{1+\nu} Z = 0 \quad . \tag{A-32}$$

Elimination of ψ_3 and ϕ_3, at the fictitious node from Eq. A-32 using Eqs. A-3 and A-4 gives

$$\phi_1 - 2\phi_0 - 2\psi_1 + [1-2\nu]\left[\phi_1 + \phi_2 + \phi_4 - 4\phi_0 + \frac{h}{2\rho}[\phi_4 - \phi_2]\right]$$

$$- \frac{2\rho^2}{1+\nu}[\delta + \nu h Z] = 0 \quad . \tag{A-33}$$

Thus Eqs. A-27 and A-33 are the most useful forms for the determination of stress function on this boundary for this end condition.

(b) For a free end but with unsymmetrical loading, the boundary conditions are the same as for the end $\eta = H$ and may be reduced to the form

$$\psi = \left[\frac{\rho^2 - \alpha^2}{2}\right][\Pi_1 + \eta Z] \tag{A-34}$$

or, since $\eta = 0$,

$$\psi = \left[\frac{\rho^2 - \alpha^2}{2}\right] \Pi_1 \tag{A-35}$$

and

$$\frac{h}{2\rho}[\phi_4 - \phi_2] + \phi_2 + \phi_4 - 2\phi_0 + 2\psi_1 - 2\psi_0 = 0 \quad . \tag{A-36}$$

Eqs. A-35 and A-36 suffice for the boundary equations on this boundary for this end condition.

Corner Nodes

At the corner nodes special consideration must be made since boundary conditions for both boundaries must apply. Since this consists mainly of algebraic manipulation of equations previously derived, details will be omitted and only the essential steps will be mentioned.

Corner $\eta = H$, $\rho = \alpha$

Boundary conditions Eqs. 22, 23, and 24 can be satisfied by direct calculation of ψ using Eqs. A-10 and A-13. Eq. 21 will be satisfied by applying Eq. A-11 directly.

Corner $\rho = 1$, $\eta = H$

The boundary conditions at this node are

$$u_\rho = 0 \qquad \epsilon_\theta = 0$$

or, equivalently, (A-37)

$$u_\eta = 0 \qquad \epsilon_\eta = 0$$

and

$$\sigma_\eta = -\Pi_3$$

$$\sigma_{\rho\eta} = 0 \ . \tag{A-38}$$

Applying stress-strain relations of the form

$$\epsilon_\theta - \delta = \sigma_\theta - \nu\left[\sigma_\eta + \sigma_\rho\right]^* , \tag{A-39}$$

the state of stress and strain at this corner is completely determined to be

$$\sigma_\eta = -\Pi_3$$

$$\sigma_\theta = -\Pi_3$$

$$\sigma_\rho = \frac{\delta - [1-\nu]\Pi_3}{\nu} \tag{A-40}$$

$$\epsilon_\rho = \frac{[1+\nu]\left\{\delta - [1-2\nu]\Pi_3\right\}}{\nu}$$

and

$$\sigma_{\rho\eta} = \epsilon_\eta = \epsilon_\theta = \epsilon_{\rho\eta} = 0 \ .$$

Unfortunately, it is not possible to satisfy all of the relevant finite difference equations at this node in a normal manner. Difficulty with convergence of analytical solutions in similar instances has been recorded (see, for instance, Pickett [7]). The practical reason for this difficulty is that this is a region of rapidly varying stresses[1]. Finite difference approximations are valid only when functions vary slowly with respect to the interval length. It would be expected that the finite difference solution

---

[1]The possibility that a singularity exists at this point has postulated by many but, to the writer's knowledge, has not been demonstrated.

would converge to the correct solution as the mesh size approaches zero. However, for any finite grid size, the stresses in the vicinity of this corner cannot be accurately determined. The effect of this error should be negligible several nodes from this corner. This was confirmed by obtaining the solution for one particular problem with several mesh sizes.

For the actual determination of ϕ and ψ at this corner, Eqs. A-13 and A-16 are used. This allows the determination of ϕ_0 and ψ_0 directly. The fictitious nodes (to be used for calculation of stresses, strains and displacements as explained below) are determined from the other two boundary conditions and one of the two field equations. The other field equation is, in general, unsatisfied.

Corner $\eta = 0$, $\rho = 1$

1. Symmetrical Problems

For the symmetry conditions, Eqs. A-16 and A-21 are used with the substitution

$$\psi_3 = \psi_1 \quad . \tag{A-41}$$

2. Unsymmetrical Problems

(a) For the bonded end at this node, the conditions

$$u_\eta = u_\rho = \epsilon_\theta = \epsilon_\rho = \epsilon_\eta = \epsilon_{\rho r} = 0 \tag{A-42}$$

apply. These conditions are satisfied by using Eq. A-16 and A-21 with $\psi_3 = \psi_1$ in Eq. A-21.

(b) For a free end with unsymmetrical loading, this node is treated the same as the point $\rho = 1$, $\eta = H$.

Corner $\eta = 0$, $\rho = \alpha$

1. Symmetrical Problems

For the symmetry condition Eqs. A-10 and A-11 are used unchanged.

2. Unsymmetrical Problems

(a) For the bonded end Eq. A-10 and Eq. A-27 are used with the same type of error as noted for the node $\rho = 1$, $\eta = H$.

(b) Eqs. A-10 and A-11 also apply for unsymmetrical loading.

Method of Solution

If the finite difference equations are written at each node of an M x N mesh, the stress functions at each node may be found by simultaneous solution of the resulting set of $(M+1)(N+1)$ equations. In practice this may involve sets containing on the order of 1000 equations. A number of

methods may be chosen to achieve a solution, but the common method used in elasticity problems is an iterative procedure, popularized by Southwell [13], known as the relaxation method.

The Seidel iteration process using systematic over-relaxation was used [14] to obtain the values of the stress functions. New values of a stress function ϕ_i at nodal point i for the k+1 iteration are found from

$$\phi_i^{(k+1)} = \phi_i^{(k)} + \beta R_i \quad , \tag{A-43}$$

where $\phi_i^{(k)}$ is the stress function value of the i node for the kth iteration, β is the over-relaxation factor, and R_i is the residual of the finite difference equation. The speed of convergence is a strong function of β which must be in the range $1 \leq \beta < 2$. Values of 1.5 to 1.7 for β were found to be near optimum, but the optimum value varies with the input parameters of each problem. Starting with an estimate of zero for each stress function value for a 4x32 mesh with $\alpha = 1/3$, some 200 to 300 iterations on each stress function were required with $\beta = 1.7$ to obtain the solution for the stress functions with the residuals reduced to 0.000001 of the largest stress function value.

Because the stress function equations are coupled at the boundaries and the interior, instability problems can arise under certain conditions. For example, the following process was found to work satisfactorily for symmetrical loading:

1. Initially assume all stress function values to be zero.

2. Make one iteration correcting the values of ϕ on the boundaries $\rho = \alpha$ and $\eta = H$ with $\beta = 1$. Corner nodes may be treated as part of either of the intersecting boundaries.

3. Relax the interior values and boundary values at $\eta = 0$ of ϕ using $\beta = 1.7$, iterating until Eqs. A-3 and A-24 are satisfied, i.e., the absolute value of the largest residual is less than some specified value.

4. Make one iteration correcting the values of ψ on the boundary $\rho = 1$. ψ is known exactly on the boundaries $\rho = \alpha$ and $\eta = H$.

5. Relax ψ at $\eta = 0$ and in the interior until Eqs. A-4 and A-25 are satisfied to some specified degree as in step (3) above.

6. Calculate ϕ on boundary $\rho = 1$ by Eq. A-16 and return to step(2).

The problem was considered relaxed to a specified degree when the absolute value of all residuals was less than a specified number d, and the sum of all residuals was less than a specified number D, i.e.,

$$|R_i| < d \tag{A-44}$$

and

$$\sum R_i < D \quad . \tag{A-45}$$

The useful value of D is related to both d and the number of node points. D was estimated by the equation

$$D \approx \left(\frac{MN}{4}\right) d \ ,$$

where M is the number of increments in the axial direction and N is the number of increments in the radial direction.

The relaxation process was found to go faster if the value of d was initially chosen large (say 0.001 of the largest stress function value) until the problem was relaxed completely; then d was reduced by an order of magnitude, and the problem further relaxed to completion with respect to the new value of d; then the process was repeated until the desired degree of relaxation was achieved.

Calculation of Stresses, Strains and Displacements From the Stress Functions

The stresses, strains, and displacements are calculated from the stress functions by writing the finite difference forms of Eqs. 9 through 18. Since these equations involve no derivatives higher than the first this process is, in general, straightforward and results in high accuracy. In practice, two factors complicate the calculation of these quantities. First, the derivatives normal to a boundary, when written in terms of the central finite difference formulae, involve fictitious nodes; or, when written in terms of forward or backward differences, involve nodes lying only on one side of the boundary. The latter method was found to introduce unduly large errors, and recourse was made to the calculation of the fictitious nodes needed to express the normal boundary gradients in terms of central difference formulae. Secondly, the axial displacement, Eq. 10, involves integrals in the axial or η direction of derivatives with respect to the radius ρ. It was found that the application of Simpson's rule for this integration was satisfactory at even numbered nodes, although it was quite complicated to program for a computer. The accuracy of the axial displacement at odd nodes, where trapezoidal integration was necessary for one increment, was not always satisfactory.

Computation Facilities

This problem has been programmed for the IBM 7090 computer at the NASA Marshall Space Flight Center. Typical machine times for problems of this type vary from about one minute for problems with 50 nodes to 20 minutes for 500 nodes. These times are also greatly dependent on Poisson's ratio, ν, and the radius ratio, α.

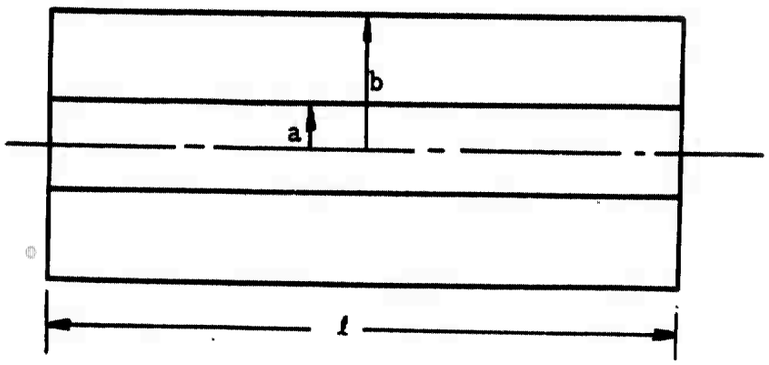

Fig. 1 Grain configuration

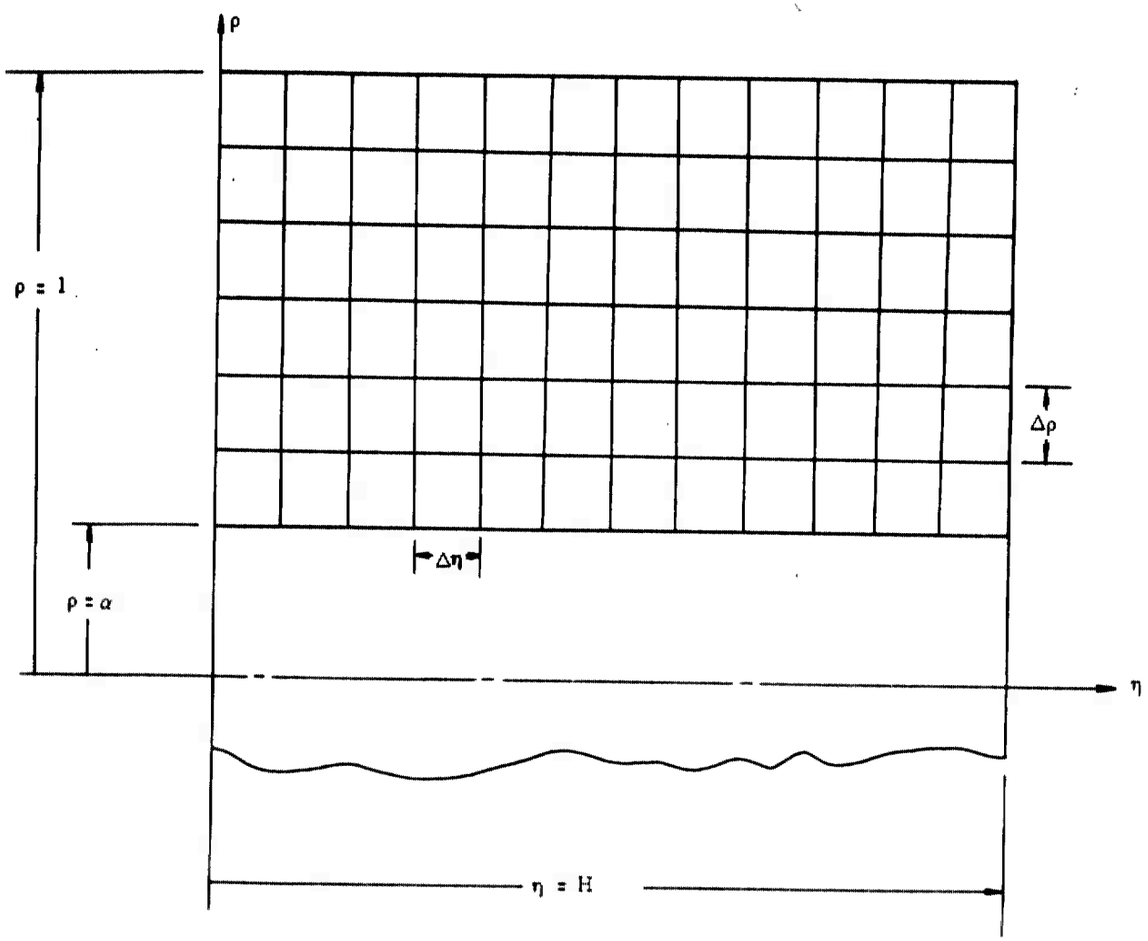

Fig. 2 Coordinate system

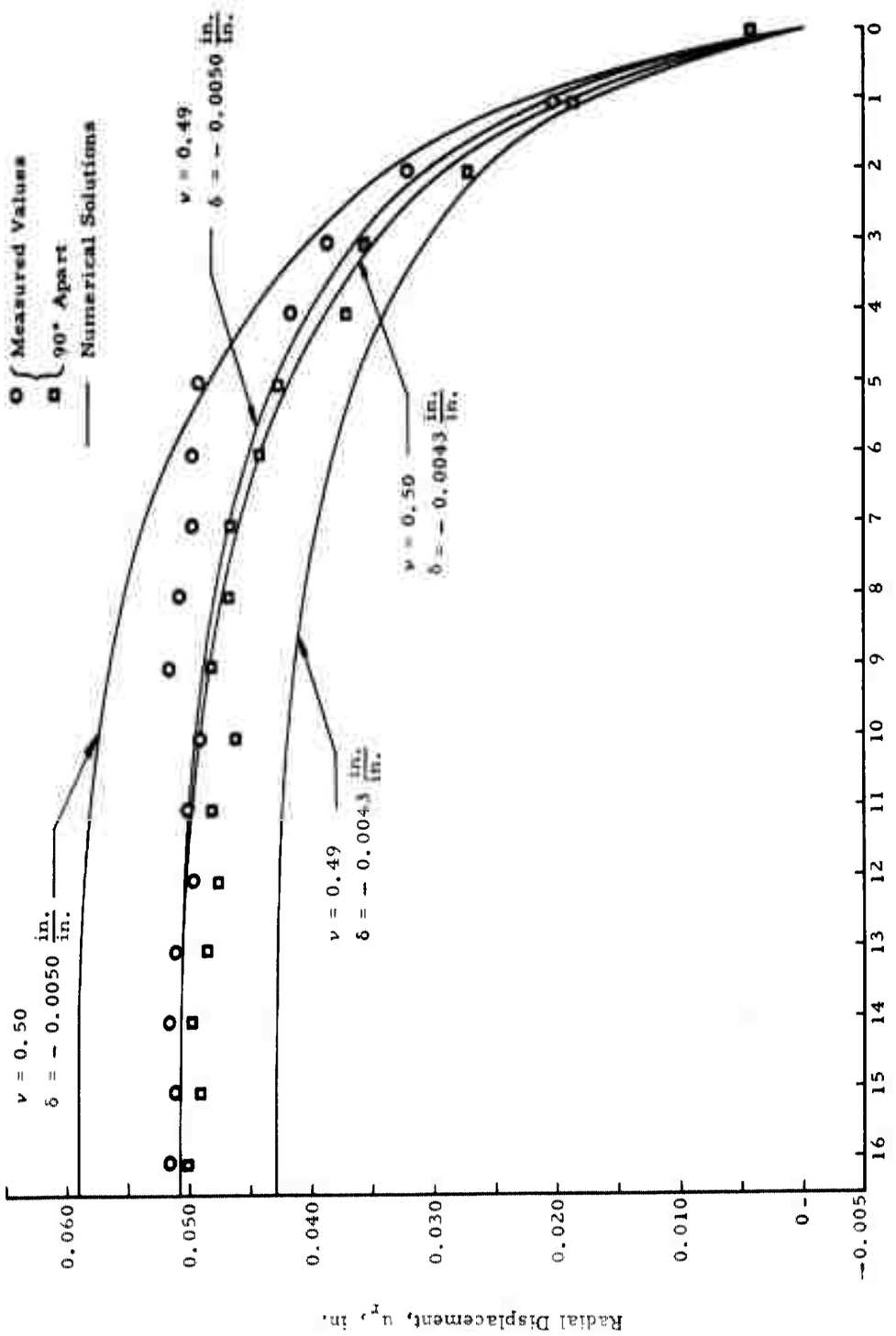

Fig. 3 Radial displacement of inner propellant surface, 6C2-33 STM with 112$_{bw}$ propellant.

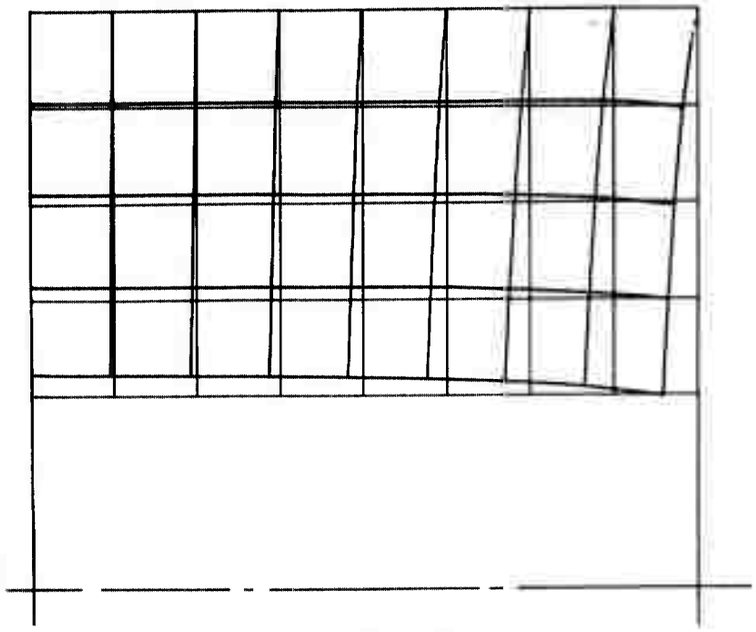

$\frac{u}{\delta b} = 60 \frac{\text{(illustrated displacement)}}{\text{(illustrated outer radius)}}$

Fig. 4 Deformation of right half of propellant grain, bonded at outer periphery, both ends free, under uniform shrinkage $\kappa=3$, $\lambda=1.33$, $\nu=0.5$

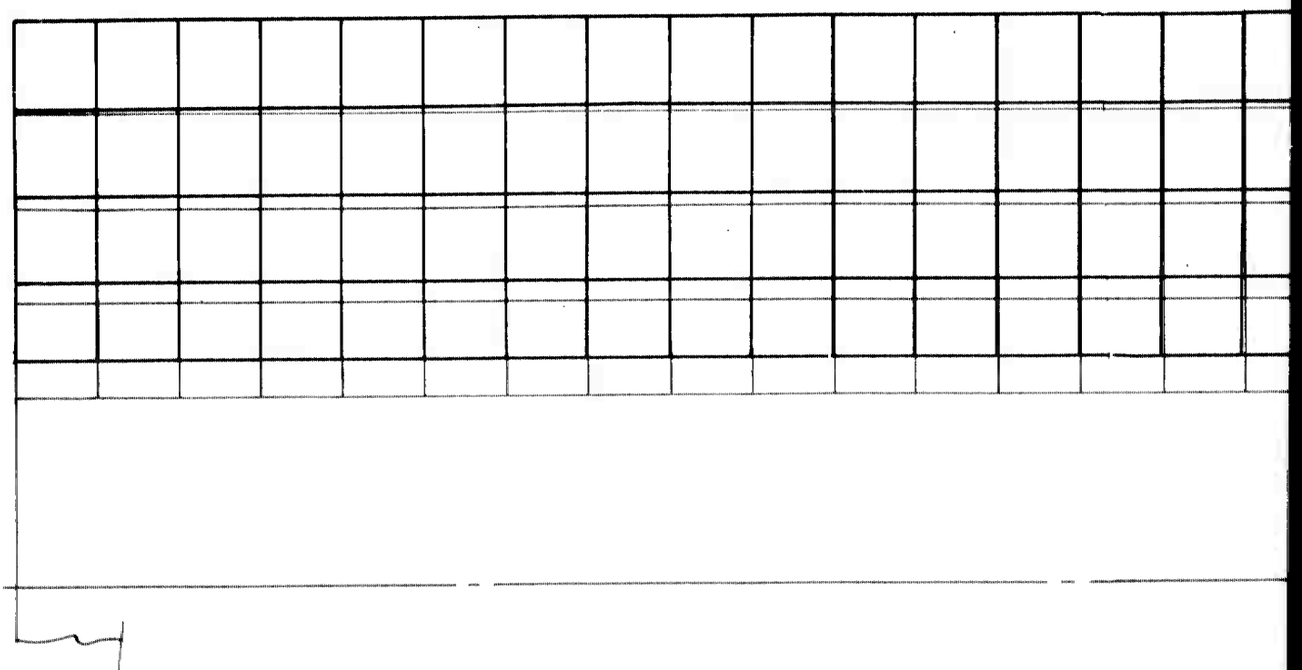

$\frac{u}{\delta b} = 60 \frac{\text{(illustrated}}{\text{(illustrated o}}$

Fig. 5 Deformation of right half of propellant grain, bonded at outer periphery, both ends f
iform shrinkage $\kappa=3$, $\lambda=5.33$, $\nu=0.5$

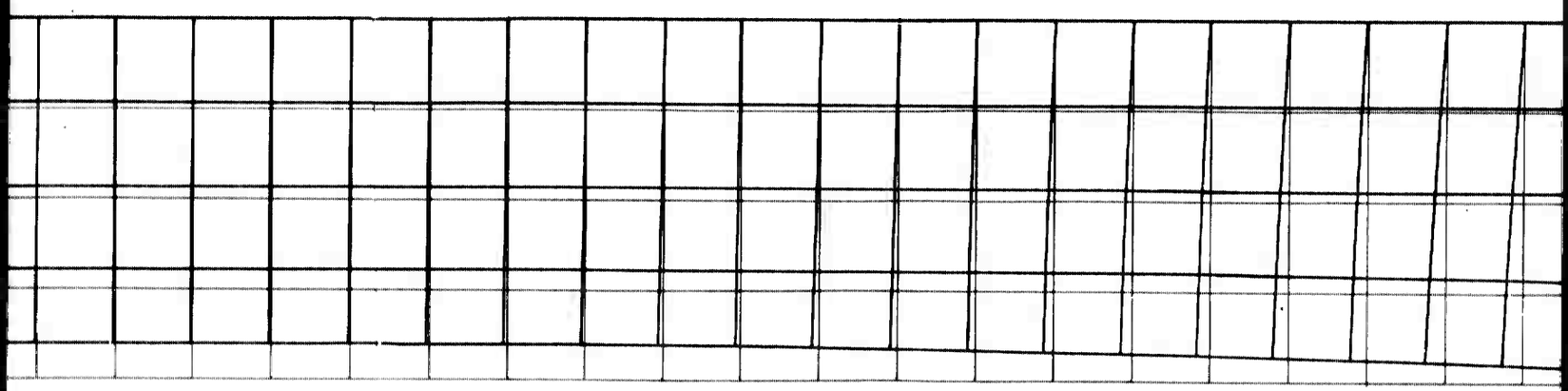

$$\frac{u}{60} = 60 \frac{\text{(illustrated deflection)}}{\text{(illustrated outer radius)}}$$

, bonded at outer periphery, both ends free, under un-

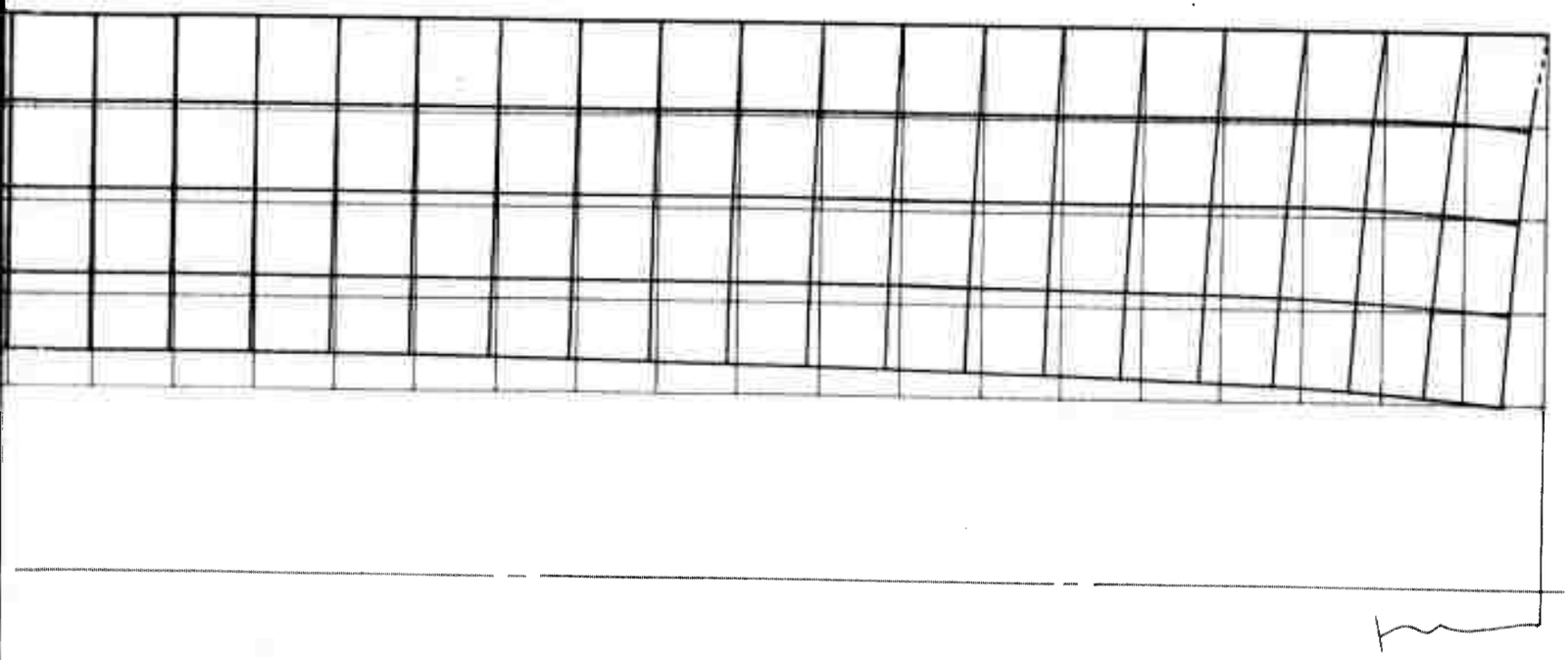

$\frac{u}{b} = 60 \frac{\text{(illustrated deflection)}}{\text{(illustrated outer radius)}}$

ry, both ends free, under un-

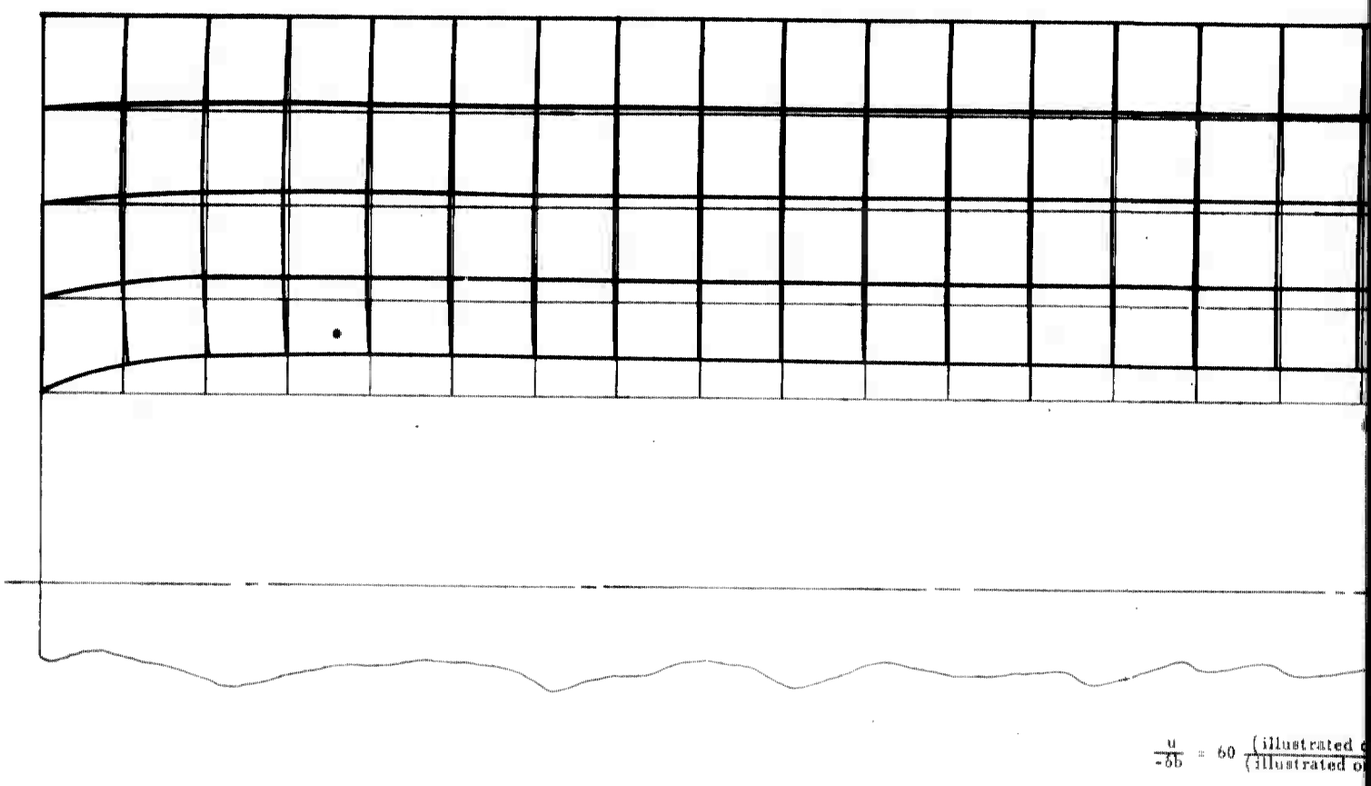

$\frac{u}{-6b} = 60 \frac{(\text{illustrated d}}{(\text{illustrated o}}$

Fig. 6 Deformation of propellant grain, bonded at outer periphery and left end, under uniform sh
$\kappa=3$, $\lambda=2.67$, $\nu=0.5$

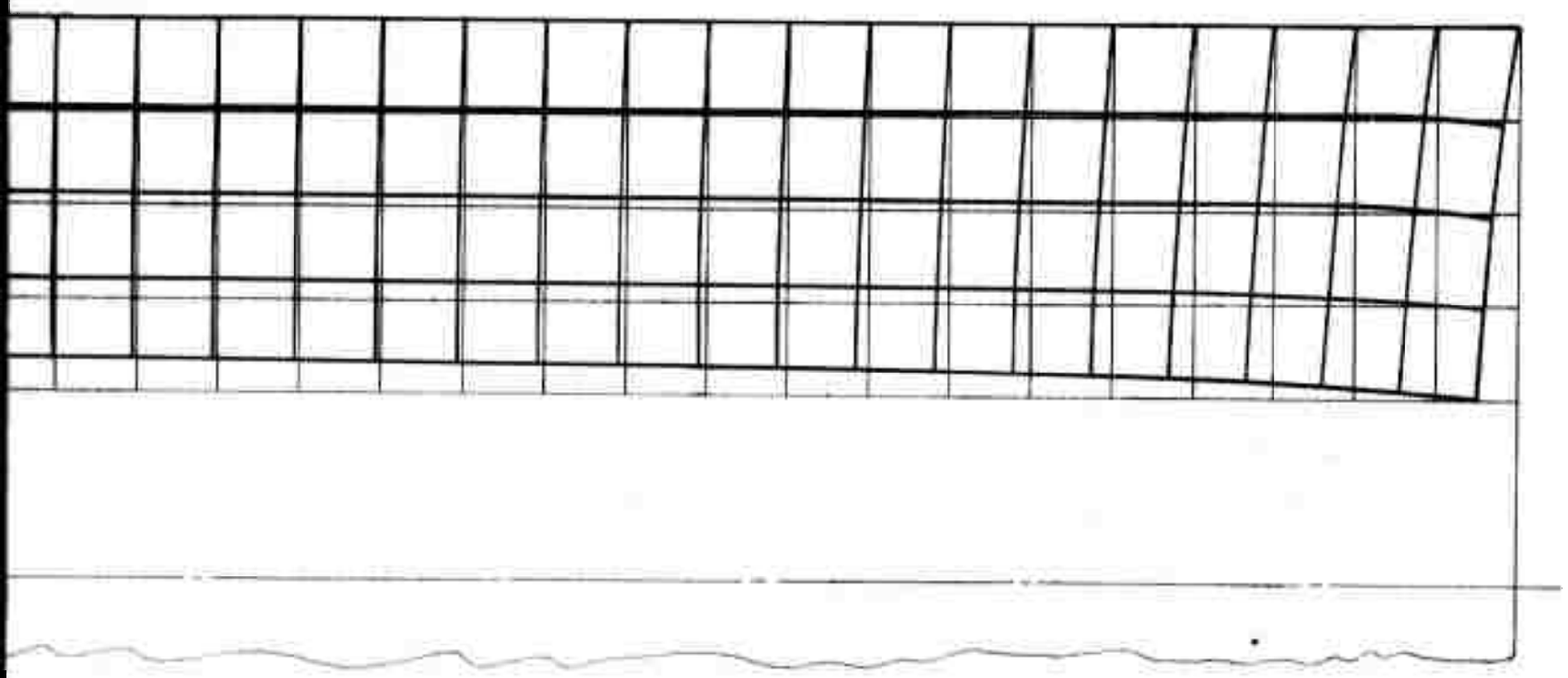

$\frac{u}{b} = 60 \frac{\text{(illustrated deflection)}}{\text{(illustrated outer radius)}}$

under uniform shrinkage

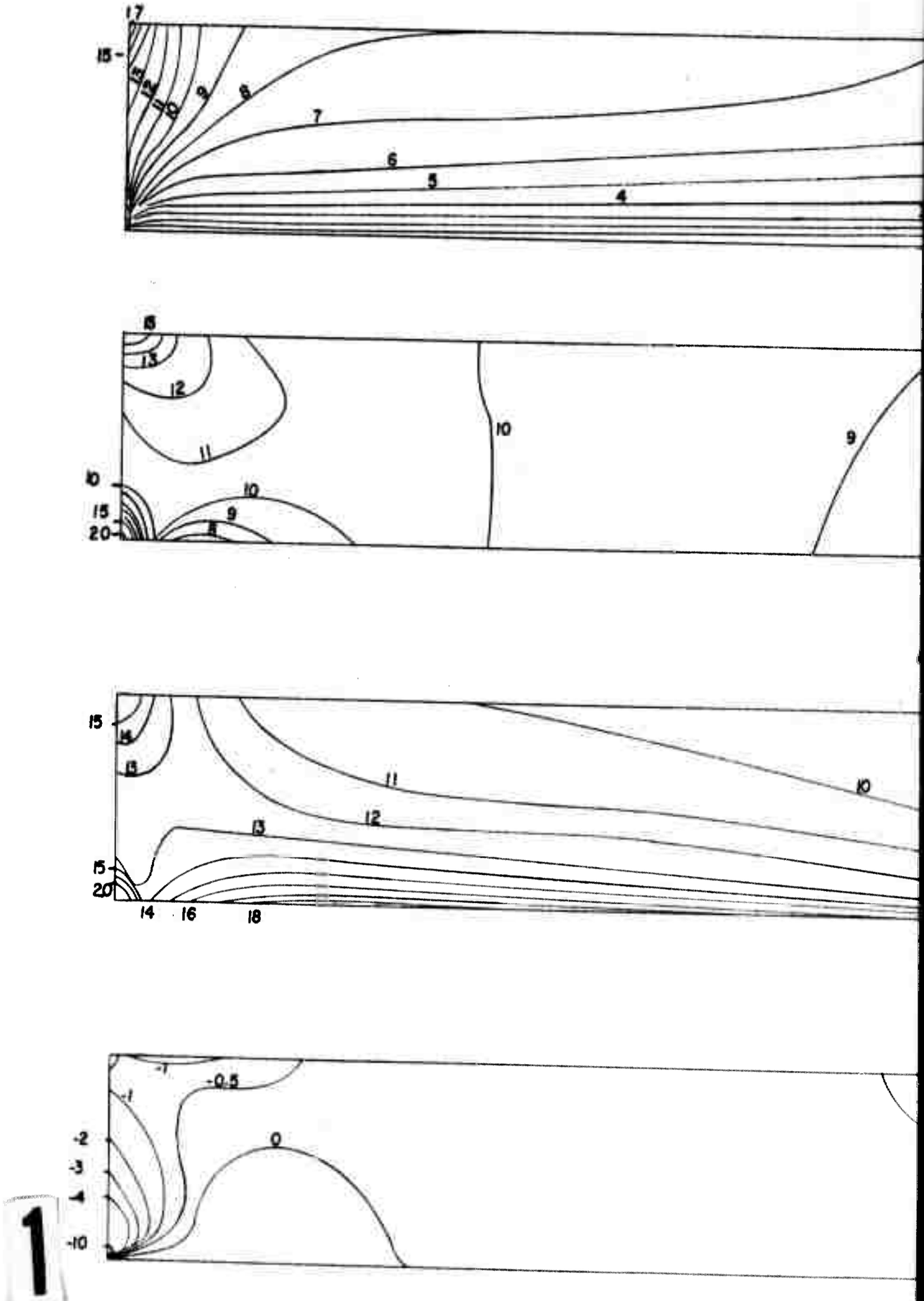

Fig. 7 Dimensionless stress contours $\frac{\sigma}{-\delta E}$, in propellant grain, bonded at outer periphery uniform shrinkage $\kappa=3$, $\lambda=2.67$, $\nu=0.5$

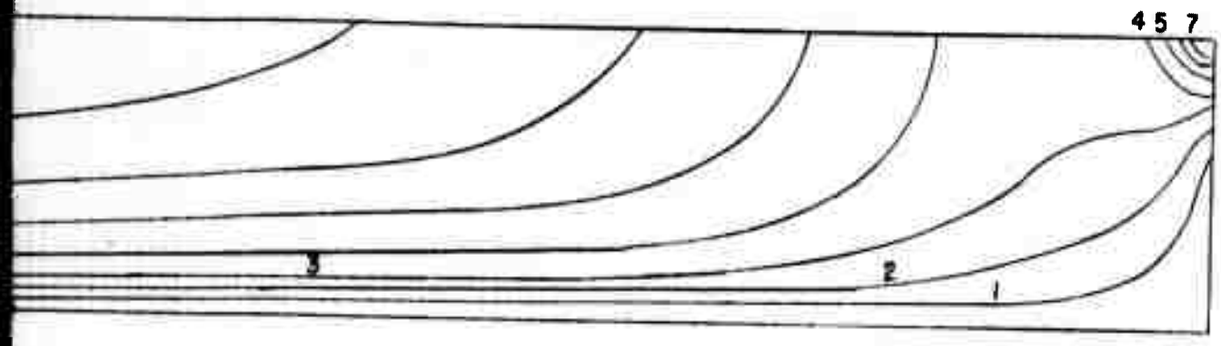

Dimensionless radial stress $\frac{\sigma_r}{-\delta E}$

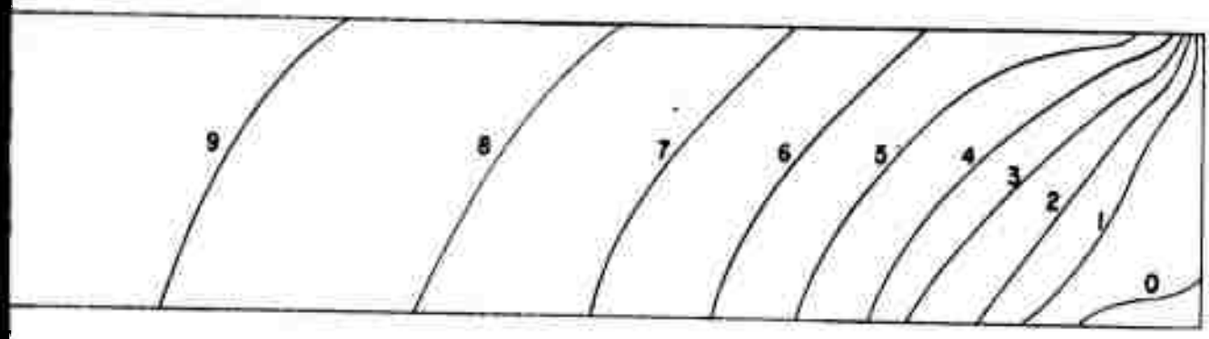

Dimensionless axial stress $\frac{\sigma_z}{-\delta E}$

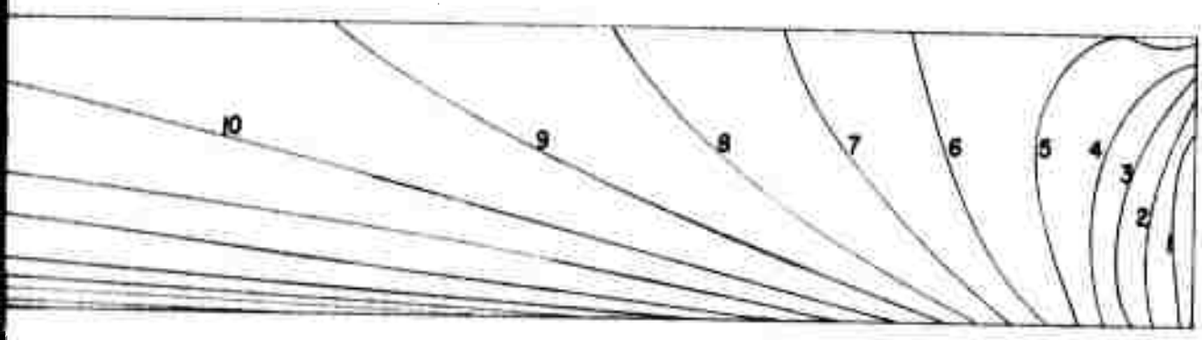

Dimensionless circumferential stress $\frac{\sigma_\theta}{-\delta E}$

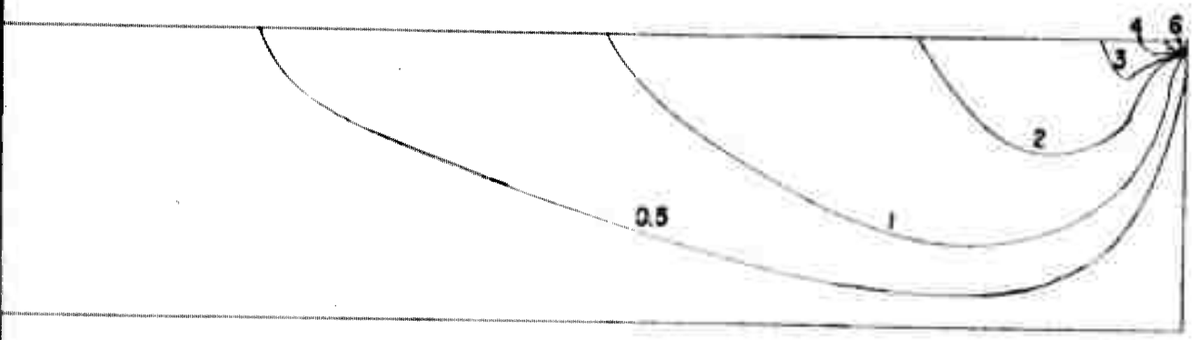

Dimensionless shear stress $\frac{\sigma_{rz}}{-\delta E}$

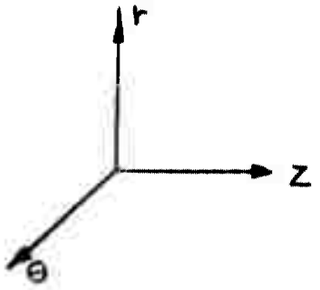

ded at outer periphery and left end, under

2

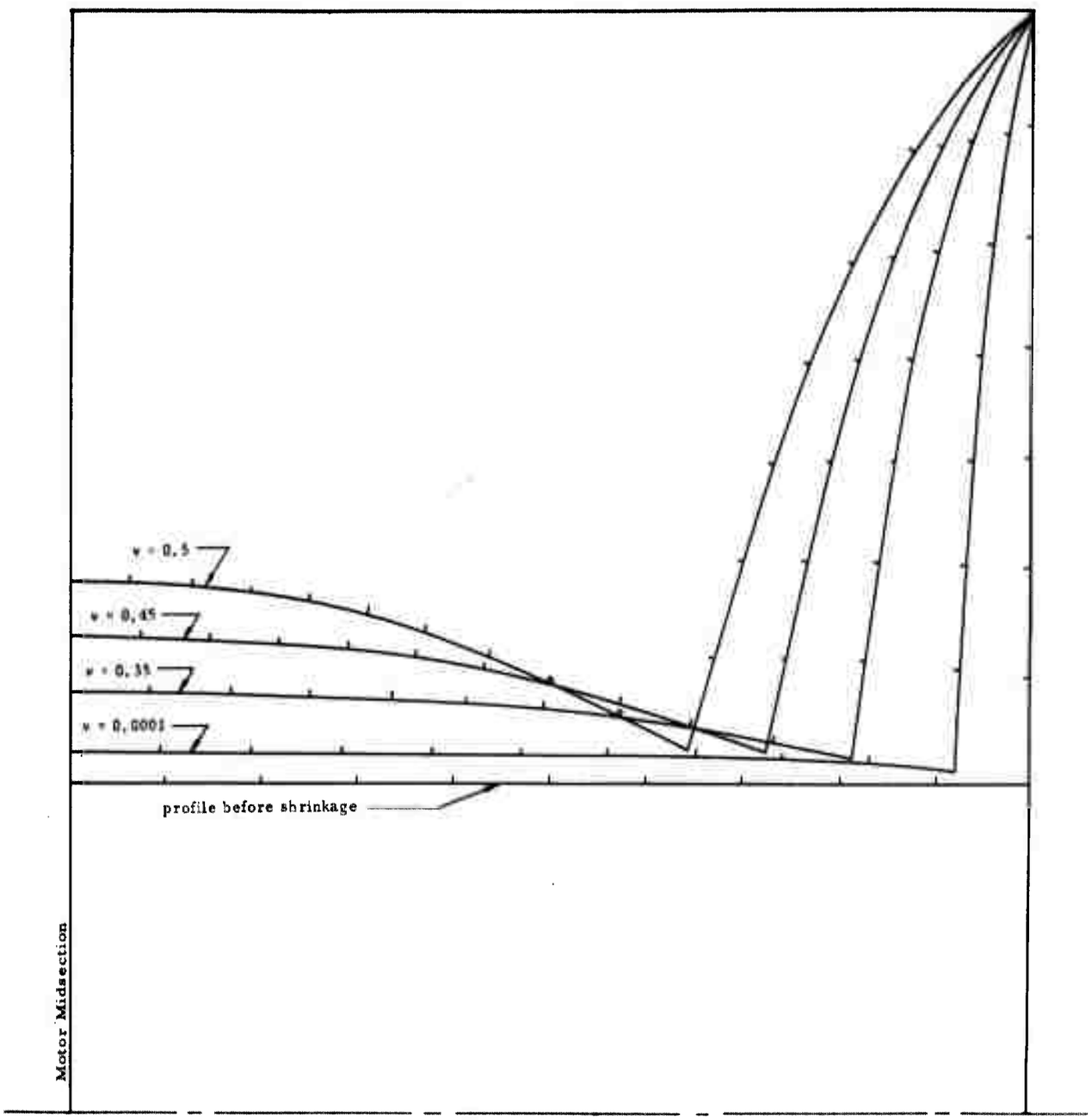

$$\frac{u}{-\delta b} = 10\,\frac{\text{(illustrated displacement)}}{\text{(illustrated outer radius)}}$$

Fig. 8 Effect of Poisson's ratio, ν, on profile, propellant bonded at outer periphery, both ends free, under uniform shrinkage
$\kappa = 3.33$, $\lambda = 1$

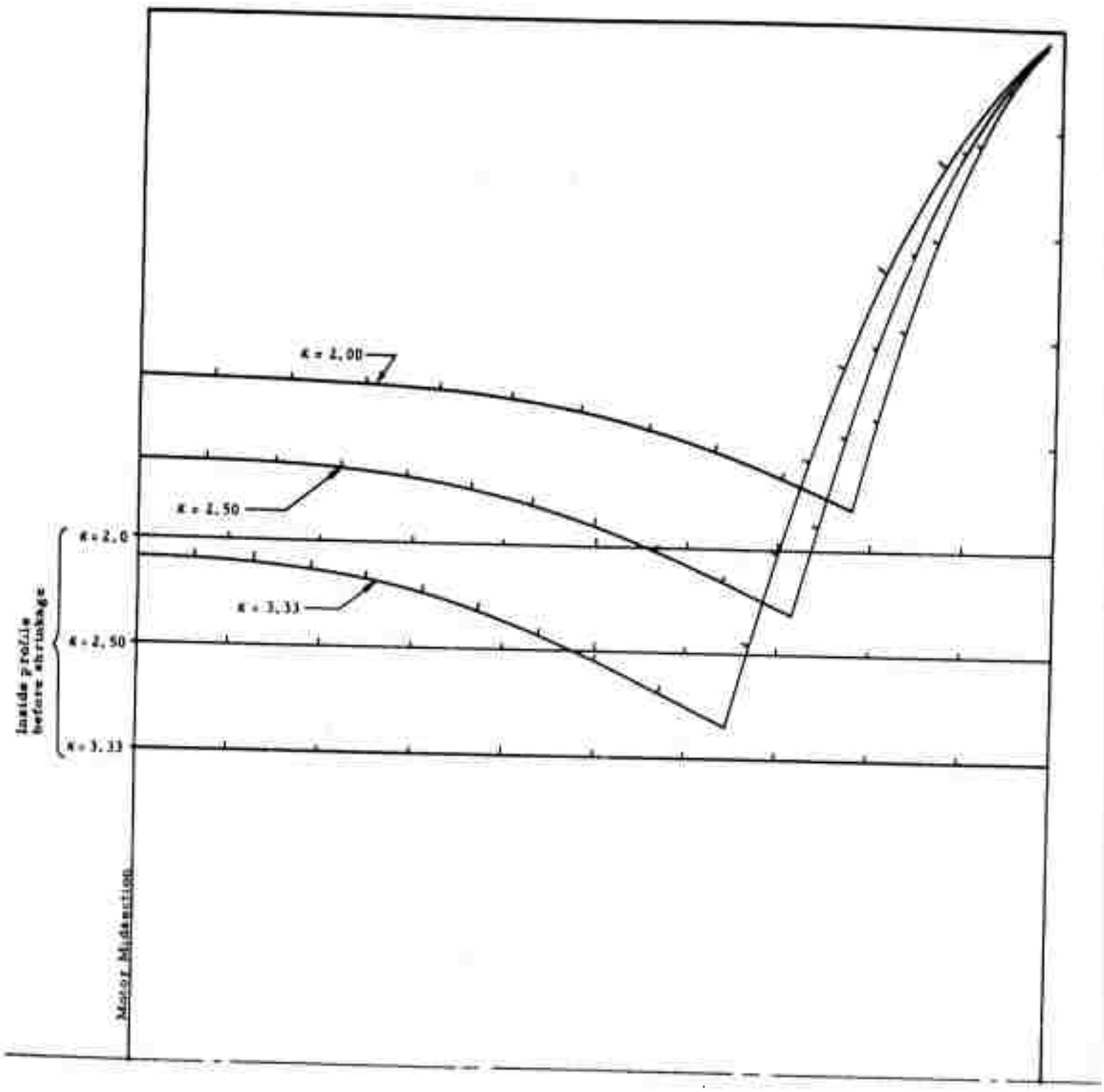

$$\frac{u}{-\delta b} = 10 \frac{\text{(illustrated displacement)}}{\text{(illustrated outer radius)}}$$

Fig. 9 Effect of radius ratio, κ, on profile, propellant bonded at outer periphery, both ends free, under uniform shrinkage $\lambda=1$, $\nu=0.5$

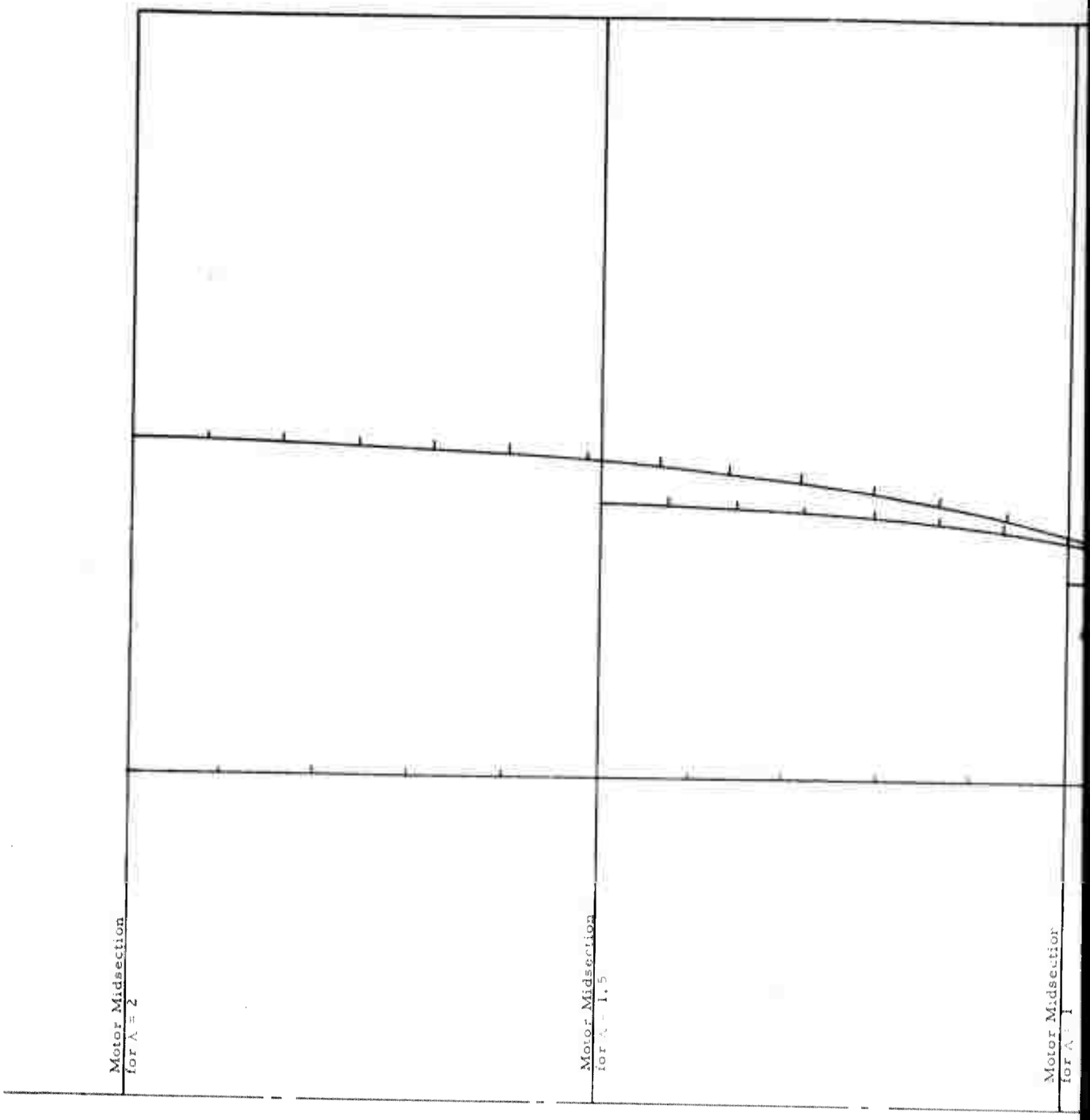

$\frac{u}{-\delta b} = 10$ (illustrated
(illustrated

Fig 10 Effect of length-to-diameter ratio, λ, on profile, propellant bonded at outer periphe
under uniform shrinkage $\kappa = 3.33, \nu = 0.5$

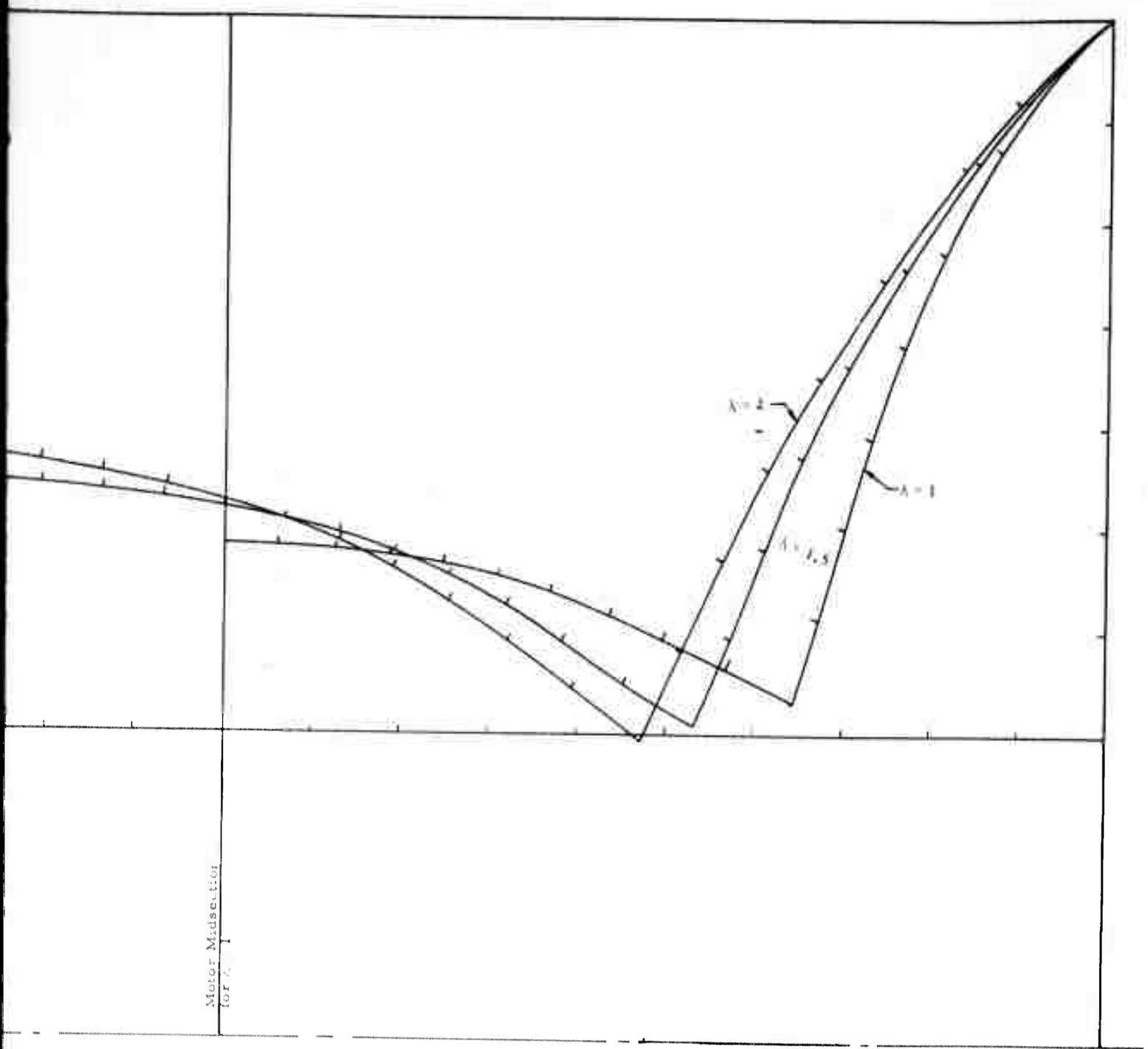

$$\frac{u}{-\delta b} = 10 \frac{\text{(illustrated displacement)}}{\text{(illustrated outer radius)}}$$

bonded at outer periphery, both ends free,

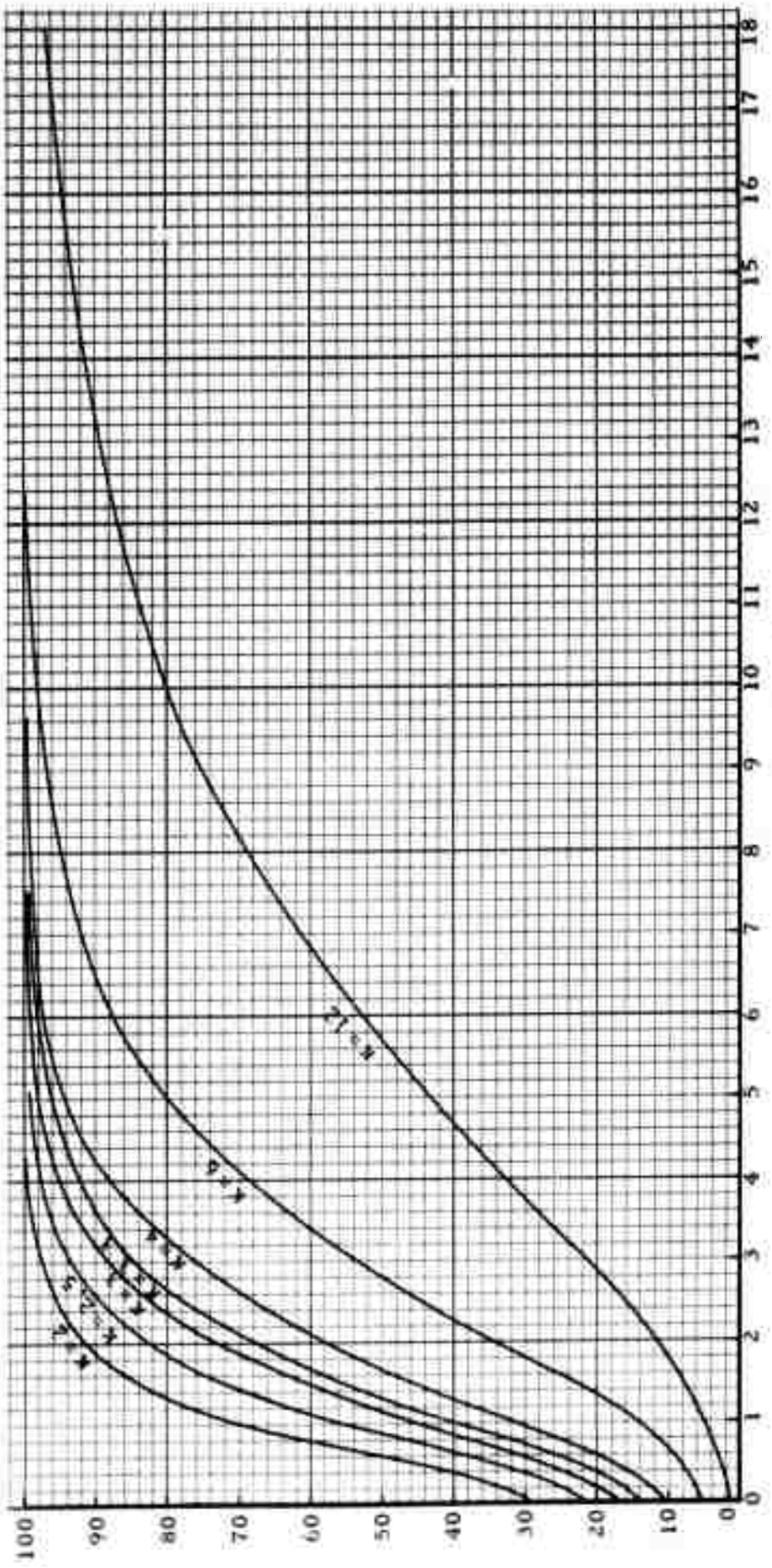

Fig. 11 Radial displacement at inner radius in middle of cylinder of finite length as percentage of radial displacement in equivalent cylinder of infinite length, propellant bonded at outer periphery, both ends free, under uniform shrinkage $\nu=0.50$

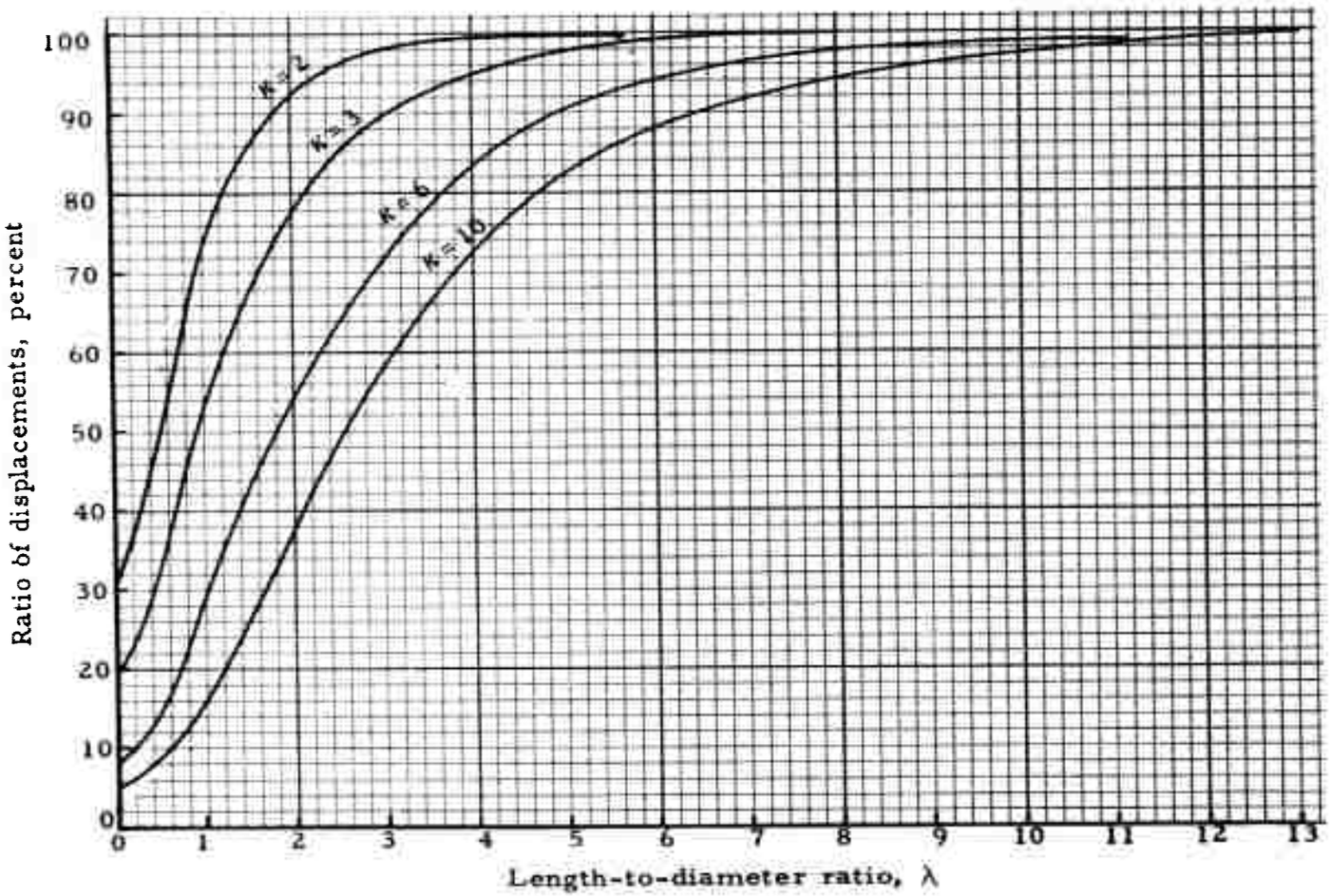

Fig. 12 Radial displacement at inner radius in middle of cylinder of finite length as percentage of radial displacement in equivalent cylinder of infinite length, propellant bonded at outer periphery, both ends free, under uniform shrinkage $\nu = 0.49$

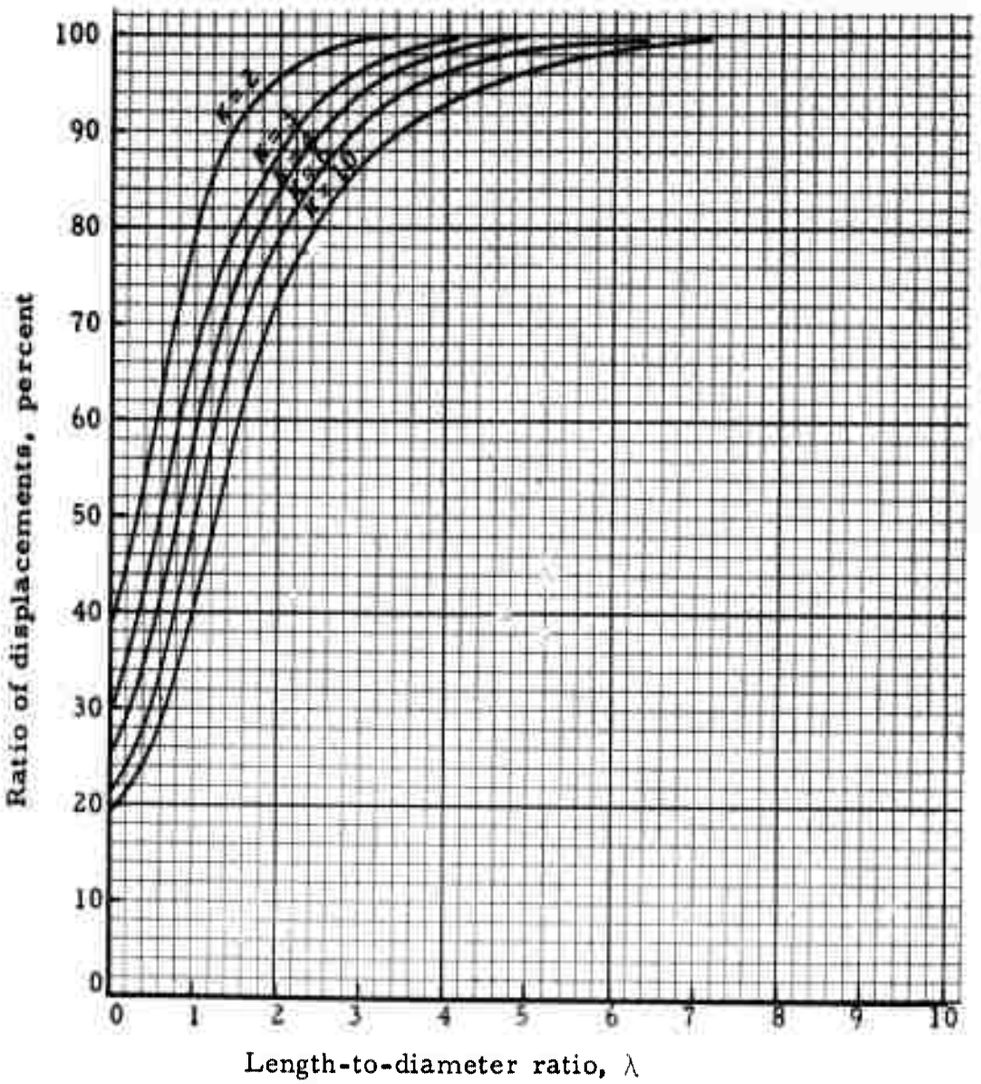

Fig. 13 Radial displacement at inner radius in middle of cylinder of finite length as percentage of radial displacement in equivalent cylinder of infinite length, propellant bonded at outer periphery, both ends free, under uniform shrinkage $\nu = 0.45$

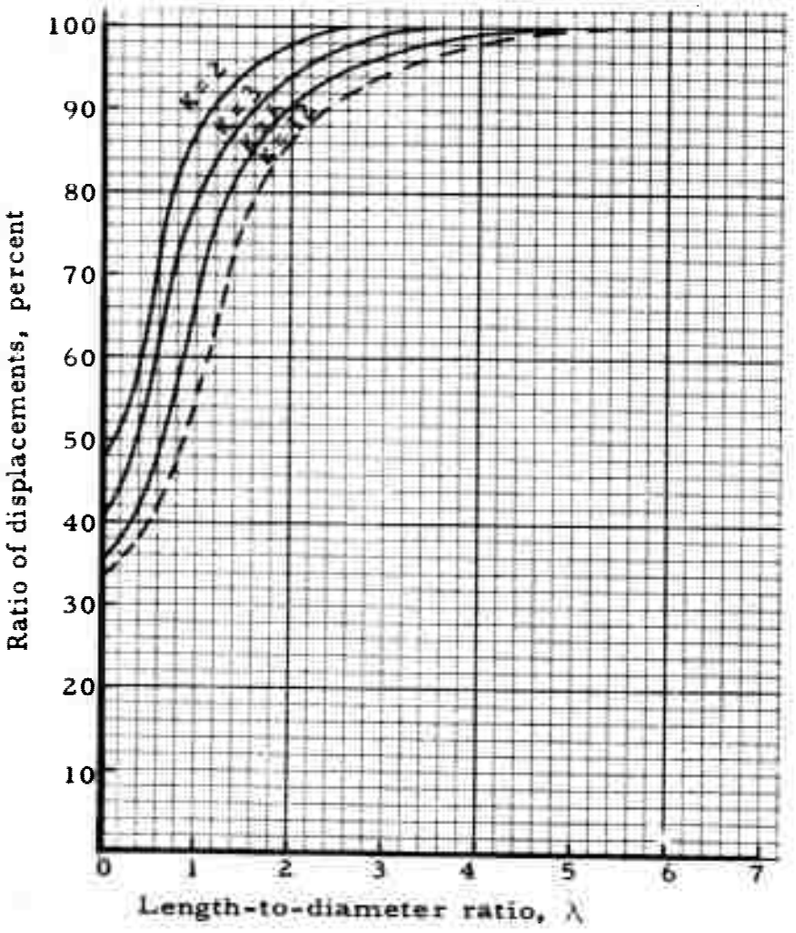

Fig. 14 Radial displacement at inner radius in middle of cylinder of finite length as percentage of radial displacement in equivalent cylinder of infinite length, propellant bonded at outer periphery, both ends free, under uniform shrinkage $\nu = 0.40$

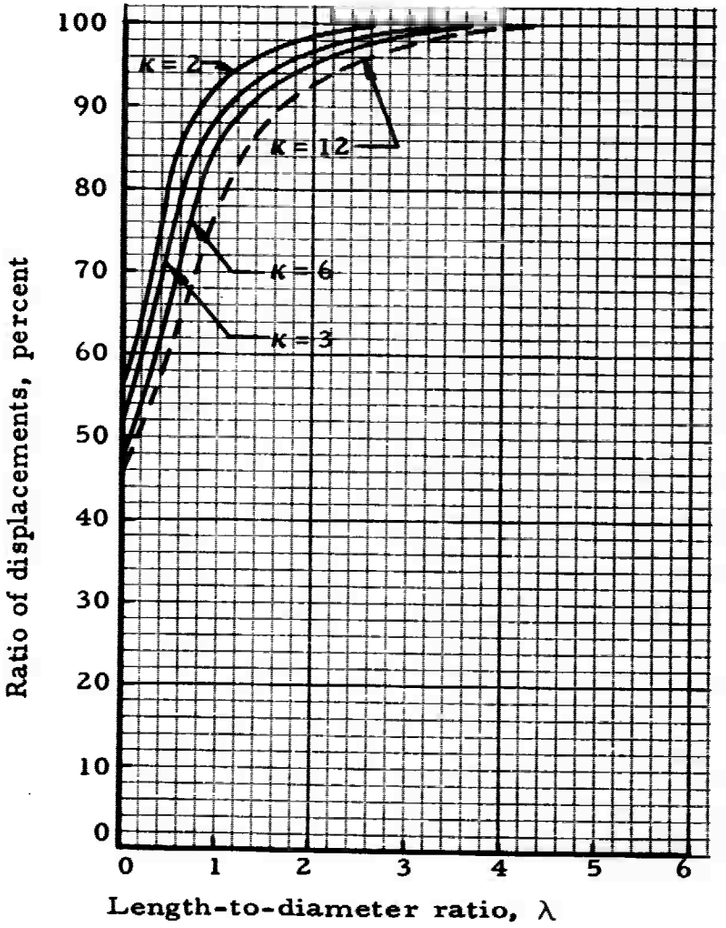

Fig. 15 Radial displacement at inner radius in middle of cylinder of finite length as percentage of radial displacement in equivalent cylinder of infinite length, propellant bonded at outer periphery, both ends free, under uniform shrinkage $\nu = 0.35$

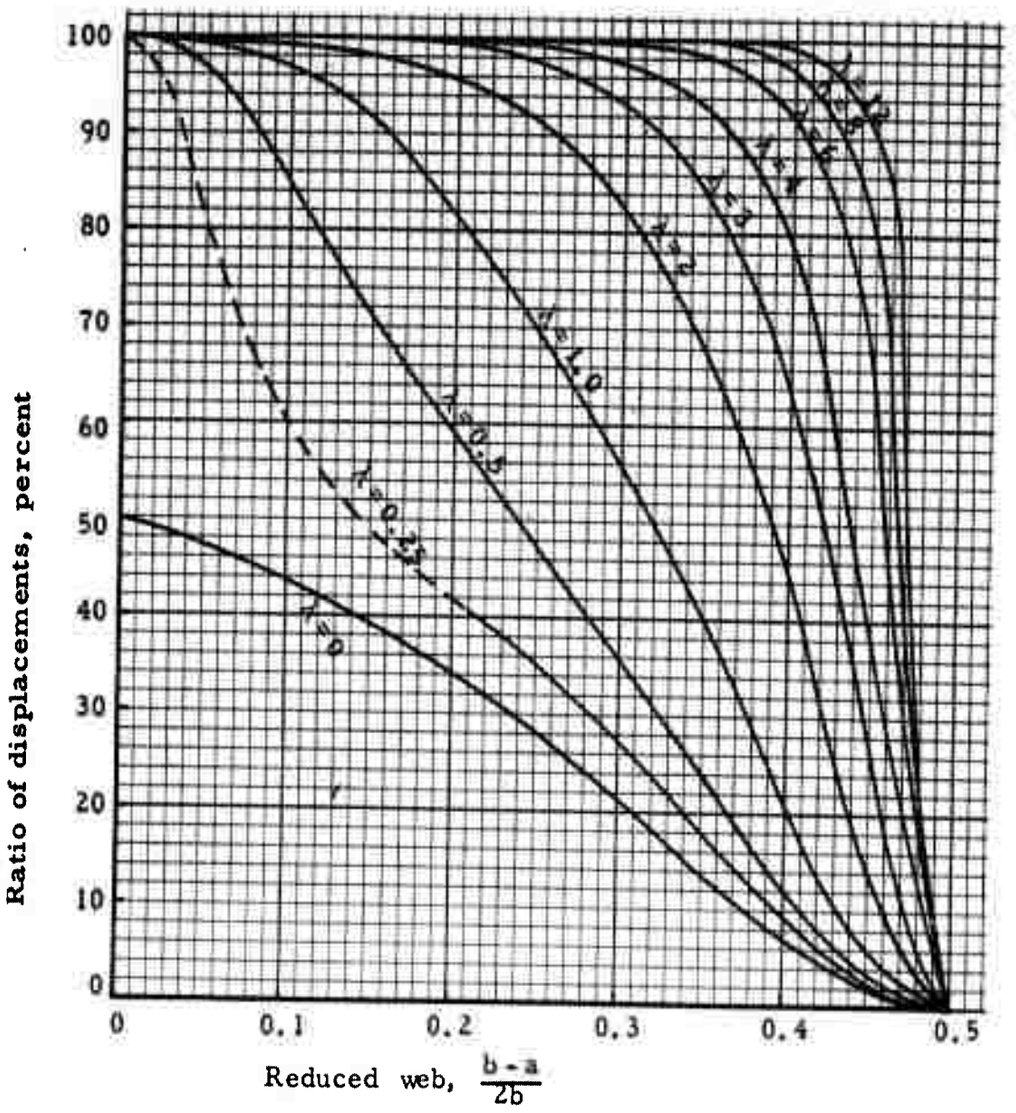

Fig. 16 Radial displacement at inner radius in middle of cylinder of finite length as percentage of radial displacement in equivalent cylinder of infinite length, propellant bonded at outer periphery, both ends free, under uniform shrinkage $\nu = 0.50$

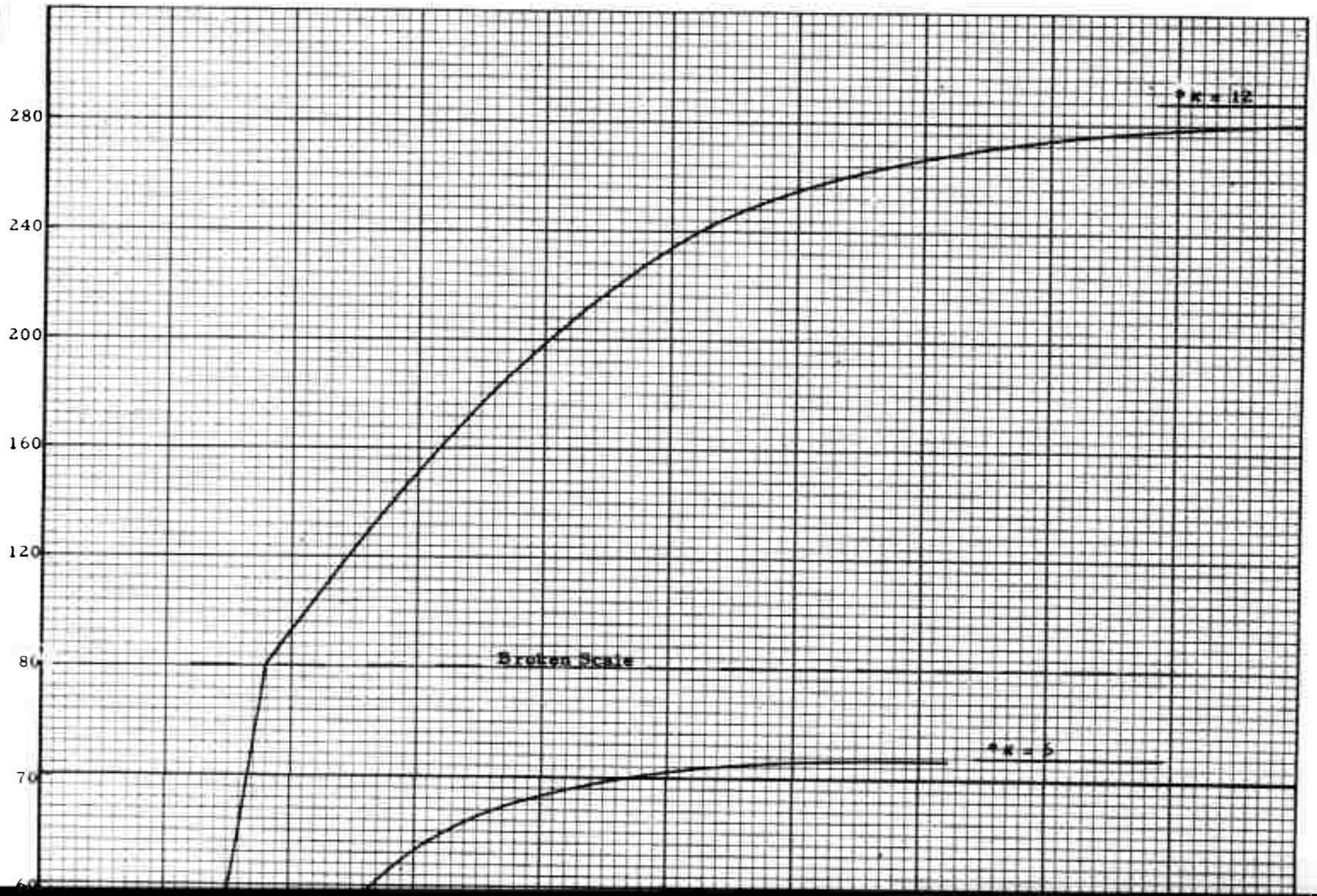
280
240
200
160
120
80
70
60
$\sigma_\theta / -\delta E$
$\phi_K = 12$
Broken Scale
$\phi_K = 5$

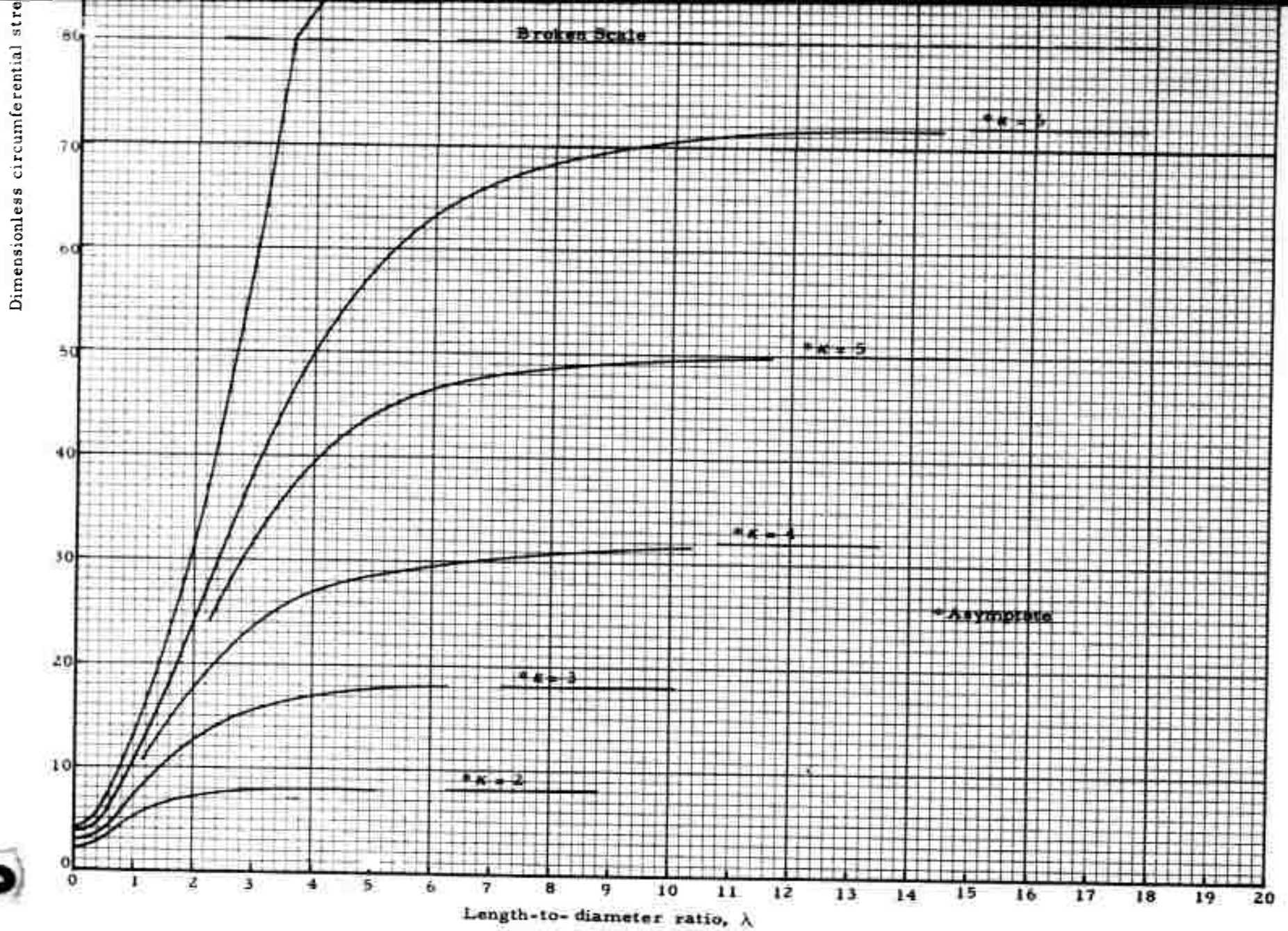

Fig. 17 Dimensionless circumferential stress at inner radius in middle of cylinder, propellant bonded at outer periphery, both ends free, under uniform shrinkage $\nu = 0.5$

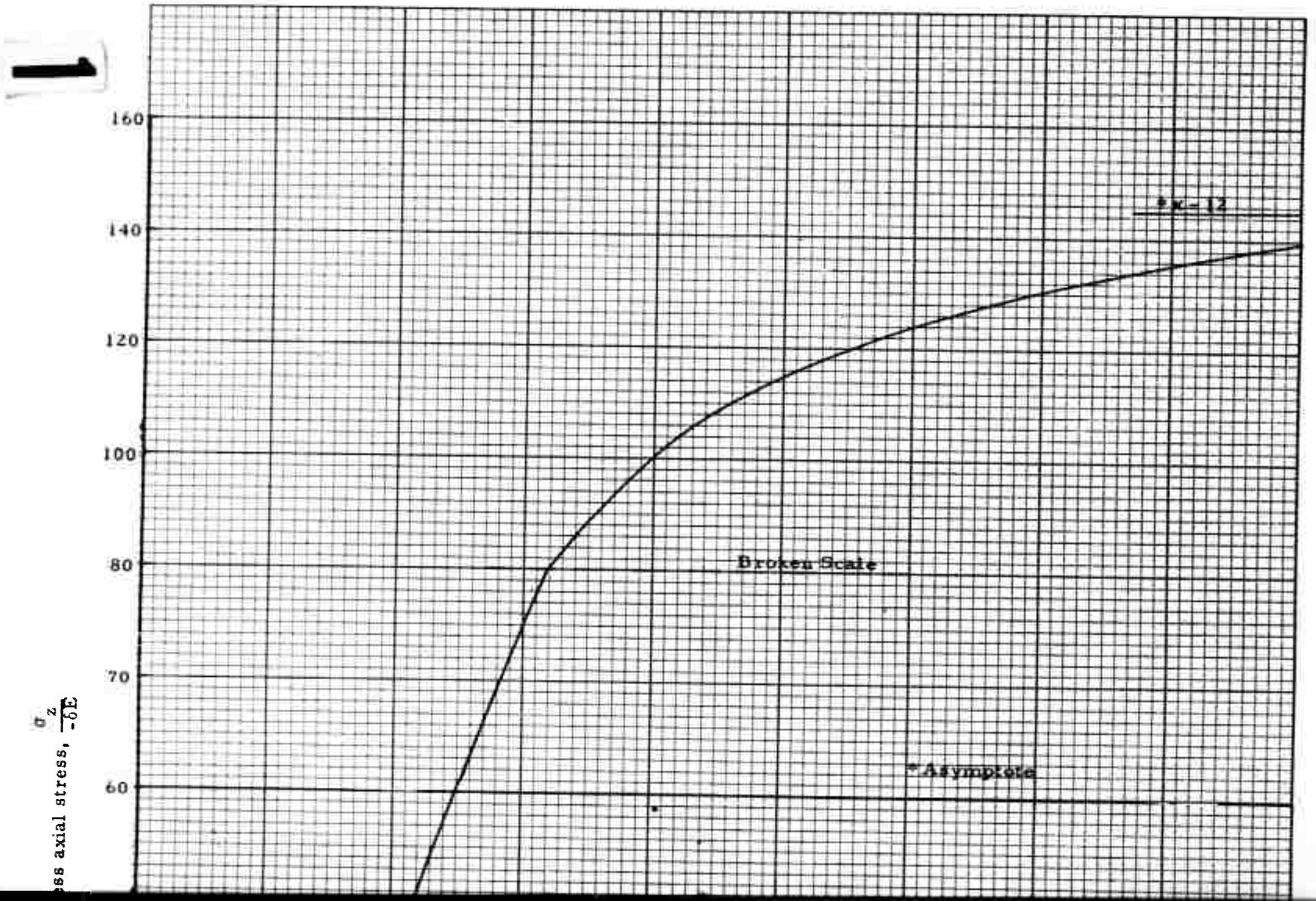
160
140
120
100
80
70
60
* x - 12
Broken Scale
* Asymptote
σ_z / $-\delta E$

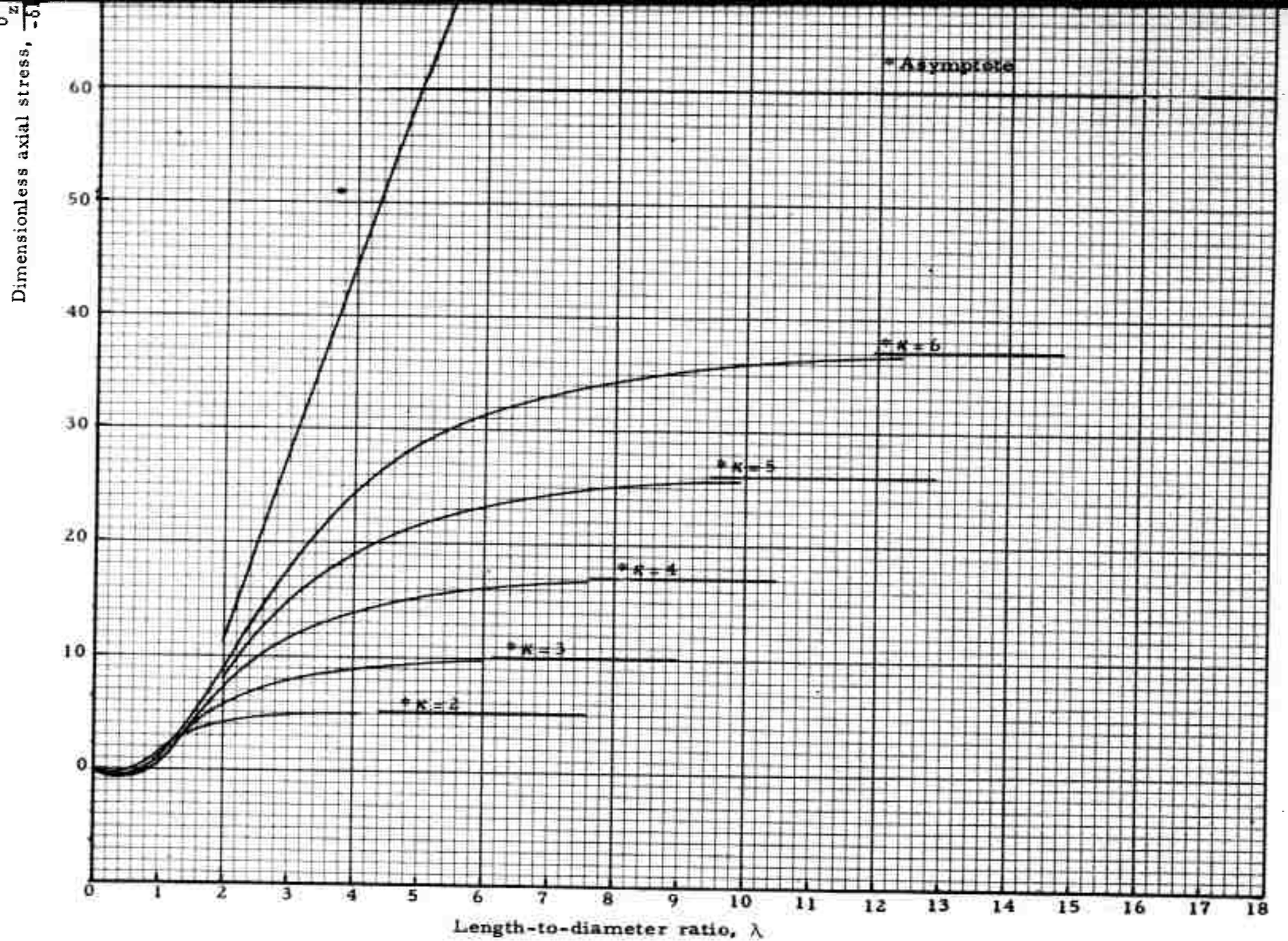

Fig. 18 Dimensionless axial stress at inner radius in middle of cylinder, propellant bonded at outer periphery, both ends free, under uniform shrinkage, ν=0.5

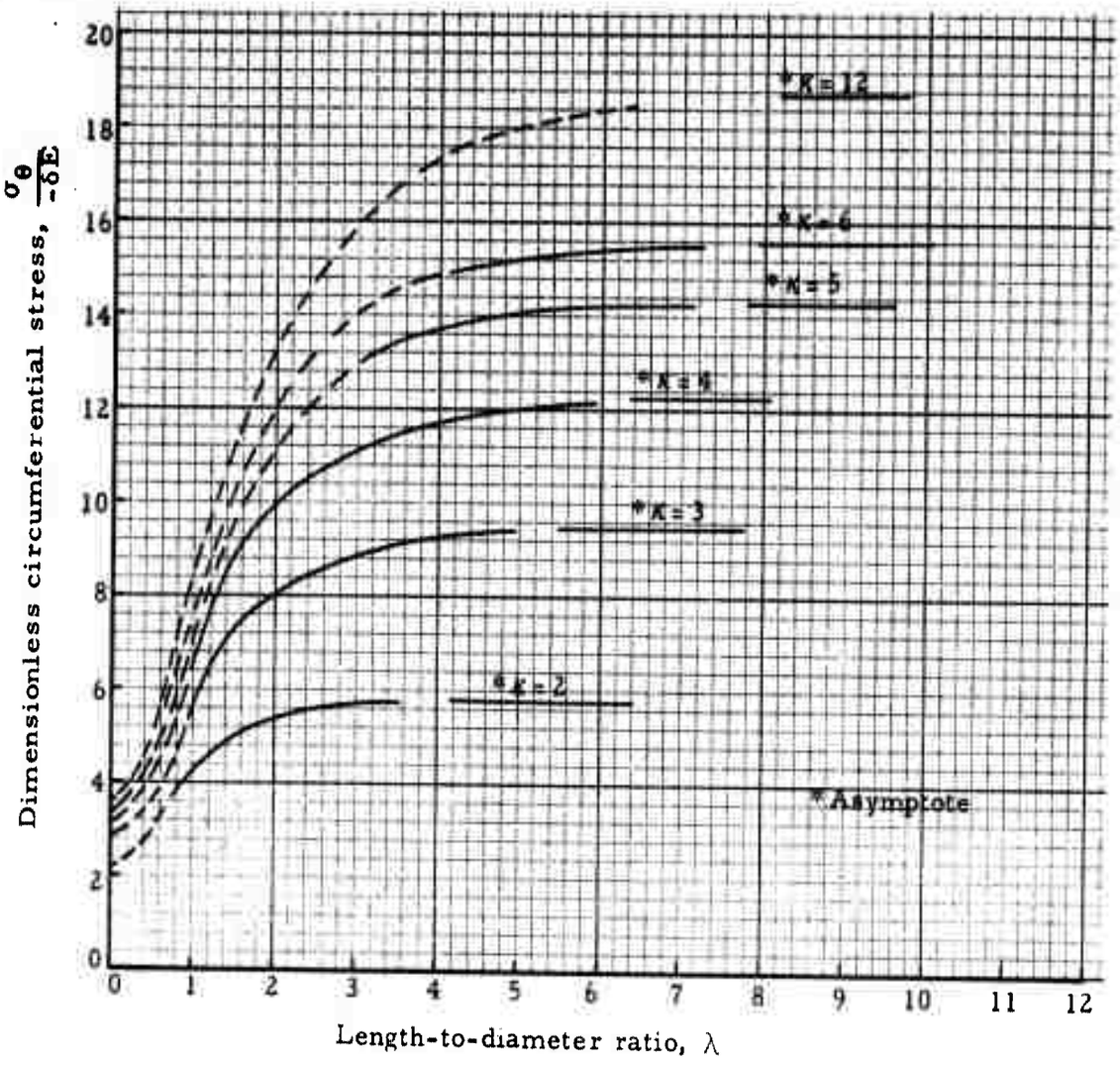

Fig. 19 Dimensionless circumferential stress at inner radius in middle of cylinder, propellant bonded at outer periphery, both ends free, under uniform shrinkage $\nu = 0.45$

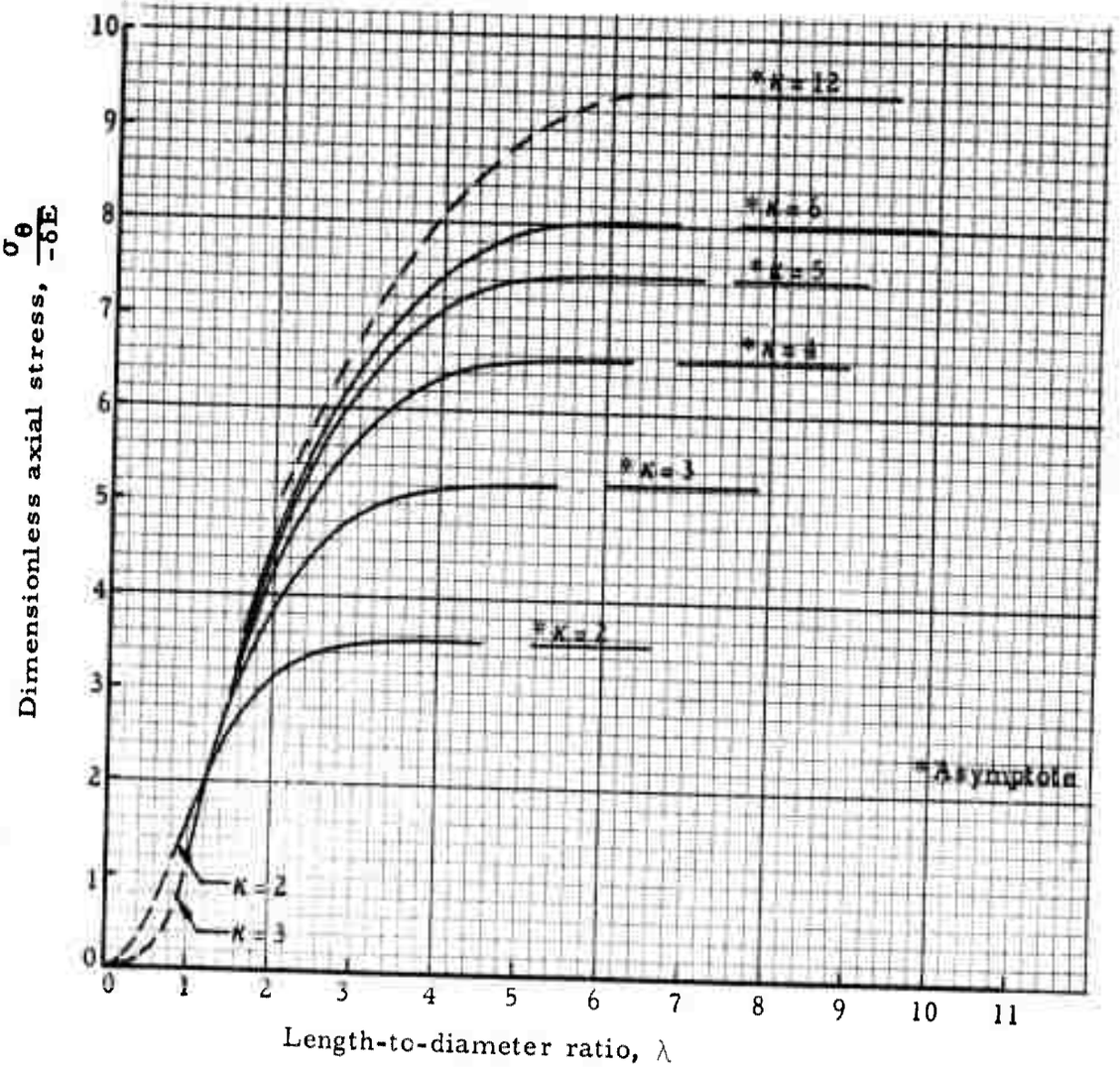

Fig. 20 Dimensionless axial stress at inner radius in middle of cylinder, propellant bonded at outer periphery, both ends free, under uniform shrinkage $\nu = 0.45$

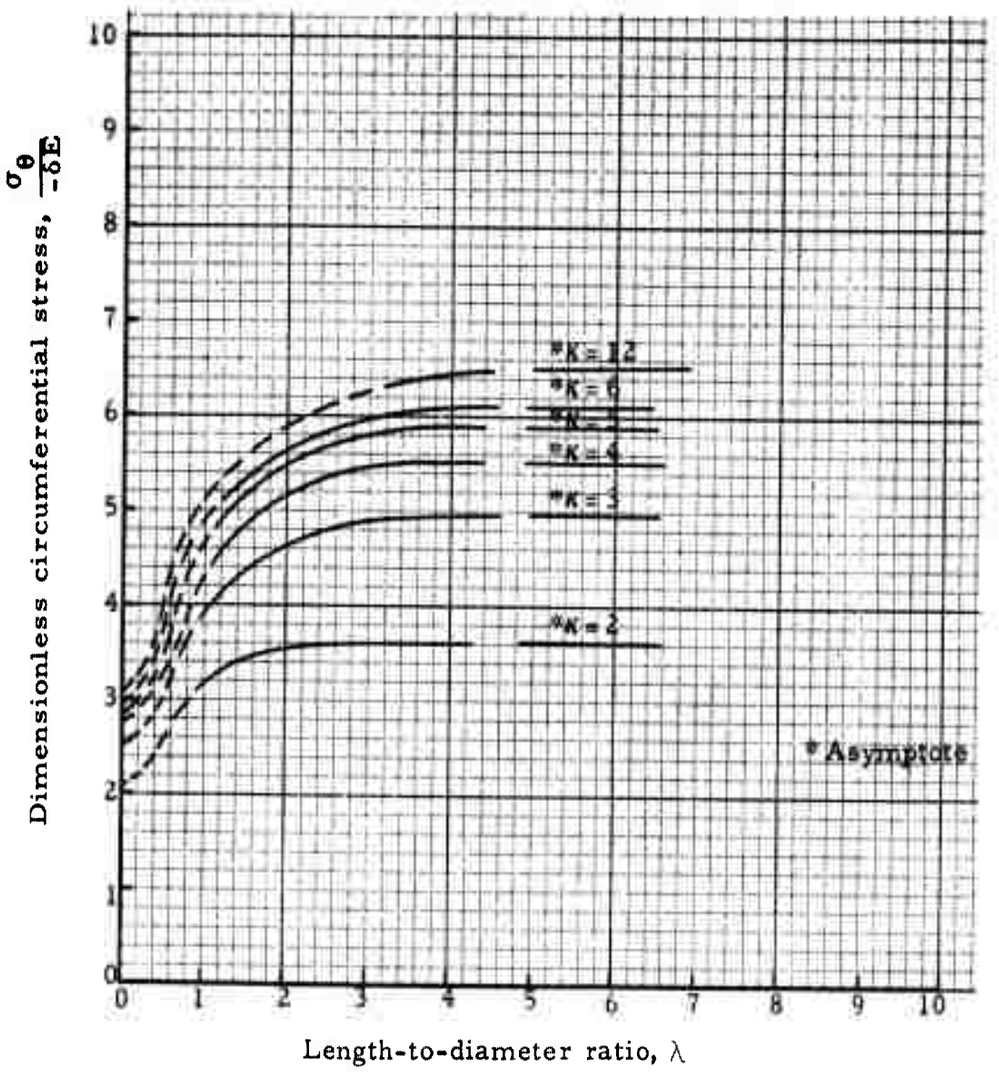

Fig. 21 Dimensionless circumferential stress at inner radius in middle of cylinder, propellant bonded at outer periphery, both ends free, under uniform shrinkage $\nu = 0.35$

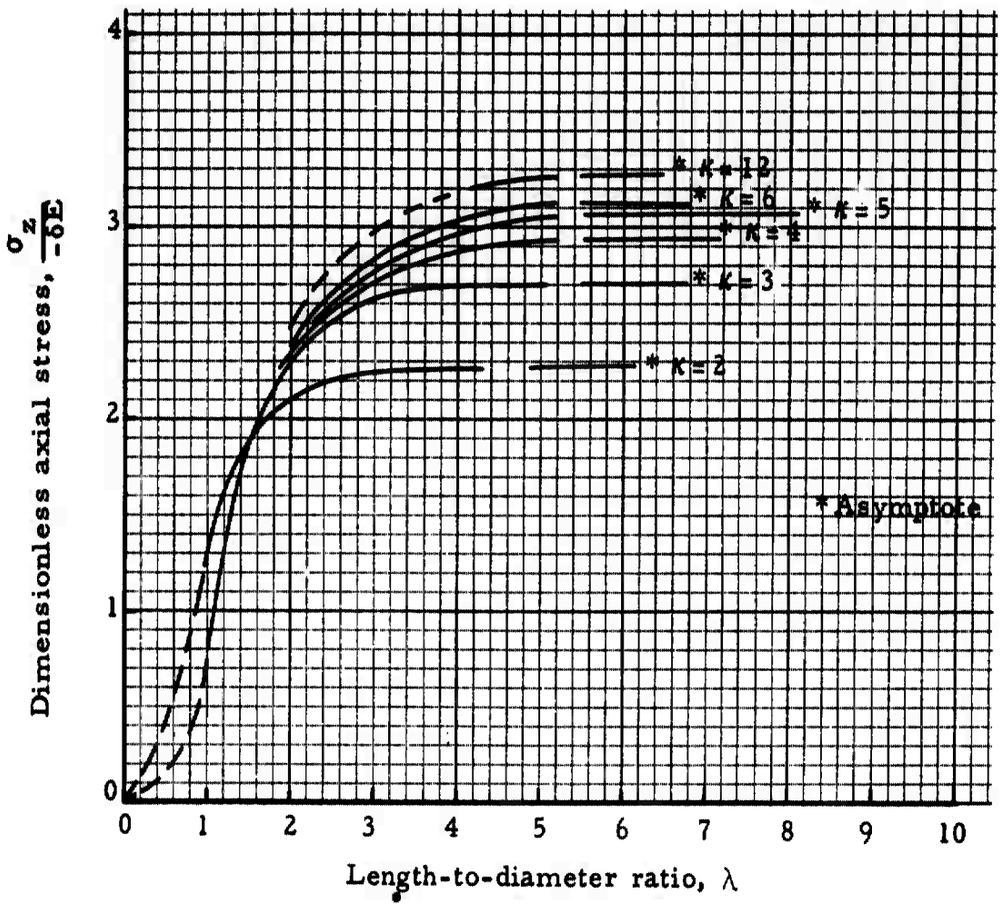

Fig. 22 Dimensionless axial stress at inner radius in middle of cylinder, propellant bonded at outer periphery, both ends free, under uniform shrinkage $\nu = 0.35$

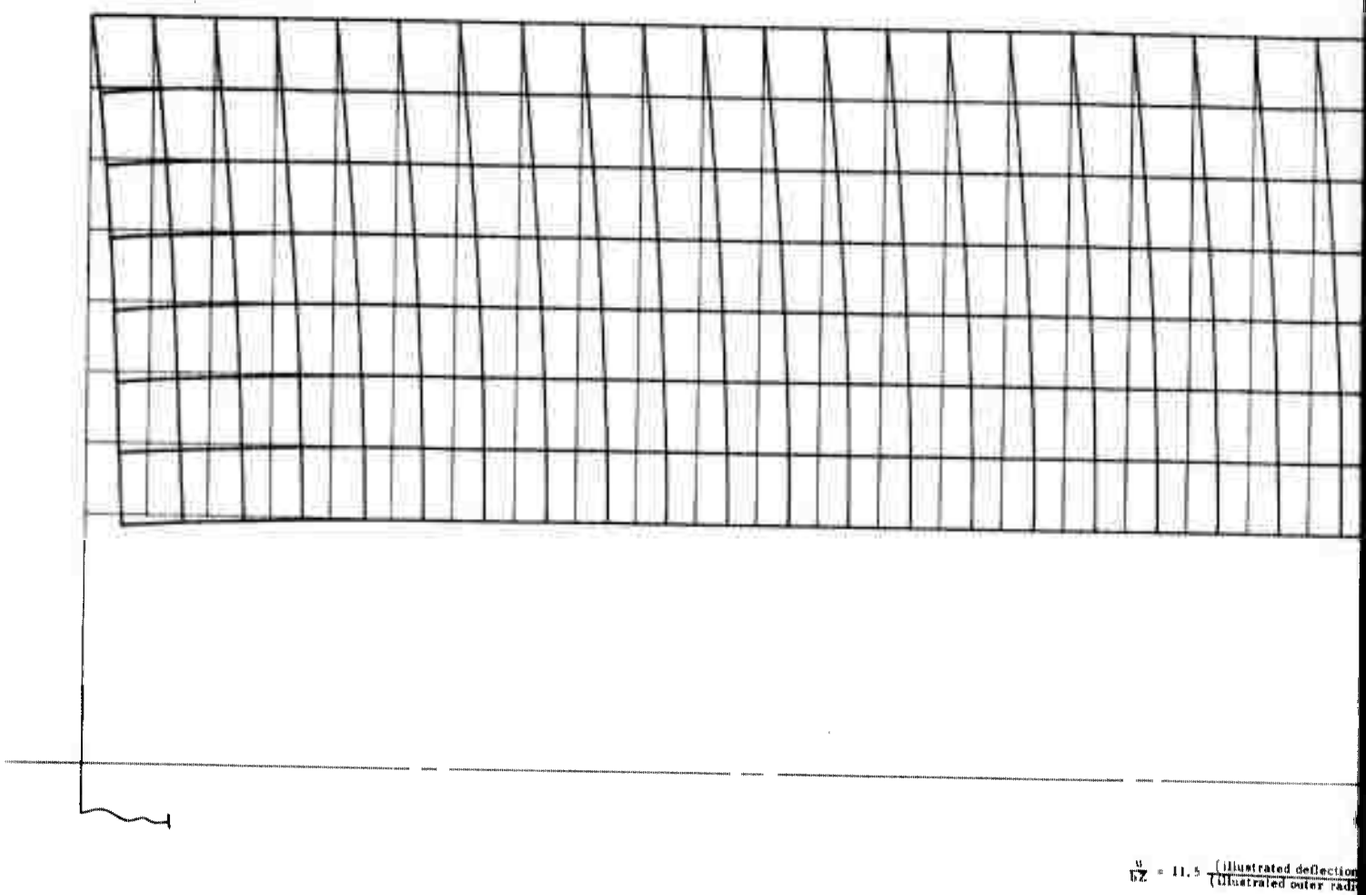

Fig. 23 Deformation of propellant grain, bonded at outer periphery, both ends free, under axi
$\kappa = 3.33$, $\lambda = 2$, $\nu = 0.5$

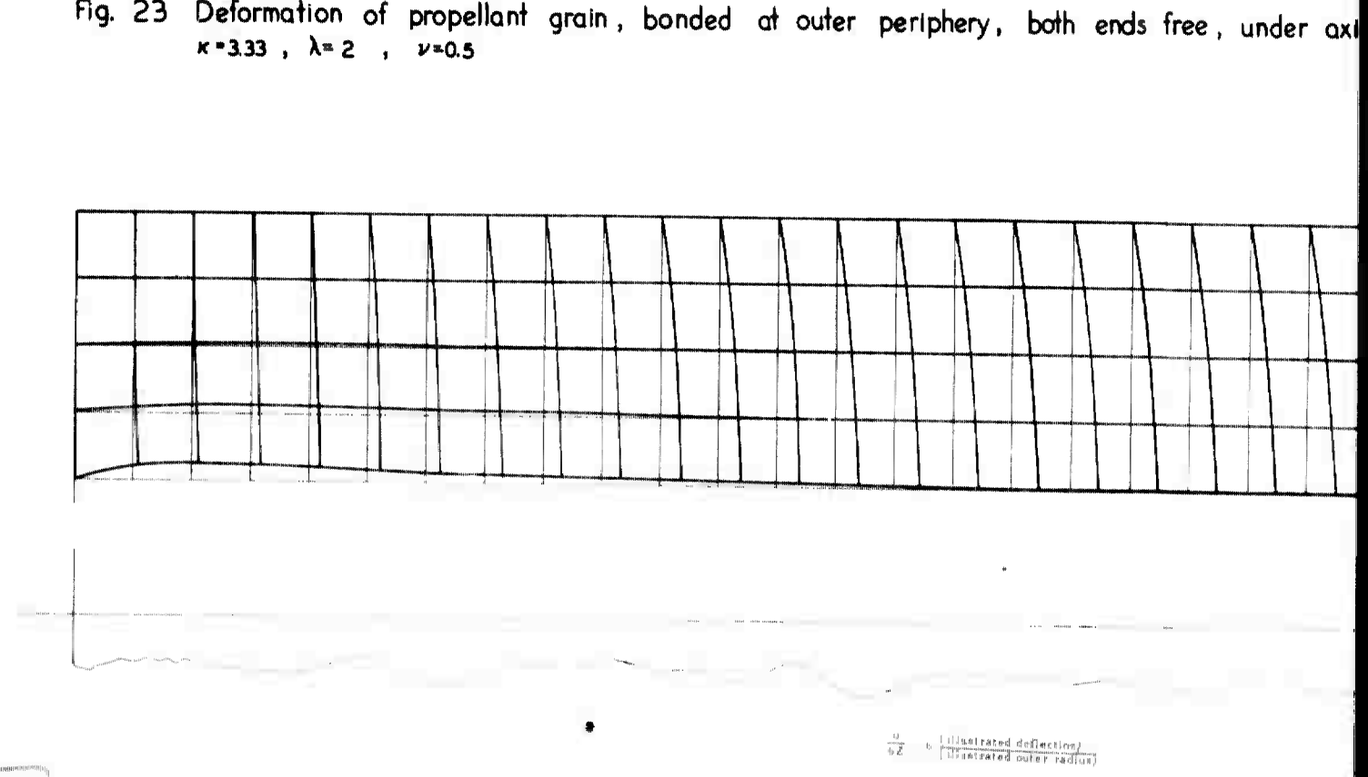

Fig. 24 Deformation of propellant grain, bonded at outer periphery and left end, under axial
$\kappa = 3$ $\lambda = 2.67$ $\nu = 0.5$

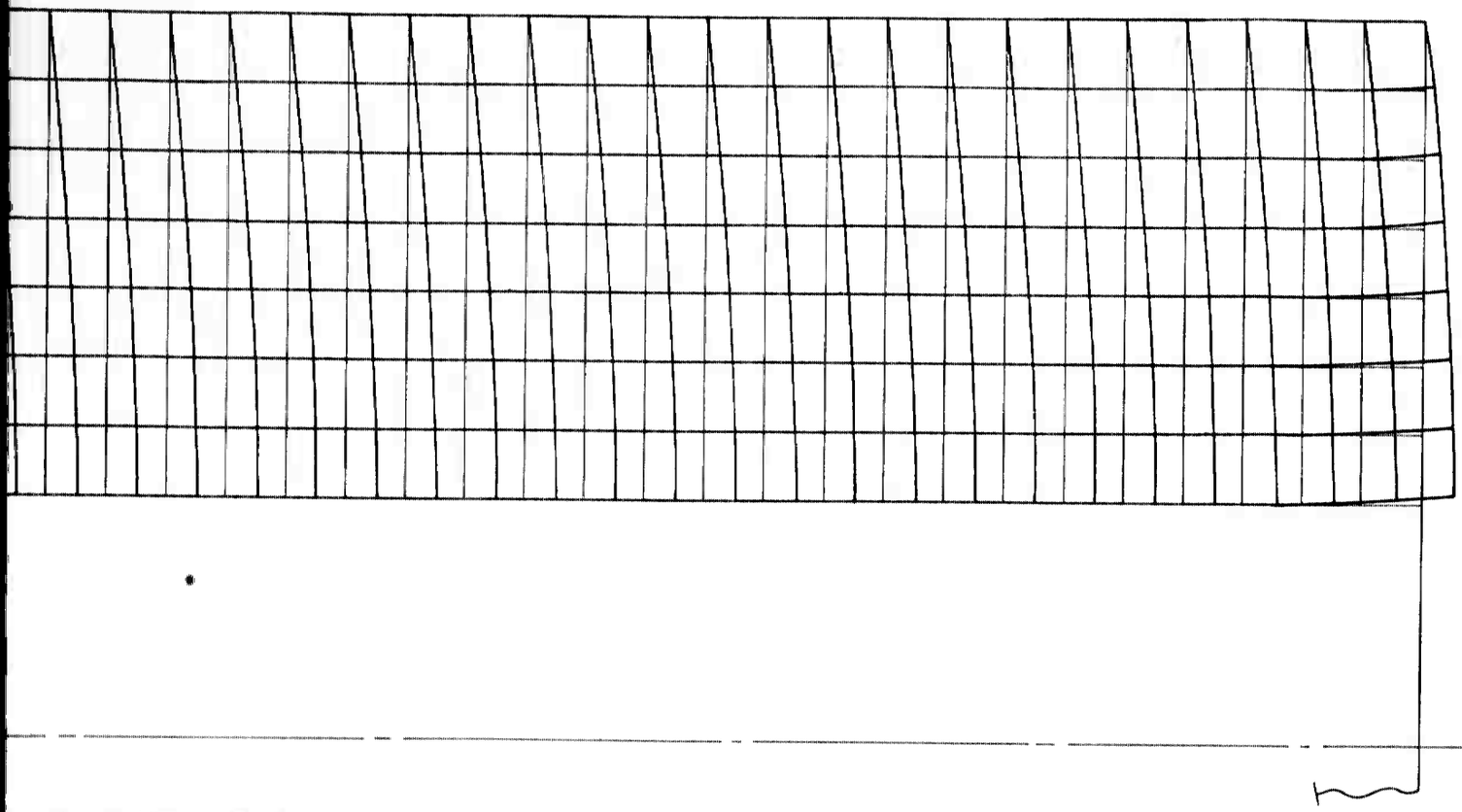

$\frac{w}{\delta z} = 11.5 \frac{\text{(illustrated deflection)}}{\text{(illustrated outer radius)}}$

ends free, under axial acceleration

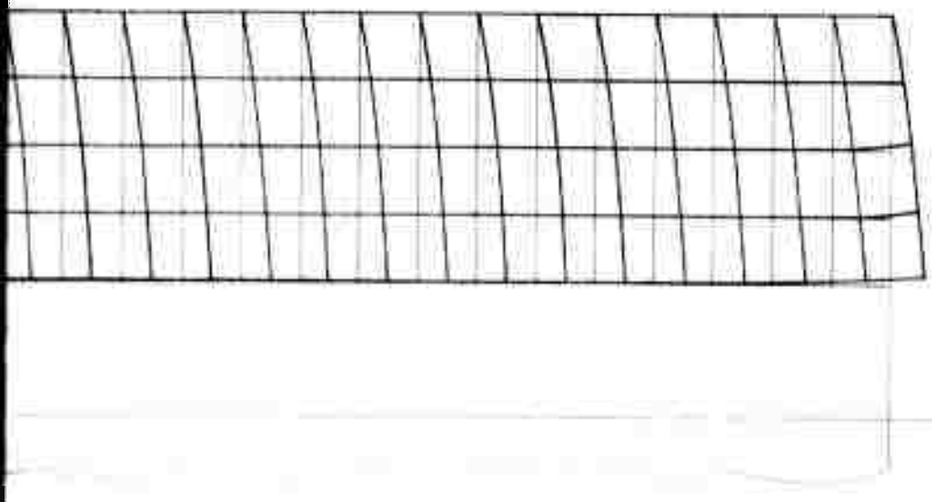

eft end, under axial acceleration

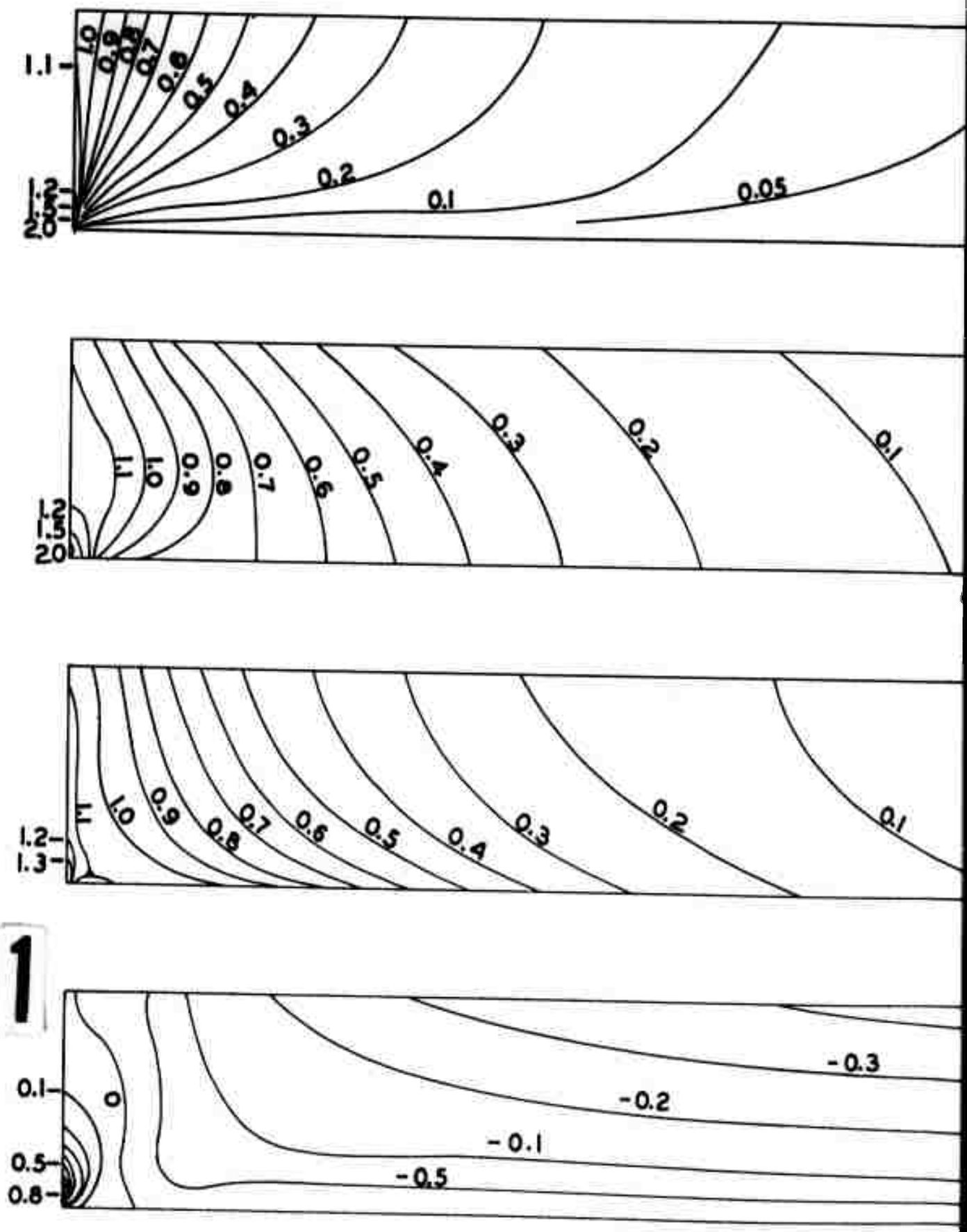

Fig. 25 Dimensionless stress contours $\frac{\sigma}{aAb}$ in propellant grain, bonded at outer periphery and left under axial acceleration $\kappa=3$, $\lambda=2.67$, $\nu=0.5$

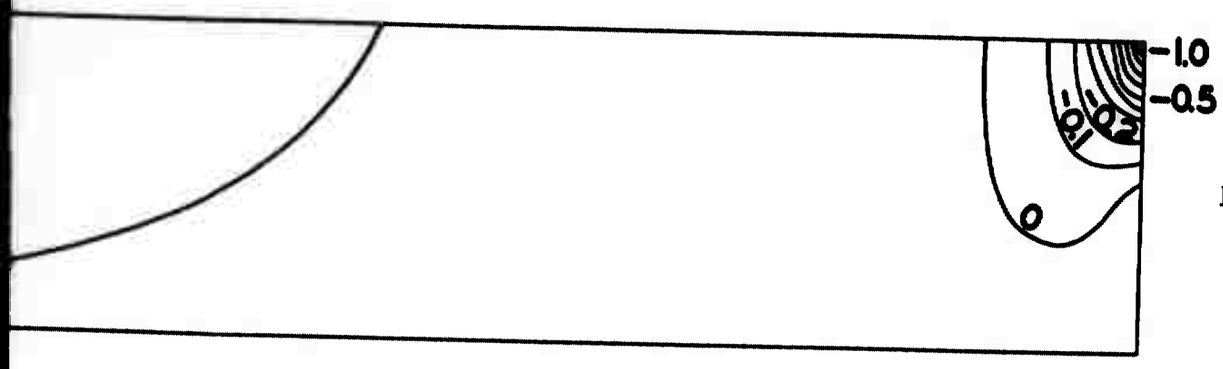

Dimensionless radial stress $\frac{\sigma_r}{\gamma A b}$

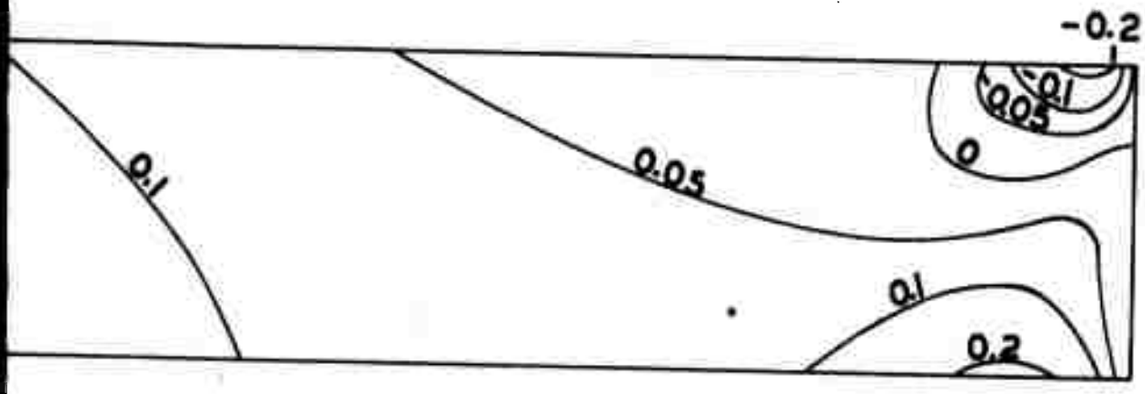

Dimensionless axial stress $\frac{\sigma_z}{\gamma A b}$

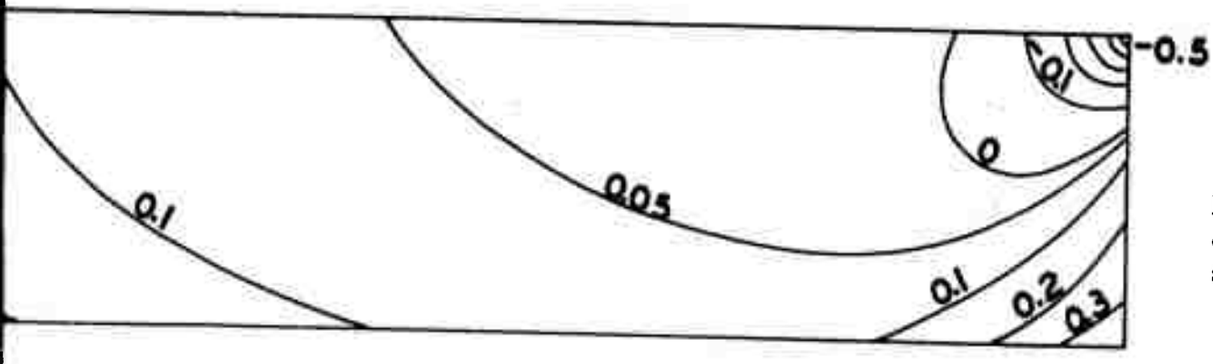

Dimensionless circumferential stress $\frac{\sigma_\theta}{\gamma A b}$

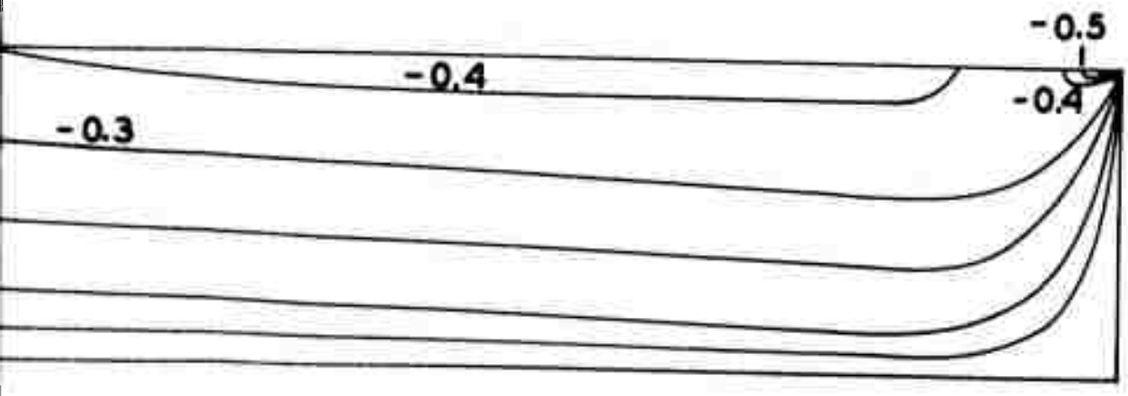

Dimensionless shear stress $\frac{\sigma_{rz}}{\gamma A b}$

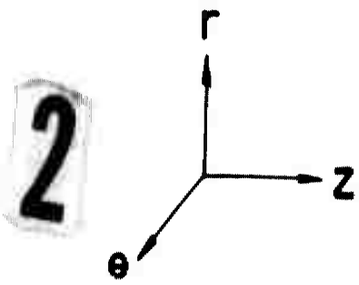

2

eriphery and left end ,

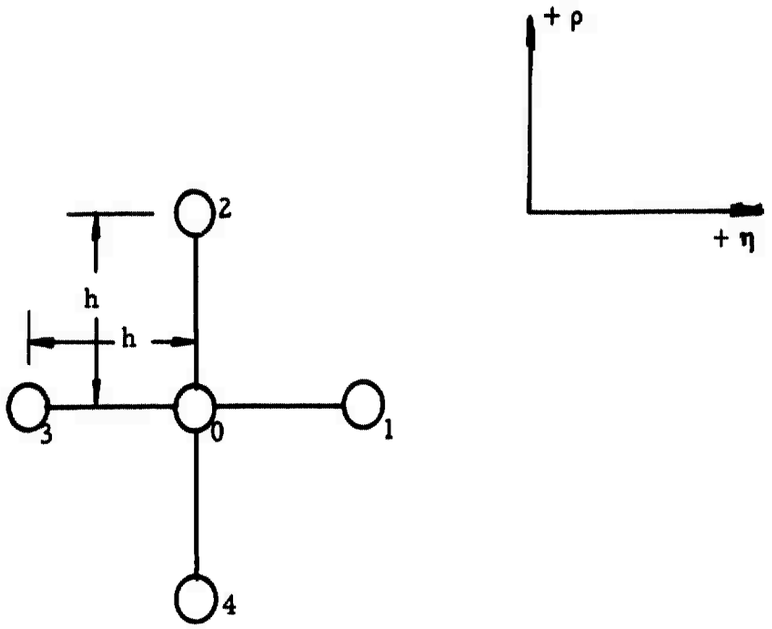

Fig. 26 Nodal notation

DISPLACEMENT ANALYSIS BY ENERGY METHODS FOR CURE SHRINKAGE OF CASE-BONDED SOLID PROPELLANT GRAINS OF FINITE LENGTH

Gerald F. Gillis

The use of energy methods for the approximate solution of elasticity problems is well established for certain types of bodies for which at least one overall dimension is small in comparison with the others, e.g., beams and plates. The investigation of the stress state and/or displacement state in bodies in which all overall dimensions are of the same magnitude has received little attention by energy methods, evidently because the simplicity evident in plate and beam problems is no longer present. This report has served as an exploratory study of the solution of problems of the latter type. The particular problem chosen for the investigation was selected because of the availability of both numerical analysis and experimental results with which to verify the solution.

PROBLEM DESCRIPTION

Strains are induced in polymeric materials as a result of thermal expansion and cure shrinkage. Due to the similarity of the two effects, they may be combined into a dimensional change function, Λ, defined as

$$\Lambda = \delta + \alpha T \quad , \tag{1}$$

where

δ = linear cure expansion (positive for expansion and negative for shrinkage) ,

α = linear coefficient of thermal expansion of the cured material, and

T = temperature relative to some reference.

With the notation of Eq. 1, $(\epsilon - \Lambda)$ represents strain due to stress whereas ϵ represents overall dimensional change. When there are no applied loads or restraints, $\epsilon = \Lambda$ and the stress induced strain is zero. If the effects of the thermal expansion and cure shrinkage are such that Λ is zero, then the stress induced strain is ϵ, as it is usually defined.

Stresses are induced in case-bonded propellant grains by cure shrinkage and by uniform temperature changes, the latter being the result of the difference in the coefficients of thermal expansion of the case and grain. In determining the stresses caused by the above effects,

T would normally be the temperature relative to the temperature at which no stresses are induced by differential thermal expansion of the case and grain.

The purpose of this analysis was to determine by energy methods the displacements of the propellant grain associated with cure shrinkage only. However, the results are general enough to include thermal expansion resulting from uniform temperature changes if the coefficient of thermal expansion of the case is negligible compared to that of the grain.

The model which was analyzed consisted of an elastic, homogeneous, isotropic, incompressible propellant grain in the form of a hollow, right, circular cylinder bonded on the outer surface to a rigid case wall. The applicability of the classical infinitesimal theory of elasticity was assumed.

Cylindrical coordinates were used with the origin located at the centroid of the cylinder (Fig. 1). The analysis was made only for the half of the cylinder extending from $z = 0$ to $z = \ell$ since it is symmetrical about the origin.

The boundary conditions for the described model are

a) $u = 0, \quad r = b$,

b) $w = 0, \quad r = b$,

c) $\sigma_r = 0, \quad r = a$,

d) $\tau_{rz} = 0, \quad r = a$,

e) $\tau_{rz} = 0, \quad z = \ell$,

f) $\sigma_z = 0, \quad z = \ell$,

g) $\tau_{rz} = 0, \quad z = 0$, and

h) $w = 0, \quad z = 0$,

where

u = radial displacement,

w = axial displacement,

τ = shear stress,

σ = normal stress,

a = inner propellant radius,

b = outer propellant radius,

ℓ = one-half the length of the propellant grain,

z = axial direction,

r = radial direction, and

θ = circumferential direction.

Boundary conditions (a) and (b) are a consequence of the rigid case assumption. The restriction to loads caused by cure shrinkage requires (c), (d), (e), and (f). Conditions (g) and (h) result from symmetry considerations. The axial symmetry of geometry and loading require that $v = \tau_{r\theta} = \tau_{\theta z} = 0$, where v is circumferential displacement.

ANALYSIS

An approximate displacement solution for the described model was obtained by applying the Rayleigh-Ritz method to the principle of minimum potential energy[1]. This was accomplished by assuming the displacements in equation form with undetermined constants such that all displacement boundary conditions were satisfied and the displacements were continuous. These displacements were substituted into the potential energy equations and the undetermined constants were evaluated by minimizing the potential energy. The approximation was improved by increasing the number of undetermined constants and repeating the minimization procedure until the potential energy approached a stationary value.

Potential Energy

The boundary conditions for the model state that the surface tractions are zero at $r = a$ and $z = \pm \ell$ and that $u = v = w = 0$ at $r = b$. Consequently, for negligible body forces, the potential energy as defined by Eq. A-8 is equal to the strain energy. That is,

$$E_p = V = \int_{\xi} V_o \, d\xi \quad , \tag{2}$$

where

ξ = volume of the body ,

E_p = potential energy ,

V = strain energy in the body, and

V_o = strain energy per unit volume .

The strain energy per unit volume for a body subjected to a linear cure expansion δ is defined by Eq. A-5 as

$$2V_o = \sigma_r[\epsilon_r - \delta] + \sigma_\theta[\epsilon_\theta - \delta] + \sigma_z[\epsilon_z - \delta] + \tau_{rz}\gamma_{rz} + \tau_{r\theta}\gamma_{r\theta} + \tau_{z\theta}\gamma_{z\theta} . \tag{3}$$

---

[1]The Appendix contains a discussion of energy methods which includes the equations and limitations of the principle of minimum complementary energy as well as the principle of minimum potential energy and the procedure for applying the Rayleigh-Ritz method to either.

Using Hooke's law in the form

$$\sigma_r = \frac{\nu}{1+\nu}\,\Theta + 2G[\epsilon_r - \delta] , \tag{4}$$

$$\sigma_\theta = \frac{\nu}{1+\nu}\,\Theta + 2G[\epsilon_\theta - \delta] , \text{ and} \tag{5}$$

$$\sigma_z = \frac{\nu}{1+\nu}\,\Theta + 2G[\epsilon_z - \delta] , \tag{6}$$

where

G = shear modulus ,

$\Theta = \sigma_r + \sigma_\theta + \sigma_z$, and

ν = Poisson's ratio ,

Eq. 3 can be written as

$$2V_o = \frac{\nu}{1+\nu}\,\Theta[e - 3\delta] + 2G[\epsilon_r^2 + \epsilon_\theta^2 + \epsilon_z^2 - 2\delta e + 3\delta^2] + G[\gamma_{rz}^2 + \gamma_{r\theta}^2 + \gamma_{z\theta}^2] , \tag{7}$$

where $e = \epsilon_r + \epsilon_\theta + \epsilon_z$. For an incompressible material, $e - 3\delta = 0$. Also, as stated above, $\tau_{r\theta} = \tau_{\theta z} = 0$ due to symmetry. Hence Eq. 7 can be written as

$$V_o = G[\epsilon_r^2 + \epsilon_\theta^2 + \epsilon_z^2 - 3\delta^2] + \frac{G}{2}\,\gamma_{rz}^2 . \tag{8}$$

Approximating Functions for the Displacements

Parr [6][1] has shown that the radial displacement in a propellant grain in the form of a hollow circular cylinder of infinite length, bonded to a rigid case and subjected to cure shrinkage, is

$$u = -\frac{[1+\nu]\,a^2\,r\,\delta}{a^2 + [1-2\nu]b^2}\left[\frac{b^2}{r^2} - 1\right] , \tag{9}$$

where $-\delta$ is the linear cure shrinkage. For an incompressible material $\nu = 0.5$, and Eq. 9 simplifies to

$$\frac{u}{b} = \frac{3}{2}\,\delta[\rho - \rho^{-1}] \tag{10}$$

where $\rho = r/b$.

The radial displacement for a cylinder of finite length can be assumed to consist of the infinite cylinder solution plus a perturbation term,

$$\frac{u}{b} = \frac{3}{2}\,\delta[\rho - \rho^{-1}] + \delta F(\rho)\,G(\zeta) , \tag{11}$$

where $\zeta = \frac{z}{l}$ and $F(\rho)$ and $G(\zeta)$ are as yet unspecified functions.

---

[1]Numbers in brackets designate references at the end of the report.

Forming an assumed expression for the axial displacement in a similar manner results in only the perturbation term since w = 0 in the infinite cylinder solution. Hence,

$$\frac{w}{l} = \delta\, f(\rho)\, g(\zeta) \quad , \tag{12}$$

where $f(\rho)$ and $g(\zeta)$ are again as yet unspecified functions.

The restriction to an incompressible material requires that

$$\epsilon_\theta + \epsilon_z + \epsilon_r = \frac{u}{r} + \frac{\partial w}{\partial z} + \frac{\partial u}{\partial r} + \frac{1}{r}\frac{\partial v}{\partial \theta} = 3\delta \quad . \tag{13}$$

Substitution of Eqs. 11 and 12 into Eq. 13 with v = 0, yields the conditions

$$g'(\zeta) = \lambda\, G(\zeta) \tag{14}$$

and

$$\frac{1}{\rho}\frac{\partial[\rho F(\rho)]}{\partial \rho} = -\lambda f(\rho) \quad , \tag{15}$$

where λ is an undetermined constant which can be evaluated by minimizing the energy. In this analysis, λ will be taken equal to unity for simplicity.

Experimental measurements of axial and radial displacements made by the Applied Physics Group of this Division on a 6C2-33 STM[1] (Figs. 2 and 4) suggest using a parabola for $f(\rho)$ of the form

$$f(\rho) = 4[1 - \rho^2] \quad , \tag{16}$$

where the factor of 4 was introduced to obtain a more convenient expression for $F(\rho)$. Substitution of Eq. 16 into Eq. 15, integration of the resulting expression, and application of boundary condition (a) yields

$$F(\rho) = [\rho^{-1} + \rho^3 - 2\rho] \quad . \tag{17}$$

These radial and axial displacement measurements further suggest the possibility of employing polynomials for $G(\zeta)$ and $g(\zeta)$. Furthermore, symmetry of the radial displacements about the $\theta - z$ plane requires that a polynomial representation of $G(\zeta)$ contain only even powers of ζ. Consequently, it was assumed that

$$g(\zeta) = \sum_{i=1}^{n} c_{2i-1}\, \zeta^{2i-1} \tag{18}$$

and

---

[1] 6C2-33 STM designates a static test motor (STM) having a case-bonded propellant grain in the form of a hollow, right, circular (C) cylinder 33 in. long with an O.D. of 6 in. and an I.D. of 2 in.

$$G(\zeta) = g'(\zeta) = \sum_{i=1}^{n} [2i-1]\, c_{2i-1}\, \zeta^{2i-2} \quad . \tag{19}$$

Substitution of Eqs. 16, 17, 18, and 19 into Eqs. 11 and 12 yields

$$\frac{u}{b} = \frac{3}{2}\,\delta\,[\rho - \rho^{-1}] + \delta\,[\rho^{-1} + \rho^{3} - 2\rho] \sum_{i=1}^{n} [2i-1]\, c_{2i-1}\, \zeta^{2i-2} \tag{20}$$

and

$$\frac{w}{\ell} = 4\delta\,[1-\rho^{2}] \sum_{i=1}^{n} c_{2i-1}\, \zeta^{2i-1} \quad . \tag{21}$$

Eqs. 20 and 21 satisfy all displacement boundary conditions and are continuous.

An exponential axial variation was also considered in an effort to determine which type of function gives the best approximation with the least expenditure of time. The solution yielding the smaller potential energy should be the better approximation.

The displacements with the exponential axial variation were assumed to be

$$\frac{u}{b} = \frac{3}{2}\,\delta\,[\rho - \rho^{-1}] + \frac{3}{2}\,B\,\delta\,[\rho^{-1} + \rho^{3} - 2\rho]\, \exp\left\{-\frac{k\ell}{b}\,[1-\zeta]\right\} \tag{22}$$

and

$$\frac{w}{\ell} = \frac{6B\delta b}{k\ell}\,[1-\rho^{2}]\, \exp\left\{-\frac{k\ell}{b}\,[1-\zeta]\right\} \tag{23}$$

where B and k are the undetermined constants and k is positive and real. These displacements are continuous and satisfy all displacement boundary conditions with the exception that the assumed form for w does not exactly satisfy the boundary condition that $w = 0$ at $z = 0$. This boundary condition will be approximately satisfied if the exponential term at $z = 0$ is small relative to its value at $z = \ell$. Eqs. 22 and 23 were written to apply only for the region $0 \le z \le \ell$ with the knowledge that, if a good approximation could be obtained for this half of the motor, symmetry about the origin will require the other half to exhibit the same behavior.

Substitution of the displacements given by Eqs. 20 and 21 and Eqs. 22 and 23 into Eq. 8 and the resulting expressions into Eq. 2 yields potential energies for the half-length of

$$\frac{E_p}{\delta^2\pi G\ell b^2} = \sum_{i=1}^{n}\sum_{j=1}^{m} c_{2i-1}\, c_{2j-1}\left\{\frac{[2i-1][2j-1]}{2i+2j-3}\,[2\gamma_1 + 32\gamma_4]\right.$$

$$+\frac{[2i-1][2j-1][2j-2][2i-2]\,b^2\gamma_6}{[2i+2j-5]\ell^2} + \frac{64\ell^2\gamma_8}{b^2[2i+2j-1]}$$

$$\left. -\frac{[2j-1][2j-2]+[2i-1][2i-2]}{2[2i+2j-3]}\,[16\gamma_4]\right\}$$

$$+ 3(3\gamma_2 - 2\gamma_5) + 12\gamma_3 \sum_{i=1}^{n} c_{2i-1} \qquad (24)$$

and

$$\frac{E_p}{\delta^2\pi G\ell b^2} = \frac{9B^2b}{2\ell}\left[\frac{\gamma_7}{k} + \frac{k\gamma_6}{4} + \frac{16\gamma_8}{k^3}\right] + \frac{18Bb\,\gamma_3}{k\ell} + 9\left[\gamma_2 - \frac{2}{3}\,\gamma_5\right] \qquad (25)$$

for the polynomial and exponential solutions, respectively, where

$$\gamma_1 = 4\eta^4 - \frac{5}{3}\,\eta^6 - 2\eta^2 + \eta^{-2} - \frac{4}{3}\ ,$$

$$\gamma_2 = -\frac{1}{2}\,[\eta^2 - \eta^{-2}]\ ,$$

$$\gamma_3 = \frac{1}{2}\,[1 - \eta^4 + \eta^2 - \eta^{-2}]\ ,$$

$$\gamma_4 = \frac{1}{2}\left[\frac{1}{3} - \eta^2 + \eta^4 - \frac{1}{3}\eta^6\right]\ ,$$

$$\gamma_5 = \frac{1}{2}\,[1 - \eta^2]\ ,$$

$$\gamma_6 = -\frac{25}{24} - \ln\,\eta - \frac{3}{2}\,\eta^4 + 2\eta^2 - \frac{1}{8}\,\eta^8 + \frac{2}{3}\,\eta^6\ ,$$

$$\gamma_7 = \frac{1}{2}\,\eta^{-2} - 3\eta^2 - \frac{3}{2}\,\eta^6 - 4\eta^4\ ,$$

$$\gamma_8 = \frac{1}{4}\,[1 - \eta^4]\ ,\ \text{and}$$

$$\eta = a/b\ .$$

A sufficient number of equations for determination of the constants may be obtained by taking the derivative of the above potential energies with respect to each constant and equating the derivative to zero. The process is much too cumbersome to be carried out here.

NUMERICAL RESULTS

Numerical calculations were made for a propellant grain with inner radius a = 1 in., outer radius b = 3 in., half length ℓ = 16 in., and a linear cure shrinkage $-\delta = 0.00428$ in./in.

Minimization of the potential energy as defined by Eq. 24 retaining only three constants (three terms) in the assumed polynomial form for the displacements yielded

$c_1 = 0.047897$,

$c_3 = -0.068692$,

$c_5 = 0.289720$, and

$$\frac{E_p}{\pi\delta^2 G\ell b^2} = 30.9525 \ .$$

The following values were obtained when the number of constants was increased to four.

$c_1 = 0.005841$,

$c_3 = 0.239486$,

$c_5 = -0.277336$,

$c_7 = 0.303037$, and

$$\frac{E_p}{\pi\delta^2 G\ell b^2} = 30.8979 \ .$$

The addition of the fourth constant resulted in an energy decrease of only 0.18%. Consequently, additional constants would not be expected to significantly improve the approximation.

Minimization of the potential energy as defined by Eq. 25 for the exponential form of the displacements yielded

$k = 0.948515$,

$B = 0.911945$, and

$$\frac{E_p}{\pi\delta^2 G\ell b^2} = 30.8979 \ .$$

With the above constants, the value of the exponential term in Eq. 23 at $z = 0$ is two orders of magnitude smaller than its value at $z = \ell$; hence, the approximation to $w = 0$ at $z = 0$ is reasonable.

The radial displacement along the inner surface of the propellant for each of the above solutions, for a solution obtained numerically using

relaxation techniques[1], and from measured values is shown in Figs. 2 and 3. The associated axial displacements at $z = \ell$ are shown in Fig. 4.

It should be noted that the numerical values for the above constants are independent of the cure shrinkage but are functions of the ratios $\frac{a}{b}$ and $\frac{b}{\ell}$; hence, they are valid for any motor where $\frac{a}{b} = \frac{1}{3}$ and $\frac{b}{\ell} = \frac{3}{16}$.

DISCUSSION

As was previously mentioned, additional undetermined constants are added to the approximating functions until the energy approaches a stationary value. The fact that a stationary value is obtained does not necessarily imply a close approximation to the exact solution. A stationary value merely assures that the solution is about as good as can be obtained from the chosen function forms. If the approximating functions are poor, the approximation may be incapable of approaching the true minimum energy or the convergence to the true minimum may require a large number of constants. Experience in applying energy methods and experimental data are valuable assets in choosing functions with the best chance of a close approximation.

The solutions obtained above could be improved by an iteration procedure. For example, definite expressions were assumed for $f(\rho)$ and $F(\rho)$ and the undetermined constants which were included in $G(\zeta)$ and $g(\zeta)$ were evaluated by minimizing the potential energy. With these expressions for $G(\zeta)$ and $g(\zeta)$, undetermined constants could then be introduced into $F(\rho)$ and $f(\rho)$ and evaluated by energy minimization. The process is then repeated as many times as desired. For the same degree of accuracy, the iteration procedure has the advantage over one which initially introduces many unknown constants in that at each iteration only a few constants must be determined through simultaneous solution of algebraic equations.

If experimental data are not available with which to compare results, upper and lower bounds on the energy should be determined, if possible, so that the maximum deviation from the true solution can be assessed. As an example, the problem considered in this analysis was concerned

---

[1]This solution, obtained by Parr, is presented in another section of this report.

with the cure shrinkage of a cylindrical propellant grain of finite length. An upper bound on the potential energy could be established from the infinite cylinder solution (plane strain) obtained by Parr [6]. A lower bound could be determined by generalizing Timoshenko's solution [8] for a thin circular disk (plane stress) subjected to a temperature variation symmetrical about the axis of the cylinder to include cure shrinkage.

These two solutions yield upper and lower bounds of

$$\frac{E_p}{\pi\delta^2 G \ell b^2} = 40.0144$$

and

$$\frac{E_p}{\pi\delta^2 G \ell b^2} = 4.00144 \quad ,$$

respectively, for $a = 1$ in., $\ell = 16$ in., $b = 3$ in., and $\delta = -0.00428$ in./in. A comparison of these values with those given in the numerical results indicates that the finite cylinder solution is closer to the infinite cylinder solution than to the one for a thin disk. Since the grain used in the example is relatively long compared to the web, it would be expected that the potential energy would be near the upper bound, as it is. For grains which are short compared to the web, it would be expected that the potential energy would be near the lower bound.

CONCLUSIONS

In general, the displacements obtained by energy methods compare favorably with measured values and those obtained by a relaxation solution. Some departure from the measured values was anticipated due to the assumption of incompressibility ($\nu = 0.5$). Present indications are that the propellant from which the measured values were obtained has a Poisson's ratio of approximately 0.495. However, a stress-strain analysis is sensitive to even such a slight variation in the value of ν when it is in the range 0.45 to 0.50.

The two-constant exponential solution was in close agreement with the one obtained using four-constant polynomial. Thus, a better approximation with fewer constants can be obtained using the exponential form. However, the fact that the polynomial form yields linear algebraic equations for the determination of the constants is a factor deserving consideration. A solution can be obtained using the polynomial form with more undetermined constants in less time than would be required for an exponential form.

REFERENCES

1. Argyris, D.E., "Energy Theorems and Structural Analysis", Aircraft Engineering, 26, 347 (1954).
2. Williams, M.L., Blatz, P.J., and Schapery, R.A., "Fundamental Studies Relating to Systems Analysis of Solid Propellants", Final Report - GALCIT 101, Appendix 1, Guggenheim Aeronautical Laboratory, California Institute of Technology, February 1961.
3. Boley, B.A. and Weiner, J.H., "Theory of Thermal Stresses", John Wiley & Sons, New York, (1960).
4. Hemp, W.S., "Fundamental Principles and Theorems of Thermo-elasticity", Aeronautical Quarterly, VII, 184 (1956).
5. Reissner, E., "On a Variational Theorem in Elasticity", Journal of Mathematics and Physics, 28, 90 (1949).
6. Rohm & Haas Company, Quarterly Progress Report on Weapons Research, Report No. P-57-5, April 1957.
7. Sokolnikoff, I.S., "Mathematical Theory of Elasticity", Second Edition, McGraw-Hill, New York, (1956).
8. Timoshenko, S. and Goodier, J. N., "Theory of Elasticity", Second Edition, McGraw-Hill, New York, (1951).
9. Westergaard, H.M., "Theory of Elasticity and Plasticity", Harvard University Press, New York, (1952).

APPENDIX

GENERAL DISCUSSION OF ENERGY METHODS AND TERMINOLOGY

Strain Energy and Complementary Strain Energy

When a uniform bar is loaded in simple tension, the forces on the ends do work which is stored in the body as strain energy. For an elastic element of unit dimensions shown in Fig. 5, the strain energy stored per unit volume is

$$V_o = \frac{1}{2} \sigma_r \epsilon_r \quad . \tag{A-1}$$

The strain energy per unit volume is equal to the area between the ϵ-axis and the stress-strain curve. The area between the σ-axis and the curve is called the complementary strain energy. If all six components of stress act on the element, the principle of the conservation of energy requires that the work done be independent of the order in which the forces are applied. Otherwise it would be possible to load in one order and unload in another such that net work would be gained from the cycle. Consequently, when all six components of stress are considered, the strain energy per unit volume can be generalized to, in cylindrical coordinates,

$$V_o = \frac{1}{2} \left[\sigma_r \epsilon_r + \sigma_\theta \epsilon_\theta + \sigma_z \epsilon_z + \tau_{r\theta} \gamma_{r\theta} + \tau_{rz} \gamma_{rz} + \tau_{\theta z} \gamma_{\theta z} \right] \quad . \tag{A-2}$$

For a body subjected to thermal effects and cure shrinkage, the strain due to stress has previously been defined as $(\epsilon - \Lambda)$, whereas the strain due to dimensional changes is denoted by ϵ. For simplicity, consider a uniform bar subjected to a uniform temperature change and then loaded in simple tension. The resulting stress-strain diagram is shown in Fig. 6. The strain energy per unit volume, the area between the ϵ-axis and the curve, is

$$V_o = \frac{1}{2} \sigma_r \left[\epsilon_r - \alpha T \right] \quad . \tag{A-3}$$

The complementary strain energy per unit volume, the area between the σ-axis and the curve, is

$$V_o^* = \frac{1}{2} \sigma_r \left[\epsilon_r + \alpha T \right] \quad . \tag{A-4}$$

These equations may also be generalized to include all stress components and the cure shrinkage. Thus,

$$V_o = \frac{1}{2}\left\{\sigma_r[\epsilon_r - \Lambda] + \sigma_\theta[\epsilon_\theta - \Lambda] + \sigma_z[\epsilon_z - \Lambda] + \tau_{r\theta}\gamma_{r\theta} + \tau_{rz}\gamma_{rz} + \tau_{\theta z}\gamma_{\theta z}\right\} \quad (A\text{-}5)$$

and

$$V_o^* = \frac{1}{2}\left\{\sigma_r[\epsilon_r + \Lambda] + \sigma_\theta[\epsilon_\theta + \Lambda] + \sigma_z[\epsilon_z + \Lambda] + \tau_{r\theta}\gamma_{r\theta} + \tau_{rz}\gamma_{rz} + \tau_{\theta z}\gamma_{\theta z}\right\}. \quad (A\text{-}6)$$

Principles of Minimum Energy

The solution of many elasticity problems can be obtained employing energy theorems based, in part, on the concepts of strain energy and complementary strain energy. Two such theorems are the theorem of minimum potential energy and the theorem of minimum complementary energy. A detailed discussion of these theorems is given by Sokolnikoff [7]. Westergaard [9] gives an informative note on the history of their development. The purpose of the present discussion is not to repeat the derivations and proofs readily available in the literature but to summarize the results as they apply to problem solution.

Sokolnikoff demonstrates that

$$\Delta_1\left\{\int_\xi V_o\, d\xi - \int_\xi [Xu + Yv + Zw]\, d\xi - \int_{S_\sigma} [\overline{X}u + \overline{Y}v + \overline{Z}w]\, dS\right\} \geq 0\,, \quad (A\text{-}7)$$

where

V_o = strain energy per unit volume,

$\int_{S_\sigma}$ = summation over the part of the surface on which the surface forces are prescribed,

$\int_\xi$ = summation throughout the volume,

Δ_1 = an arbitrary, small, continuous change which is consistent with the displacement specified boundary conditions and associated with a variation of the displacements from the equilibrium state,

X, Y, Z = the components of the body forces per unit volume in the r, θ, and z directions, respectively,

$\overline{X}, \overline{Y}, \overline{Z}$ = the components of the surface forces per unit area in the r, θ, and z directions, respectively, and

u, v, w = the equilibrium components of displacements in the r, θ, and z directions, respectively.

The expression in the parentheses is defined as the potential energy, that is,

$$E_p = \int_\xi V_o\, d\xi - \int_\xi [Xu + Yv + Zw]\, d\xi - \int_{S_\sigma} [\overline{X}u + \overline{Y}v + \overline{Z}w]\, dS\,. \quad (A\text{-}8)$$

Thus, Eq. A-7 states that of all continuous displacements satisfying given displacement specified boundary conditions, those which satisfy the equilibrium conditions make the potential energy an absolute minimum. The above statement is known as the principle of minimum potential energy.

Sokolnikoff also demonstrates that

$$\Delta_2 \left\{ \int_{\xi} V_o^* \, d\xi - \int_{S_u} [\bar{X}u + \bar{Y}v + \bar{Z}w] \, dS \right\} \geq 0 \ , \qquad \text{(A-9)}$$

where

Δ_2 = an arbitrary small change associated with a cariation from the true state of stress such that the stress specified boundary conditions and equilibrium conditions are still satisfied,

V_o^* = complementary strain energy per unit volume, and

$\int_{S_u}$ = summation over the part of the surface where displacements are specified.

The expression in the parentheses is defined as the complementary energy, that is,

$$E_c = \int_{\xi} V_o^* \, d\xi - \int_{S_u} [\bar{X}u + \bar{Y}v + \bar{Z}w] \, dS \ . \qquad \text{(A-10)}$$

With this definition, Eq. A-9 states that of all statically possible combinations of stresses that will satisfy the equilibrium equations and stress specified boundary conditions, the one that corresponds to the true state of stress (the one that also satisfies the compatibility equations) will make the complementary energy an absolute minimum. The above statement is known as the principle of minimum complementary energy.

Rayleigh-Ritz Method

An important application of the minimum principles relates to their use in obtaining approximate solutions to problems. In the Rayleigh-Ritz method, it is assumed that a nearly true solution can be represented by a set of functions involving a limited number of constants to be determined by minimizing the energy.

In applying the Rayleigh-Ritz method to the principle of minimum complementary energy, the stresses are assumed in an equation form involving undetermined constants such that the equilibrium equations and boundary conditions specified in terms of stresses are satisfied. These assumed stresses are then substituted into the complementary energy expression and the unknown constants are evaluated by minimizing the

complementary energy. The stresses obtained will approximately satisfy the compatibility equations. The accuracy of the approximation should increase with the addition of more constants. Since the compatibility equations are not, in general, exactly satisfied, the accuracy of any displacements subsequently determined from such a solution is likely to be poor.

The Rayleigh-Ritz method is applied to the principle of minimum potential energy by specifying the displacements in an equation form involving undetermined constants such that the boundary conditions given in terms of displacements are satisfied. Continuity of the assumed displacements guarantees that the compatibility equations will be satisfied. These displacements are then substituted into the potential energy expression and the constants determined by minimizing the potential energy. The displacements obtained by substituting the values of these constants into the assumed functions will not, in general, exactly satisfy the equilibrium equations. Even though this method can provide a good approximation to the displacements, the accuracy of the associated stresses is likely to be poor.

In either case, the appropriate energy function is minimized by equating to zero the derivative of the energy expression with respect to each unknown constant, that is,

$$\frac{\partial E}{\partial c_n} = 0 \ , \qquad \text{(A-11)}$$

where E is the energy and the c_n's are the unknown constants. Such a procedure will yield n equations for the evaluation of the c_n's. Normally, the number of constants is increased until the energy approaches a stationary value. When this point is reached, the addition of more constants will not significantly improve the approximation; hence, the solution is the best obtainable with the chosen approximations.

It should be noted that the accuracy of the solution is limited by the ability of the assumed stress or displacement forms to approximate the true solution.

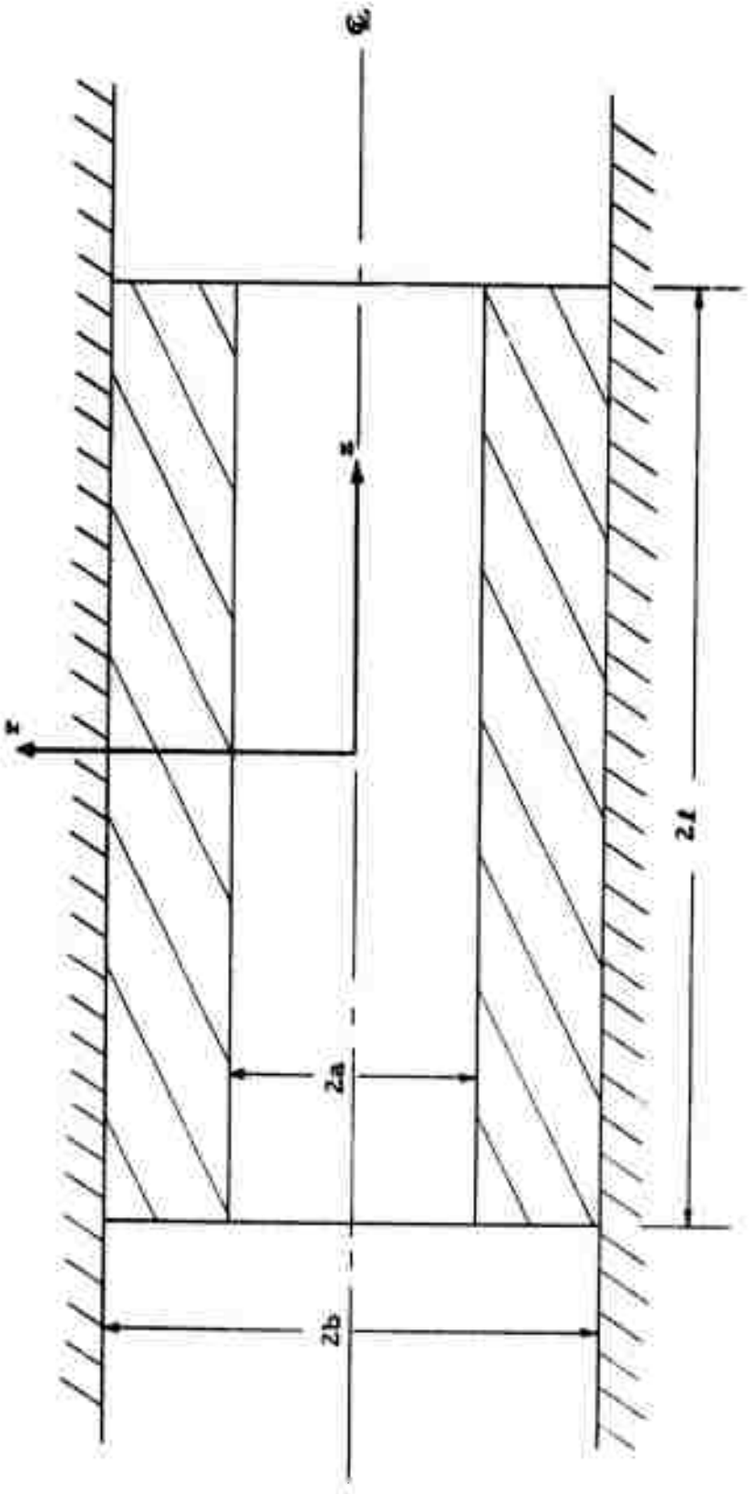

Fig. 1 Axial cross section of the propellant grain configuration.

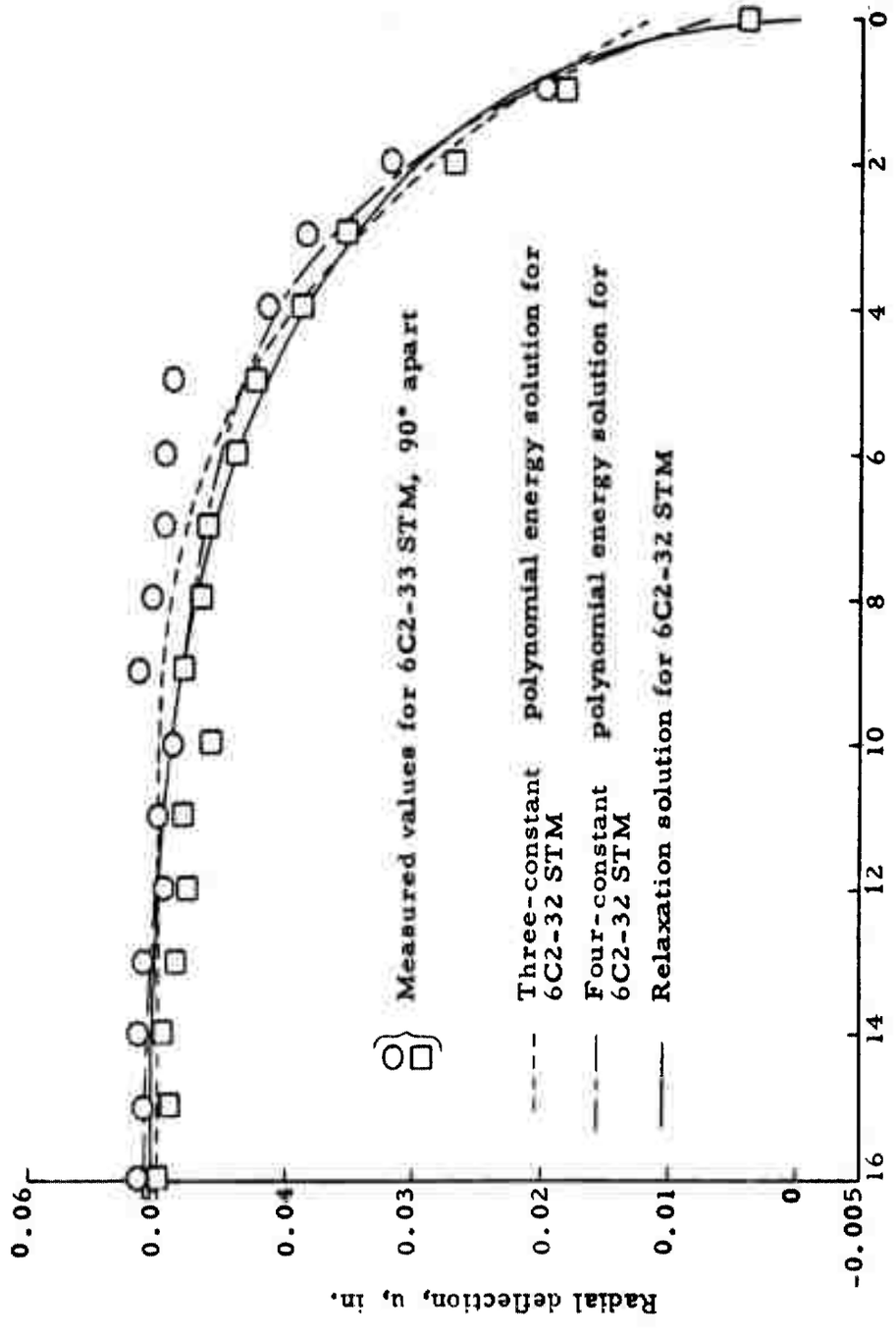

Fig. 2 Radial deflection of inner propellant surface for $112b_w$ propellant.

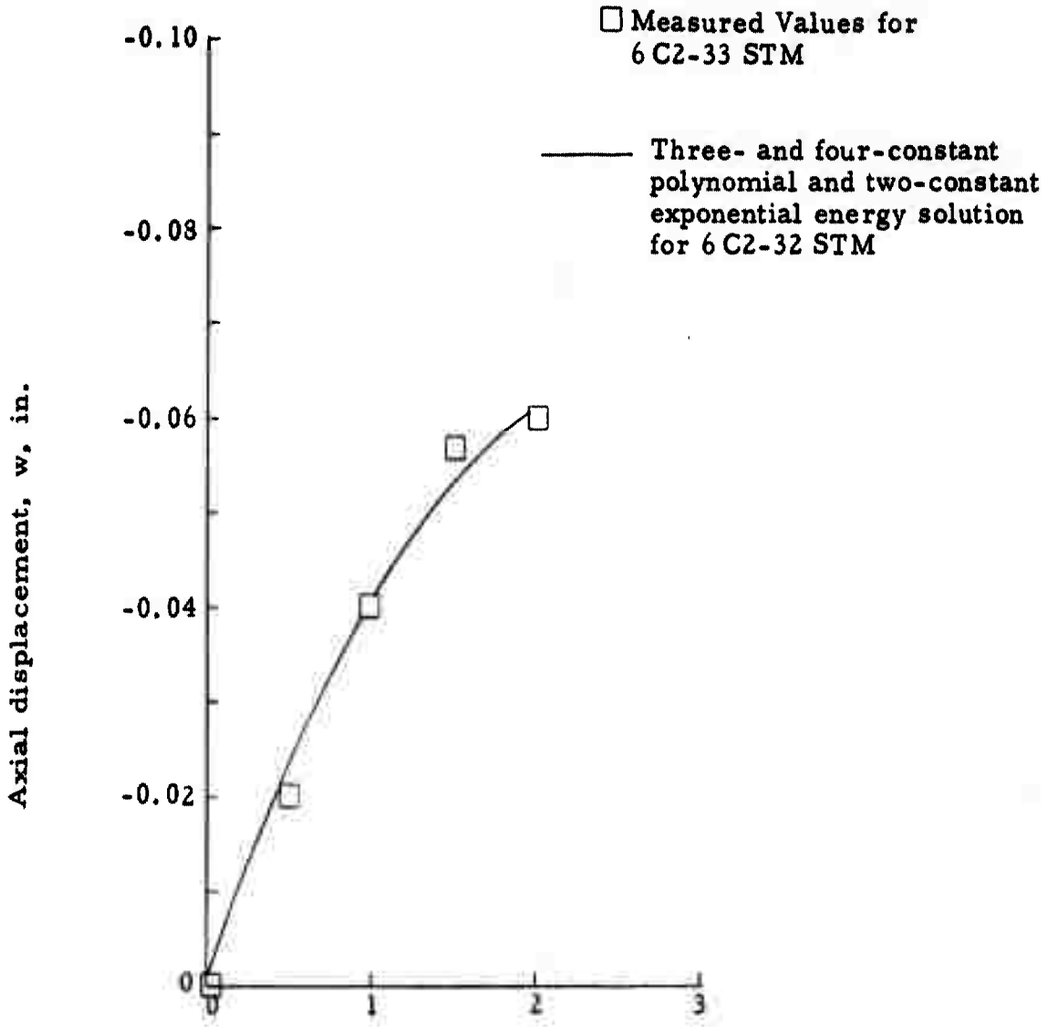

Fig. 4 Axial deflection at end (z=1) of propellant grain for il2b_w propellant.

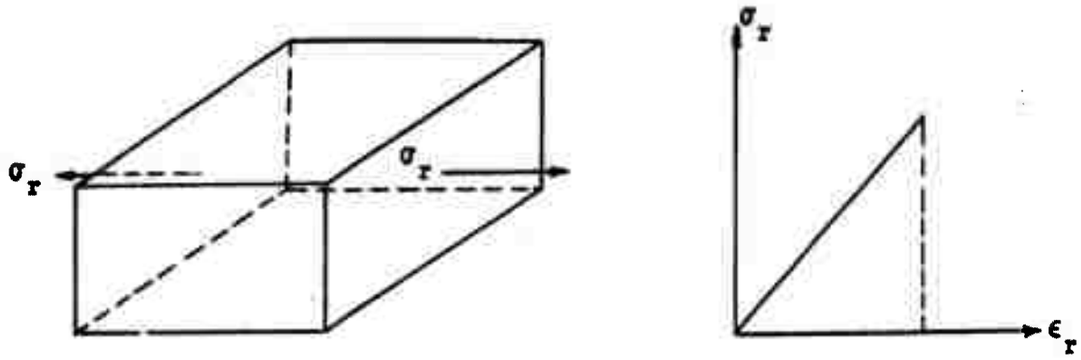

Fig. 5 Element of unit dimensions loaded in simple tension.

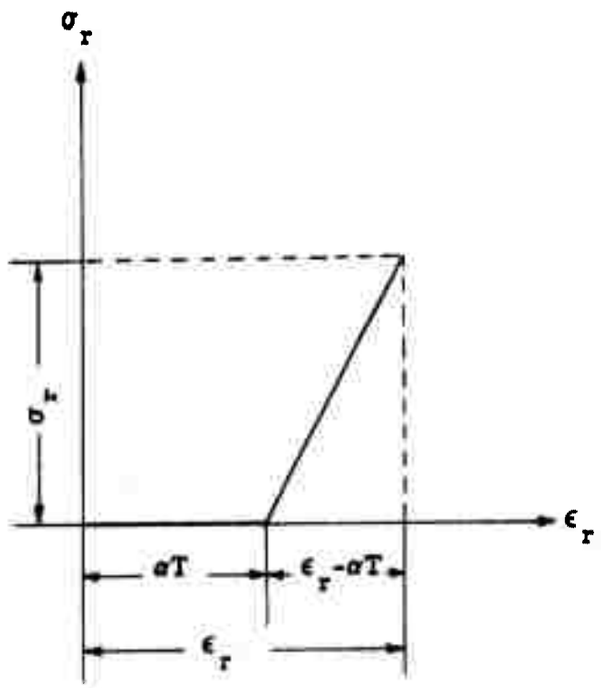

Fig. 6 Stress-strain diagram for element subjected to thermal expansion followed by simple tension.

Initial distribution of this report was made in accordance with the Joint Army-Navy-Air Force mailing lists for Solid Propellant and Liquid Propellant technical information plus approved supplements

UNCLASSIFIED

UNCLASSIFIED